
Optimal Agent-Based Coordination of Energy Communities:

A Case Study of Waste Heat Recovery from Hydrogen Technologies

Master Thesis
for a *MSc in Energy Science and Technology*

Paolo Andres Decormis Leon

Supervisors:

Dr. Hanmin Cai
Dr. Gabriele Humbert
Dr. Binod Prasad Koirala
Dr. Leonard Göke

Professor:

Prof. Dr. André Bardow

December 2024

ETH ZURICH - SWISS FEDERAL INSTITUTE OF TECHNOLOGY

Acknowledgements

I am deeply grateful for the constant, supportive, and invaluable supervision and guidance I received from my supervisors, Dr Hanmin Cai, Dr Gabriel Humbert, and Dr Binod Koirala from EMPA, and Dr Leonard Göke from EPSE. Their willingness to be available and their eagerness to assist me in every way I needed have made this journey both enjoyable and a highly rewarding learning experience. I am particularly thankful for the insightful conversations we shared beyond the scope of this work and for their thoughtful advice on career paths. These will remain valuable inputs for whatever lies ahead. I also wish to extend my gratitude to Prof André Bardow for taking my thesis under the co-supervision of his lab.

This thesis builds upon the work of numerous students who have contributed to similar research at the Urban Energy Systems Lab at EMPA and beyond. I am especially grateful to B. Bernadino for generously sharing several variable inputs and for patiently guiding me through his compiled data, which ensured a much smoother workflow from the outset. I also wish to thank Timo Laaksonlaita, Josien de Koning, and Roxanne Vandenberghe, whose previous work proved to be an invaluable resource for the development of this thesis.

As this thesis marks the conclusion of my master's studies, I want to express my heartfelt gratitude to my family for their unwavering love and support, even from afar, throughout my academic journey. I also want to thank my friends, who continuously inspire me, and remind me of what I find truly valuable in my life.

Andres Decormis

Abstract

Energy communities are increasingly recognised as pivotal elements in the transition to a sustainable energy system. These communities empower citizens to manage their energy production and consumption locally, enhancing efficiency and reducing costs. Decentralised district heating networks (DHNs) play a significant role in this transition by integrating renewable heat sources and reutilising waste heat. This thesis explores the potential of integrating waste heat from hydrogen technologies into energy communities, utilising low-temperature DHNs to further improve system efficiency and reduce costs.

This thesis addresses key questions regarding the dynamic valuation of heat, the economic potential of waste heat recovery from hydrogen technologies, and the optimal coordination of multi-agent, multi-energy communities. A model of a multi-energy community incorporating various energy technologies was developed, with operations optimised over a year to meet energy demands. The findings indicate that while simple systems with heat pumps exhibit low demand flexibility and high operational costs, the introduction of hydrogen technologies with waste heat recovery can significantly enhance flexibility and reduce costs under certain conditions.

Optimal operation of hydrogen technologies is dependent on specific energy values within the system, influenced by factors such as hydrogen prices and electrochemical efficiencies. Current hydrogen-to-electricity price ratios indicate that hydrogen technologies have limited value and may not be profitable investments at present. However, future hydrogen prices could lead to hydrogen technologies becoming financially viable investments with the potential to reduce yearly operational costs by over 80%. The presence of waste heat recovery broadens the optimal operating regions, enhancing the economic viability of hydrogen technologies. The study also formulates a distributed optimisation approach using the exchange ADMM algorithm, enabling energy agents to coordinate effectively while maintaining privacy and achieving near-optimal solutions in a suitable computational time for real-life applications.

To assess the economic value of energy technologies, the Fair Operational Cost Savings (FOCS) value based on the Shapley value is developed. This analysis considers various boundary conditions, highlighting the economic contributions of different technologies and their synergies. In the case studied, installation of PV could lead to over a 30% decrease in yearly operational costs under current price conditions. However, optimistic forecasts of hydrogen prices indicate that a fuel cell with waste heat recovery might become the most valuable technology in the energy system with a FOCS value of over 900 CHF per kW of electricity output.

Contents

| | |
|--|------|
| Acknowledgements | i |
| Abstract | ii |
| List of Figures | vi |
| List of Tables | x |
| List of Acronyms | xii |
| Nomenclature | xiii |
| 1 Introduction | 1 |
| 1.1 Motivation | 1 |
| 1.2 Research questions | 2 |
| 1.3 Thesis contributions | 3 |
| 1.4 Structure of the thesis | 3 |
| 2 Methodology | 4 |
| 2.1 System boundaries | 4 |
| 2.1.1 Energy system components | 5 |
| 2.1.2 System modelling | 7 |
| 2.2 Centralised optimisation | 13 |
| 2.2.1 Objective function | 14 |
| 2.2.2 Constraints | 14 |
| 2.3 Distributed optimisation | 15 |
| 2.3.1 Alternating Direction Method of Multipliers (ADMM) | 15 |

| | | |
|----------|--|-----------|
| 2.3.2 | ADMM in a multi-energy community | 18 |
| 2.4 | Economic assessment | 20 |
| 2.4.1 | Operational cost savings | 20 |
| 2.4.2 | Investment prioritisation | 23 |
| 3 | Case study | 25 |
| 3.1 | Energy community | 25 |
| 3.2 | Inputs | 25 |
| 3.2.1 | Boundary Conditions | 25 |
| 3.2.2 | Energy community demands | 27 |
| 3.2.3 | Techno-economic parameters | 29 |
| 3.3 | Scenarios | 30 |
| 4 | Results | 31 |
| 4.1 | Optimal operation and energy values | 31 |
| 4.1.1 | Baseline scenario | 31 |
| 4.1.2 | Hydrogen system scenario | 34 |
| 4.1.3 | Complete energy community | 53 |
| 4.2 | Multi-agent distributed coordination | 56 |
| 4.2.1 | Convergence to a feasible solution | 56 |
| 4.2.2 | Convergence to an optimal solution | 58 |
| 4.3 | Economics assessment results | 59 |
| 4.3.1 | FOCS values | 59 |
| 4.3.2 | Investment prioritisation | 63 |
| 5 | Conclusion & Discussion | 66 |
| 5.1 | Conclusions | 66 |
| 5.2 | Limitations & future work | 68 |
| A | Optimisation problems | 74 |
| A.1 | Centralised optimisation | 74 |
| A.1.1 | Objective function | 74 |

| | | |
|----------|-----------------------------------|-----------|
| A.1.2 | Constraints | 75 |
| A.2 | Distributed optimisation | 78 |
| A.2.1 | Hydrogen system agent | 78 |
| A.2.2 | Heat pump agent | 79 |
| A.2.3 | TES agent | 80 |
| A.2.4 | BES agent | 80 |
| A.2.5 | Grid connection agent | 80 |
| A.2.6 | Consumer agent c | 81 |
| B | Techno-economic parameters | 82 |

List of Figures

| | | |
|-----|--|----|
| 2.1 | Schematic representation of the elements constituting the methodology. | 4 |
| 2.2 | Schematic representation of the multi-energy system, indicating the energy flows consisting of electricity (yellow), hydrogen (blue), and heat (red); and outlining the boundary of the district. | 5 |
| 2.3 | Schematic representation of the hydrogen system, indicating the energy flows and system's boundary. | 6 |
| 2.4 | Schematic representation of the heat flows and heat sources considered for modelling the heat demand of a consumer's household. | 8 |
| 2.5 | A normalised piecewise affine (PWA) approximation (with $n = 4$ breakpoints) of electrolyser output power, indicating the detailed electrolyser model and the constant efficiency approach. | 11 |
| 2.6 | A comparison of the relative error between a linear and a PWA approximation (with $n = 4$ breakpoints) of the output power of a PEM electrolyser. | 11 |
| 2.7 | A comparison of the required compression power of hydrogen, under adiabatic and isothermal conditions, for different output pressures. | 13 |
| 2.8 | Flowchart of the Exchange ADMM algorithm applied to a multi-agent, multi-energy community. | 21 |
| 2.9 | Schematic representation of the computation carried out by each prosumer agent $i = 1, \dots, N$ and the central coordinator, indicating the information exchanged between the agents over each iteration k under the Exchange ADMM algorithm. | 22 |
| 3.1 | Ambient temperature in the city of Basel over the modelled period (year 2023). | 26 |
| 3.2 | Solar irradiance in the city of Basel over the modelled period (year 2023). | 26 |
| 3.3 | Import and export electricity prices in the city of Basel over the modelled period (year 2023). | 27 |
| 3.4 | Electricity demand profiles for lighting and electric appliances as a percentage of total yearly electricity demand for a (a) summer weekday and (b) winter weekend. | 28 |

| | |
|--|----|
| 3.5 Schematic representation of the three energy system scenarios modelled, and the corresponding sub-scenarios that were modelled for each configuration. | 30 |
| 4.1 Cumulative space heating and electricity demands of energy community over one year in the <i>baseline scenario</i> | 32 |
| 4.2 Scatter plot of heat pump power consumption at different ambient temperatures for different allowable indoor temperature ranges. | 34 |
| 4.3 Heat value over ambient temperature, indicating periods with low and high electricity import tariffs. Subfigure (a) displays all periods, while subfigure (b) filters out periods with no heat demand. | 35 |
| 4.4 Comparison of total heat generation by technology for the baseline and hydrogen scenarios with different prices. | 36 |
| 4.5 Comparison of expenses and revenues of the energy system for the baseline scenario and hydrogen scenarios with different hydrogen prices, indicating the net yearly operating costs. | 37 |
| 4.6 Comparison of the heat value distributions for the baseline and hydrogen scenarios with different hydrogen prices. The dashed and dotted lines represent the heat values associated with producing heat with the heat pump with electricity imported during the high and low tariff periods, respectively. The heat values only correspond to periods when there is heat demand. | 39 |
| 4.7 Scatter plot comparing the heat value vs ambient temperature for the baseline and hydrogen scenarios with low forecasted hydrogen prices. The heat values only correspond to periods when there is heat demand. | 40 |
| 4.8 Schematic representation of the electrolyser and fuel cell with the energy flows and the corresponding price or value associated with it. | 41 |
| 4.9 Scatter plot showing the relationship between the heat value and the electricity value for the hydrogen scenario with a high price forecast of 6 CHF/kg. The time periods from the optimisation results when the fuel cell is consuming hydrogen and producing electricity are indicated with a different marker. The black dashed line is obtained from the analytical optimal frontier function for the fuel cell. The optimal operating region is shaded in blue. | 42 |
| 4.10 Scatter plot showing the relationship between the heat value and the electricity value for the hydrogen scenario with a low price forecast of 2 CHF/kg. The time periods from the optimisation results when the fuel cell is consuming hydrogen and producing electricity are indicated with a different marker. The black dashed line is obtained from the analytical optimal frontier function for the fuel cell. The optimal operating region is shaded in blue. | 43 |

| | | |
|------|---|----|
| 4.11 | Optimal frontiers of a fuel cell as a function of the heat and electricity values in an energy system at different hydrogen prices. | 44 |
| 4.12 | Optimal frontiers of a fuel cell as a function of the heat and electricity values in an energy system for different electrochemical efficiencies. | 45 |
| 4.13 | Scatter plot of the heat value vs the electricity value for the hydrogen scenario with low price forecast of 2 CHF/kg, modelling the fuel cell as a PWA function with 3 breakpoints, indicating with a hue the output power of the fuel cell. | 46 |
| 4.14 | Scatter plot showing the relationship between the heat value and the electricity value for the hydrogen scenario with a low price forecast of 2 CHF/kg, modelling the fuel cell with a constant efficiency, indicating with a hue the output power of the fuel cell. | 47 |
| 4.15 | Optimal yearly electricity consumption of the electrolyser for multiple scenarios with different hydrogen-to-electricity price ratios, indicating the approximated optimal boundaries at low and high electricity tariffs. The shaded region represents an approximation of the optimal operating region. | 49 |
| 4.16 | Optimal yearly hydrogen consumption of the fuel cell for multiple scenarios with different hydrogen-to-electricity price ratios, indicating the approximated optimal boundaries at low and high electricity tariffs. The shaded region represents an approximation of the optimal operating region. | 50 |
| 4.17 | Comparison of the optimal yearly electricity consumption of the electrolyser for multiple scenarios with different hydrogen-to-electricity price ratios, with and without a WHR system to reutilise heat. The shaded regions represent an approximation of the optimal operating region in both cases. | 51 |
| 4.18 | Optimal yearly hydrogen consumption of the fuel cell for multiple scenarios with different hydrogen-to-electricity price ratios, with and without a WHR system to reutilise heat. The shaded regions represent an approximation of the optimal operating region in both cases. | 52 |
| 4.19 | Comparison of expenses and revenues of the energy system for the baseline scenario and complete system scenario with different hydrogen prices, indicating the net yearly operating costs. | 53 |
| 4.20 | Comparison of total electricity consumption (positive) and generation (negative) by technology for the baseline scenario and complete system scenario with different hydrogen prices. | 54 |
| 4.21 | Plot of the convergence of ℓ_1 -norm of the electricity primal residual over multiple iterations for the complete energy system scenario, for various combinations of heat and electricity penalty parameters. | 57 |
| 4.22 | Plot of the convergence of ℓ_1 -norm of the heat primal residual over multiple iterations for the complete energy system scenario, for various combinations of heat and electricity penalty parameters. | 57 |

| | |
|--|----|
| 4.23 Plot of the optimal cost gap, comparing the relative difference in the operational cost from the distributed optimisations at different penalty parameters over the iterations. | 58 |
| 4.24 Comparison of the fair operational cost savings of each technology for the different hydrogen prices scenarios. | 60 |
| 4.25 Plot of the fair operational cost saving values for each technology in the complete system scenario at different hydrogen-to-electricity import prices. | 61 |
| 4.26 Plot of the specific fair operational cost saving values for PV and BES for different PV installed capacities. | 62 |
| 4.27 Net present value of investments into different energy technologies for different hydrogen price scenarios. | 64 |

List of Tables

| | | |
|-----|--|----|
| 3.1 | Values of hydrogen prices for different scenarios. | 27 |
| 3.2 | Temperature ranges used for different scenarios. | 29 |
| 3.3 | Parameters to model the heat demand of households. | 29 |
| 4.1 | Comparison of main results for the baseline scenario between an allowable temperature range of 5°C and 0.1°C. The percentages indicate their relative difference. | 33 |
| 4.2 | Comparison of the main results obtained for the baseline scenario and hydrogen scenarios with three different prices for hydrogen. The percentages indicate the relative difference to the baseline scenario. | 38 |
| 4.3 | Comparison of the main results obtained for the baseline and complete system with three different prices for hydrogen. The percentages indicate the relative difference to the baseline scenario. | 55 |
| 4.4 | Coalition values of the hydrogen system and complete system scenarios at three different hydrogen prices. Indicating the marginal contribution of having the complete energy system in addition to the hydrogen system. . | 56 |
| 4.5 | Comparison of the FOCS values obtained for each technology under the complete system scenario with three different prices for hydrogen. The values are presented in absolute and in percentage term. The percentages in parenthesis indicate the relative difference to the baseline scenario. . | 61 |
| 4.6 | Specific fair operational cost saving values for BES and TES for combinations of inflexible and flexible heating demand, and an energy system excluding and including a BES. | 63 |
| 4.7 | Comparison of net present values and internal rates of return of multiple energy technologies for three different hydrogen price scenarios. IRR values for some technologies are missing because their FOCS values are too low to compute an internal rate of return. | 64 |
| 4.8 | Comparison of net present values and internal rates of return of multiple energy technologies for three different PV installed capacities. IRR values for some technologies are missing because their FOCS values are too low to compute an internal rate of return. | 65 |

| | |
|--|----|
| B.1 Economic-related parameters for the energy technologies modelled in the energy system. | 82 |
| B.2 Technical parameters for the energy technologies modelled in the energy system. | 83 |

List of Acronyms

- 4GDH** Fourth-Generation District Heating
5GDHC Fifth-Generation District Heating & Cooling
ADMM Alternating Direction Method of Multipliers
BES Battery Energy Storage
CO Compressor
COP Coefficient of Performance
DHN District Heating Network
EL Electrolyser
FC Fuel Cell
FOCS Fair Operational Cost Savings
H₂ Hydrogen
HHV Higher Heating Value
HP Heat Pump
IRR Internal Rate of Return
LCOH Levelised Cost of Heat
LHV Lower Heating Value
LP Linear Programming
LT Low Temperature
MILP Mixed-Integer Linear Programming
NPV Net Present Value
PEM Proton-Exchange Membrane
PV Photovoltaics
PWA Piecewise Affine
ROI Return on Investment
SOC State-of-Charge
TES Thermal Energy Storage
WACC Weighted Average Cost of Capital
WHR Waste Heat Recovery

Nomenclature

Variables and parameters

| Symbol | Definition | Units |
|-----------------------------|--|--------|
| <i>Electricity</i> | | |
| $P_{\text{cons},c}$ | Electricity demand of consumer c | kW |
| P_{HP} | Electricity consumption of heat pump | kW |
| P_{PV} | Electricity production of PV panels | kW |
| $P_{\text{BES,ch}}$ | Charging power of battery | kW |
| $P_{\text{BES,dis}}$ | Discharging power of battery | kW |
| P_{EL} | Electricity consumption of electrolyser | kW |
| $P_{\text{H}_2,\text{in}}$ | Electricity consumption by hydrogen system | kW |
| $P_{\text{H}_2,\text{out}}$ | Electricity production by hydrogen system | kW |
| P_{FC} | Electricity production of fuel cell | kW |
| P_{imp} | Electricity imported from the grid | kW |
| P_{exp} | Electricity exported to the grid | kW |
| P_{prod} | Power produced | kW |
| P_{cons} | Power consumed | kW |
| <i>Energy</i> | | |
| E_{BES} | Energy stored in battery | kWh |
| SOC | State of charge of battery | - |
| E_{TES} | Energy stored in thermal energy storage | kWh |
| <i>Rates</i> | | |
| $r_{\text{BES,ch}}$ | Charging power rate of battery | kW/kWh |
| $r_{\text{BES,dis}}$ | Discharging power rate of battery | kW/kWh |
| $r_{\text{TES,in}}$ | Charging power rate of thermal energy storage | kW/kWh |
| $r_{\text{TES,out}}$ | Discharging power rate of thermal energy storage | kW/kWh |
| <i>Heat</i> | | |
| $Q_{\text{cons},c}$ | Heat demand of consumer c | kW |
| Q_{HP} | Heat output of heat pump | kW |
| $Q_{\text{TES,in}}$ | Heat input to thermal energy storage | kW |
| $Q_{\text{TES,out}}$ | Heat output from thermal energy storage | kW |
| $Q_{\text{EL,total}}$ | Total heat generated by electrolyser | kW |

| | | |
|----------------------------|--|------|
| $Q_{FC,\text{total}}$ | Total heat generated by fuel cell | kW |
| $Q_{EL,\text{used}}$ | Heat recovered from electrolyser | kW |
| $Q_{FC,\text{used}}$ | Heat recovered from fuel cell | kW |
| $Q_{EL,\text{waste}}$ | Heat wasted by electrolyser | kW |
| $Q_{FC,\text{waste}}$ | Heat wasted by fuel cell | kW |
| Q_{H_2} | Heat supplied to the district from hydrogen system | kW |
| $Q_{\text{solar},c}$ | Heat gain from solar irradiance | kW |
| $Q_{\text{amb},c}$ | Heat exchange with the ambient | kW |
| Q_{prod} | Heat produced | kW |
| Q_{cons} | Heat consumed | kW |
| <hr/> | | |
| <i>Temperature</i> | | |
| T_c | Indoor temperature of consumer c | °C |
| T_{amb} | Ambient temperature | °C |
| T_c^{\min} | Minimum desired indoor temperature | °C |
| T_c^{\max} | Maximum desired indoor temperature | °C |
| <hr/> | | |
| <i>Efficiencies</i> | | |
| η_{EL} | Nominal electrochemical efficiency of electrolyser | - |
| η_{FC} | Nominal electrochemical of fuel cell | - |
| $\eta_{EL,\text{th}}$ | Thermal efficiency of electrolyser | - |
| $\eta_{FC,\text{th}}$ | Thermal efficiency of fuel cell | - |
| $\eta_{BES,\text{ch}}$ | Charging efficiency of battery | - |
| $\eta_{BES,\text{dis}}$ | Discharging efficiency of battery | - |
| ϵ_{BES} | Self-discharge of battery | - |
| $\eta_{\text{TES,in}}$ | Heat input efficiency of thermal energy storage | - |
| $\eta_{\text{TES,out}}$ | Heat output efficiency of thermal energy storage | - |
| ϵ_{TES} | Self-discharge of thermal energy storage | - |
| η_{PV} | Efficiency of PV panels | - |
| COP | Coefficient of performance of heat pump | - |
| <hr/> | | |
| <i>Mass flow</i> | | |
| $\dot{m}_{H_2,\text{lp}}$ | Hydrogen mass flow (low pressure) | kg/h |
| $\dot{m}_{H_2,\text{FC}}$ | Hydrogen mass flow to fuel cell | kg/h |
| $\dot{m}_{H_2,\text{hp}}$ | Hydrogen mass flow (high pressure) | kg/h |
| $\dot{m}_{H_2,\text{imp}}$ | Hydrogen mass flow imported | kg/h |
| $\dot{m}_{H_2,\text{exp}}$ | Hydrogen mass flow exported | kg/h |
| <hr/> | | |
| <i>Pressure</i> | | |
| $P_{H_2,\text{sto}}$ | Pressure of hydrogen storage | Pa |
| P_{out} | Output pressure of compressor | Pa |
| P_{in} | Input pressure of compressor | Pa |
| <hr/> | | |
| <i>PWA</i> | | |
| $\alpha_{EL,j}$ | Intercept of PWA efficiency segment j for electrolyser | - |
| $\beta_{EL,j}$ | Slope of PWA efficiency segment j for electrolyser | - |
| $\alpha_{FC,j}$ | Intercept of PWA efficiency segment j for fuel cell | - |
| $\beta_{FC,j}$ | Slope of PWA efficiency segment for j fuel cell | - |

| | | |
|----------------------------------|---|-------------------|
| <i>Demand</i> | | |
| $L_{\text{li},c}$ | Yearly demand for lighting | kWh |
| $L_{\text{ea},c}$ | Yearly demand for electric appliances | kWh |
| $\beta_{\text{li}}(t)$ | Hourly demand profile for lighting | - |
| $\beta_{\text{ea}}(t)$ | Hourly demand profile for electric appliances | - |
| R_c | Thermal resistance | °C/kW |
| C_c | Thermal capacitance | kWh/°C |
| ϕ_{solar} | Solar irradiance | kW/m ² |
| $A_{\text{irr},c}$ | Irradiated area of household c | m ² |
| α_c | Absorptivity of household c | - |
| ζ_c | Exponential decay term for temperature response | - |
| a_c | Integrating factor for thermal inertia equation | - |
| <hr/> | | |
| <i>Others</i> | | |
| A_{PV} | Area of PV panels | m ² |
| Δt | Time step for discretised equations | h |
| <hr/> | | |
| <i>Prices</i> | | |
| $p_{\text{imp}}^{\text{E,low}}$ | Electricity import price (low-tariff) | CHF/kWh |
| $p_{\text{imp}}^{\text{E,high}}$ | Electricity import price (high-tariff) | CHF/kWh |
| $p_{\text{exp}}^{\text{E}}$ | Electricity export price | CHF/kWh |
| $p_{\text{imp}}^{\text{H}_2}$ | Hydrogen import price | CHF/kWh |
| $p_{\text{exp}}^{\text{H}_2}$ | Hydrogen export price | CHF/kWh |
| <hr/> | | |
| <i>Optimisation</i> | | |
| J_{op} | Total operational cost (objective function) | CHF |
| λ^{H} | Heat value (dual variable) | CHF/kWh |
| λ^{E} | Electricity value (dual variable) | CHF/kWh |
| <hr/> | | |
| <i>Constants</i> | | |
| HHV_{H_2} | Higher heating value of hydrogen | kWh/kg |
| R | Common gas constant | J/(mol°C) |
| M_{H_2} | Molar mass of hydrogen | kg/mol |
| <hr/> | | |
| <i>Economic</i> | | |
| $\xi(s)$ | Marginal contribution of energy agent s | CHF |
| $v(\mathcal{S})$ | Value of coalition \mathcal{S} | CHF |
| ϕ^{FOCS} | Fair Operational Cost Savings (FOCS) value | CHF |
| <hr/> | | |

Notation of ADMM

| Symbol | Definition |
|--------------------------|--|
| \mathbf{x} | Decision variable vector of agent 1 |
| \mathbf{y} | Decision variable vector of agent 2 |
| \mathbf{A} | Coefficient matrix for agent 1's variables |
| \mathbf{B} | Coefficient matrix for agent 2's variables |
| \mathbf{c} | Right-hand side vector in equality constraint |
| $f(\mathbf{x})$ | Cost function of agent 1 |
| $g(\mathbf{y})$ | Cost function of agent 2 |
| $\boldsymbol{\lambda}$ | Dual variable associated with equality constraint |
| ρ | Penalty parameter in the augmented Lagrangian |
| \mathcal{L} | Unaugmented Lagrangian function |
| \mathcal{L}_ρ | Augmented Lagrangian function |
| \mathbf{r}^k | Primal residual at iteration k |
| \mathbf{s}^k | Dual residual at iteration k |
| ϵ^{pri} | Feasibility tolerance for primal residual |
| ϵ^{dual} | Feasibility tolerance for dual residual |
| $\bar{\mathbf{x}}$ | Average contribution of all agents |
| N | Number of agents in the system |
| θ^* | Optimal objective function value |
| \mathbf{x}_i | Decision variable vector of agent i in Exchange ADMM |
| $f_i(\mathbf{x}_i)$ | Cost function of agent i in Exchange ADMM |

Sets

| Symbol | Definition |
|---------------|---|
| \mathcal{C} | Set of consumers |
| \mathcal{T} | Set of time periods in time horizon |
| Ω | Set of decision variables in optimisation problem |
| \mathcal{V} | Set of energy carriers in multi-energy community |
| \mathcal{S} | Set of energy agents/players in a coalition |

Units

| Symbol | Definition |
|--------|--------------------------------|
| kWh | kilowatt hour |
| MWh | megaowatt hour |
| kW | kilowatt |
| CHF | Swiss francs |
| Rp. | Swiss Rappen (cent of a franc) |
| mol | moles |
| °C | degree Celsius |
| y | year |
| m | meter |
| kg | kilogram |

Subscripts and superscripts

| Symbol | Definition |
|---------|---------------------------------|
| H | heat |
| E | electricity |
| H_2 | hydrogen |
| k | iteration |
| v | energy carrier |
| c | consumer |
| s | energy agent |
| \star | global optimum |
| max | Maximum value or total capacity |

Chapter 1

Introduction

In first place, section 1.1 presents the motivation of this thesis while introducing the most relevant concepts. Then, section 1.2 states the research questions to be answered throughout the thesis. Section 1.3 points out the main contributions of this thesis. Lastly, section 1.4 outlines the structure of the remaining of this report.

1.1 Motivation

Energy communities are becoming increasingly prominent within the energy system and are expected to play a crucial role in the energy transition towards reducing the total carbon emissions [1]. These communities empower citizens to manage their energy consumption and production locally, achieving higher energy efficiency levels and lower overall costs [2]. The benefits extend beyond individual households: energy communities provide greater flexibility to energy suppliers and help to reduce grid congestion [3] [4]. Typically, they leverage shared energy resources, which can be optimised in response to local demand and fluctuating energy prices.

In Switzerland, despite a measurable reduction in household emissions from domestic heating, two-thirds of Swiss households still rely on fossil fuels to cover this demand [5]. By connecting households through shared thermal networks, energy communities could facilitate the decarbonization of Switzerland’s household heating sector. Switzerland is exploring these decentralised district heating approaches through projects like *Nanoverbund* [6], which leverage shared heating resources to drive sustainable heat distribution across communities. Moreover, the latest electricity act *Mantelerlass* released by the Swiss Federal Council seeks to incentivise active citizen participation through local energy communities, as a measure to reach the overarching objective of increasing the security of energy supply in Switzerland [7].

District Heating Networks (DHNs) are anticipated to play a crucial role in decarbonising the heating sector by facilitating the integration of multiple renewable heat sources [8]. Traditional DHNs have a centralised, high temperature heat energy generation [9]. However, new district heating systems—such as Fourth-Generation District

Heating (4GDH) and Fifth-Generation District Heating & Cooling (5GDHC)—enable the use of low-temperature heat sources, which then allows to leverage additional technologies, contributing to a cleaner heating sector [8] [10]. An example of this is the integration of excess or waste heat sources into the system. Studies have investigated the integration of several waste heat sources into DHNs, such as energy-intensive industrial processes or data centres [11]. Small scale, low temperature DHNs, such as the one investigated in the *Nanoverbund* project are a feasible application of integrating waste heat sources to provide ambient heating in households.

In addition, multiple studies have examined the potential for the utilisation of excess heat from hydrogen technologies, such as fuel cells and electrolyzers, in different applications [12] [13] [14] [15]. One instance of such applications is as a heat source in decentralised heating networks. These studies indicate that the utilisation of waste heat from hydrogen technologies significantly increases the overall system efficiency, since it increases the overall useful energy extracted from the system [16]. Studies have also found that the Levelised Cost of Heat (LCOH) coming from excess heat of hydrogen technologies is price competitive to other heat sources, especially when integrated into Low Temperature (LT) networks, since it does not require additional heat pump to raise the temperature in such cases [17].

Energy communities provide an effective framework for integrating waste heat from hydrogen technologies, such as electrolyzers and fuel cells, into local heating systems. By utilising shared LT DHNs, they enable the use of this excess heat, increasing overall system efficiency. This collaborative approach to resource optimisation supports the broader transition to a more sustainable and decarbonised heating sector.

1.2 Research questions

To tackle these challenges and capitalise on the opportunities associated with energy communities and the integration of waste heat from hydrogen technologies, this thesis poses several key research questions. These questions are intended to deepen our understanding of the dynamic value of heat, optimal coordination in multi-energy communities, and the economic potential of energy technologies, including hydrogen devices. Through this investigation, this research seeks to provide insights that support the effective design and operation of distributed energy systems that leverage local resources and enhance the potential of energy communities. The research questions are the following:

1. How can we dynamically value heat in a multi-energy community under dynamic boundary conditions and alternative heating solutions?
2. What is the economic potential of Waste Heat Recovery (WHR) from hydrogen technologies in a multi-energy community?
3. How can a multi-agent, multi-energy community coordinate production and consumption in an optimal and distributed manner?
4. How do different energy technologies compare in terms of their economic potential for a multi-energy community?

1.3 Thesis contributions

In addressing these research questions, the primary contributions of this thesis are:

- Development of a model of a multi-energy community with a comprehensive investigation of the main drivers of the dynamic value of heat and its impact by the integration of waste heat.
- Comprehensive analysis and derivation of the operational dynamics of hydrogen technologies with waste heat recovery in an energy system.
- Formulation and implementation of an agent-based, distributed, optimal coordination mechanism for a multi-agent energy system that simulates a local energy market for heat and electricity.
- Quantification of the fair operational cost savings contributions from multiple energy agents within an energy community with an economic assessment on the profitability of investment alternatives.

1.4 Structure of the thesis

This report is structured as follows: Chapter 2 firstly describes the energy system used throughout the thesis, then it discusses the proposed optimisation problem, formulates this problem in a multi-agent distributed optimisation framework, and finally presents the method followed for the economic assessment of energy technologies. Chapter 3 introduces the case study used in this work to obtain numerical results, mentioning the parameters and boundary conditions used as input to the model. After this, Chapter 4 presents the results obtained from the case study and an interpretation of these numerical results. Finally, Chapter 5 summarises and discusses the main conclusions from the thesis, mentions the main limitations of this work, and proposes future research directions.

Chapter 2

Methodology

This chapter presents the energy system and the methodology followed to answer the research questions. Firstly, section 2.1 introduces the energy system, with all of its components and the modelling approach adopted. Then, section 2.2 describes the optimisation problem of the energy community from a centralised perspective. After this, section 2.3 outlines the distributed optimisation framework that coordinates the multi-agent, multi-energy community to achieve optimality. Finally, section 2.4 presents the approach used to assess the economic impact of the energy system, from operational cost savings to investment prioritisation. To better understand the elements constituting the methodology of this work, Figure 2.1 presents a schematic representation of them.

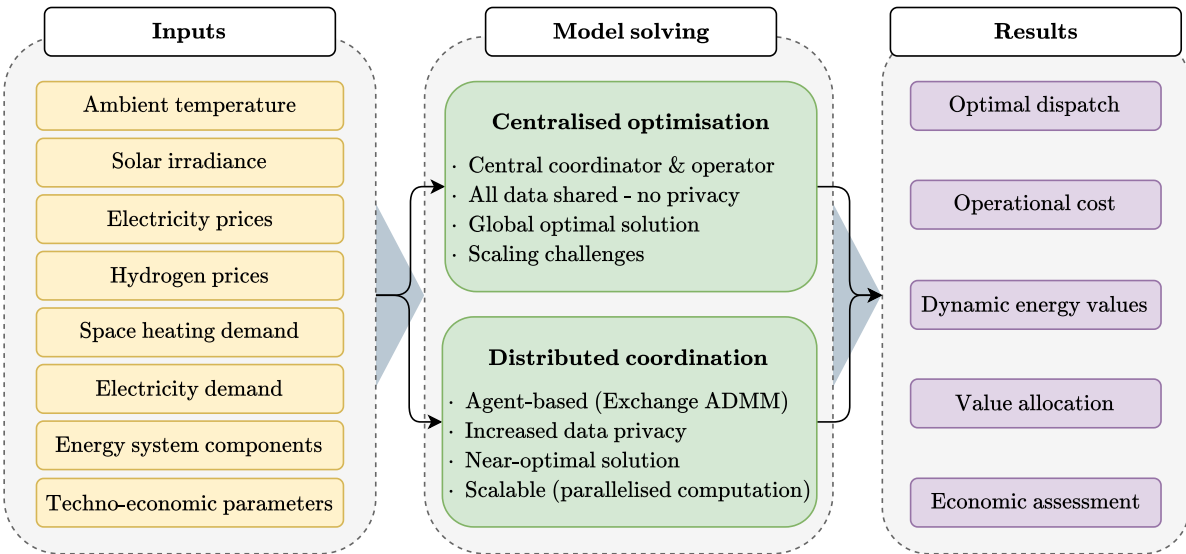


Figure 2.1: Schematic representation of the elements constituting the methodology.

2.1 System boundaries

The energy system modelled in this thesis is built upon the existing pilot project set out to demonstrate the potential of a *nanoverbund* - an energy community with a shared

thermal network to cover the heating demand of a set of households in a more efficient manner. In addition, the energy system considers hydrogen technologies to (i) enable long-term storage of energy and (ii) provide heat recovered during hydrogen conversion processes to the thermal network. The hydrogen technologies considered are based on the systems analysed within the *H2districts* project, which investigates the use of hydrogen technologies to provide operational flexibility to an energy system [11]. The specific details and techno-economic parameters of this pilot project will be described in the upcoming Chapter 3. This section presents the energy system and its components, and describes the modelling approach followed for each of them.

2.1.1 Energy system components

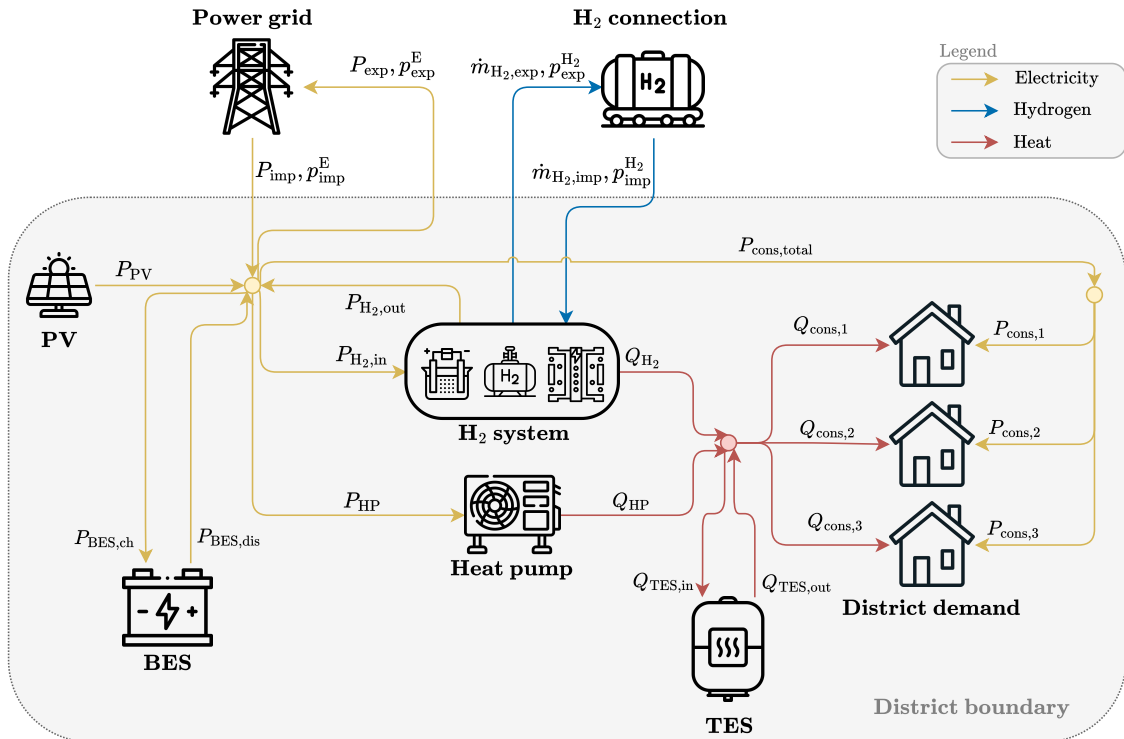


Figure 2.2: Schematic representation of the multi-energy system, indicating the energy flows consisting of electricity (yellow), hydrogen (blue), and heat (red); and outlining the boundary of the district.

Figure 2.2 shows a schematic representation of the modelled energy system. The **district demand** in this case consists of the energy demands of three households. The demands consist of an electricity demand $P_{\text{cons},c}$ and heat demand $Q_{\text{cons},c}$ for each consumer $c \in \mathcal{C}$. In the specific case of the energy system modelled based on the pilot project there are three households, i.e. $\mathcal{C} = \{1, 2, 3\}$. The energy community consists of a **Battery Energy Storage (BES)** for electricity storage, **Thermal Energy Storage (TES)** for heat storage, **Heat Pump (HP)** for electricity-to-heat conversion, **Hydrogen (H₂)** system which in itself counts with multiple components described in upcoming paragraphs, and a **Photovoltaics (PV)** system to generate electricity from solar irradiation. In

addition to these technologies, the district is assumed to have two external connections, one to the **power grid** for electricity imports and exports, and one to a **H₂ connection** for imports and exports of H₂. The H₂ system, as already mentioned, consists of multiple components. A schematic of these components is displayed in Figure 2.3. As shown in the diagram, the system consists of:

- **Proton-Exchange Membrane (PEM) electrolyser**, using electric energy P_{EL} to produce hydrogen $\dot{m}_{H_2,lp}$ and generating excess heat $Q_{EL,total}$
- **PEM fuel cell**, using hydrogen $\dot{m}_{H_2,FC}$ to generate electric energy P_{FC} and generating excess heat $Q_{FC,total}$
- **H₂ compressor**, compressing hydrogen from $\dot{m}_{H_2,lp}$ to $\dot{m}_{H_2,hp}$
- **H₂ storage tank**, which can be filled-in either from the H₂ produced by the electrolyser, providing hydrogen to the fuel cell, and allowing for hydrogen imports and exports to the H₂ connection $\dot{m}_{H_2,imp}$, $\dot{m}_{H_2,exp}$, respectively
- **WHR system**, represented by the heat exchangers which can make use of the excess heat extracted from the electrolyser and the fuel cell ($Q_{EL,used}$, $Q_{FC,used}$) to supply heat (Q_{H_2}) to the district heating network
- **Air cooling**, dumping any excess heat that is not used by the district to maintain the temperature of the electrochemical devices within their respective operating boundaries, focusing on temperature limits

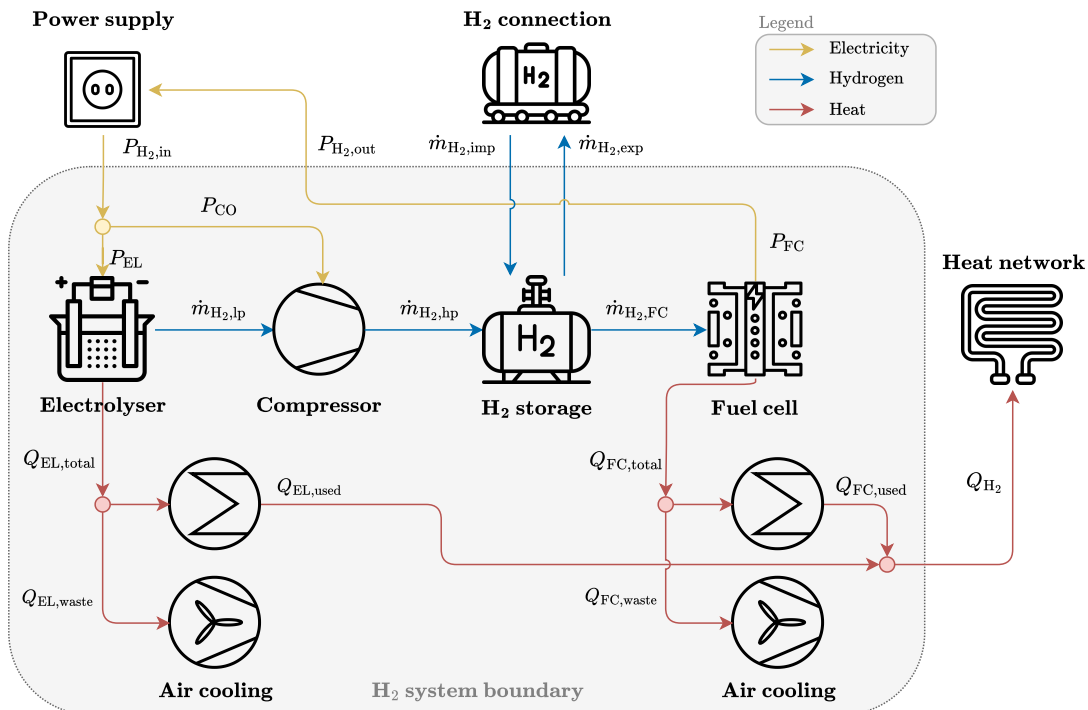


Figure 2.3: Schematic representation of the hydrogen system, indicating the energy flows and system's boundary.

2.1.2 System modelling

This subsection describes the modelling approach followed for each of the elements in the energy system, illustrated in Figure 2.2.

Electricity demand

The electricity demand, P_{cons} , of each consumer, c , is modelled as a summation of electricity demand for lighting and electric appliances. Each of these demands follows a fixed profile with an hourly resolution that distinguishes between weekdays and weekends, and different seasons of the year, which is represented as a fraction of the total yearly demand $\beta_{\text{li}}(t)$ and $\beta_{\text{ea}}(t)$. These demands are then scaled according to the estimated total yearly electricity demand of each consumer for lighting and electric appliances, $L_{\text{li},c}$ and $L_{\text{ea},c}$, respectively.

$$P_{\text{cons},c}(t)\Delta t = \beta_{\text{li}}(t)L_{\text{li},c} + \beta_{\text{ea}}(t)L_{\text{ea},c} \quad (2.1)$$

Heat demand

The heat demand, Q_{cons} , of each consumer, c , is represented as a flexible demand. The flexibility arises from the modelled thermal inertia of each household and its desired temperature range $[T_c^{\min}, T_c^{\max}]$ to be maintained indoors, shown in Equation 2.2.

$$T_c^{\min} < T_c(t) < T_c^{\max} \quad (2.2)$$

The consumer thermal boundary and heat flows are illustrated in Figure 2.4. As shown in the diagram, there are three heat exchanges for each consumer: (1) the heat consumed from the thermal network by consumer c , $Q_{\text{cons},c}$, (2) the heat gained by the solar irradiance in the house, $Q_{\text{solar},c}$, and (3) the heat exchanged between the consumer and the environment $Q_{\text{amb},c}$.

The dynamic behaviour of the consumer's indoor temperature, T_c , is modelled through the differential equation expressed in Equation 2.3, where C_c is the thermal capacitance of the consumer's household.

$$C_c \frac{dT_c}{dt} = Q_{\text{cons},c} + Q_{\text{solar},c} - Q_{\text{amb},c} \quad (2.3)$$

The heat exchanged with the ambient can be approximated by a linear relationship to the difference between the consumer's temperature, T_c , and the ambient temperature, T_{amb} , through the thermal resistance of the consumer, R_c . It is worth noting that this relationship, shown in Equation 2.4, can lead to a heat gain or heat loss of the consumer at different times, depending on the the temperature difference.

$$Q_{\text{amb},c}(t) = \frac{1}{R_c} [T_c(t) - T_{\text{amb}}(t)] \quad (2.4)$$

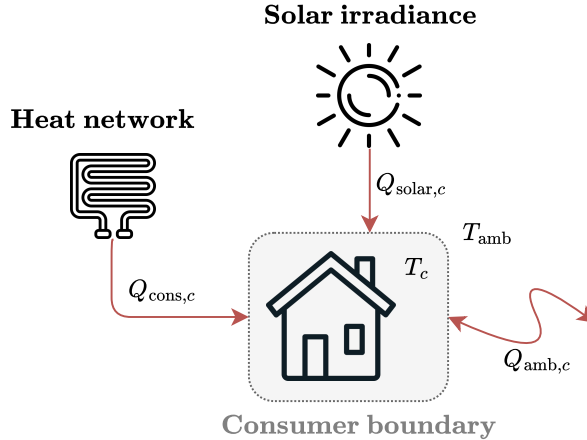


Figure 2.4: Schematic representation of the heat flows and heat sources considered for modelling the heat demand of a consumer's household.

The heat gained from solar radiation is modelled as a linear relationship of the solar irradiance ϕ_{solar} , the irradiance area of the household $A_{\text{irr},c}$, and the absorptivity of the household's irradiated area α_c .

$$Q_{\text{solar},c}(t) = \phi_{\text{solar}}(t) A_{\text{irr},c} \alpha_c \quad (2.5)$$

From the formulations described in Equations 2.4 and 2.5, and solving Equation 2.3 as a linear first-order differential equation with the integrating factor $a_c = e^{\frac{t}{R_c C_c}}$, the discretised, linear relationship displayed in Equation 2.6 can be derived, where ζ_c is the exponential decay term, which is formulated in Equation 2.7 [18].

$$T_c(t) = \zeta_c T_c(t-1) + [1 - \zeta_c] [T_{\text{amb}}(t-1) + R_c [Q_{\text{cons},c}(t-1) + Q_{\text{solar},c}(t-1)]] \quad (2.6)$$

$$\zeta_c = e^{-\frac{\Delta t}{R_c C_c}} \quad (2.7)$$

Heat pump

The heat pump is modelled with a constant Coefficient of Performance (COP), which indicates the conversion of electric energy, P_{HP} , into heat, Q_{HP} , as displayed in Equation 2.8. The maximum load on the heat pump is determined by a constant maximum electricity consumption P_{HP}^{\max} .

$$Q_{\text{HP}}(t) = \text{COP} P_{\text{HP}}(t) \quad (2.8)$$

Photovoltaic system

The electricity production of the PV panels, P_{PV} , at time t in the district is modelled as shown in Equation 2.9, where A_{PV} is the panel area normal to the solar irradiance ϕ_{solar} and η_{PV} is the efficiency of the solar panel. Both parameters are assumed to be constant throughout the modelling period.

$$P_{\text{PV}}(t) = \phi_{\text{solar}}(t) A_{\text{PV}} \eta_{\text{PV}} \quad (2.9)$$

Battery energy storage

The energy stored in the BES at each timestep t is modelled through the equation shown in Equation 2.10. Where, E_{BES} represents the energy stored in the battery, ϵ_{BES} the self-discharge of the battery, $P_{\text{BES,}ch}$ and $P_{\text{BES,}dis}$ represent the charge and discharge power over period t , and $\eta_{\text{BES,}ch}$ and $\eta_{\text{BES,}dis}$ the charge and discharge efficiencies, respectively.

$$E_{\text{BES}}(t) = E_{\text{BES}}(t - 1) [1 - \epsilon_{\text{BES}}] + \eta_{\text{BES,}ch} P_{\text{BES,}ch}(t) \Delta t - \frac{1}{\eta_{\text{BES,}dis}} P_{\text{BES,}dis}(t) \Delta t \quad (2.10)$$

The battery charge and discharge rates are limited within the battery's boundaries, and the battery's charge within its State-of-Charge (SOC) limits. These constraints are shown in Equations 2.11, 2.12, and 2.13.

$$0 \leq P_{\text{BES,}ch}(t) \leq r_{\text{BES,}ch}^{\max} E_{\text{BES}}(t) \quad (2.11)$$

$$0 \leq P_{\text{BES,}dis}(t) \leq r_{\text{BES,}dis}^{\max} E_{\text{BES}}(t) \quad (2.12)$$

$$\text{SOC}_{\text{BES}}^{\min} \leq E_{\text{BES}}(t)/E_{\text{BES}}^{\max} \leq \text{SOC}_{\text{BES}}^{\max} \quad (2.13)$$

Thermal energy storage

The TES component is modelled almost identically to the BES described in the previous paragraph, where the energy stored by the TES is given by E_{TES} , and now $Q_{\text{TES,in}}$ and $Q_{\text{TES,out}}$ represent the heat input and output during period t , respectively. This model is displayed in Equation 2.14. The limits on the heat input and output rates, and the energy stored are modelled as shown in Equations 2.15, 2.16, and 2.17.

$$E_{\text{TES}}(t) = E_{\text{TES}}(t - 1) [1 - \epsilon_{\text{TES}}] + \eta_{\text{TES,in}} Q_{\text{TES,in}}(t) \Delta t - \frac{1}{\eta_{\text{TES,out}}} Q_{\text{TES,out}}(t) \Delta t \quad (2.14)$$

$$0 \leq Q_{\text{TES,in}}(t) \leq r_{\text{TES,in}}^{\max} E_{\text{TES}}(t) \quad (2.15)$$

$$0 \leq Q_{\text{TES,out}}(t) \leq r_{\text{TES,out}}^{\max} E_{\text{TES}}(t) \quad (2.16)$$

$$0 \leq E_{\text{TES}}(t) \leq E_{\text{TES}}^{\max} \quad (2.17)$$

PEM Electrolyser

Since a focus of the thesis is on the WHR system and the value of waste heat from H₂ technologies, the modelling of the electrolyser and the fuel cell is more detailed than the traditional, constant efficiency approach. For H₂ components we use Piecewise Affine (PWA) approximations of the corresponding conversion efficiencies.

In other works [19] [20], the PWA approximation of the true efficiency curve of H₂ technologies is implemented making use of binary variables, which determine the section of the load curve under which the component is operating at time t . This usual implementation requires a Mixed-Integer Linear Programming (MILP) formulation of an optimisation problem, which is drastically more computationally expensive to solve than

a Linear Programming (LP) optimisation problem. For this reason, and making use of the concavity of the *true* efficiency curves, we are able to formulate the PWA approximation as $n + 1$ linear inequality constraints. The mathematical representation of this modelling approach is shown in Equation 2.18. Where P_{EL} is the electrolyser load, P_{EL}^{\max} is the maximum load capacity of the electrolyser, $\dot{m}_{\text{H}_2,\text{lp}}$ is the hydrogen produced, HHV_{H_2} is the Higher Heating Value (HHV)¹ of hydrogen, and $\alpha_{\text{EL},j}$ and $\beta_{\text{EL},j}$ are the y -intercepts and slopes of each of the $n + 1$ linear constraints. These linear functions are obtained by interpolating the true efficiency curves at n breakpoints.

$$\frac{\dot{m}_{\text{H}_2,\text{lp}}(t)\text{HHV}_{\text{H}_2}}{P_{\text{EL}}^{\max}} \leq \alpha_{\text{EL},j} + \beta_{\text{EL},j} \frac{P_{\text{EL}}(t)}{P_{\text{EL}}^{\max}}, \quad \forall j \in [1, n + 1] \quad (2.18)$$

A comparison of the estimated output power based on the input power is shown in Figure 2.5. It can be seen from the figure that the PWA approximation results in a much closer approximation to the Electrolyser (EL) model than the constant efficiency approximation. This is made more evident observing by plotting the relative error of both approximations, shown in Figure 2.6. It is evident that following these approaches, the largest discrepancy is at low partial loads in the operation of the electrolyser.

It is important to remark that since PEM H₂ technologies can operate at low partial loads [21], and in order to avoid introducing binary variables to the problem formulation, the electrolyser is modelled as following a single operating state. Although this decreases the detail in component modelling, it is assumed to have a small impact in the output of the optimisation. Therefore, the power limits on the electrolyser are as shown in Equation 2.19.

$$0 \leq P_{\text{EL}}(t) \leq P_{\text{EL}}^{\max} \quad (2.19)$$

PEM Fuel cell

As mentioned in the previous paragraphs, the H₂ technologies are modelled using PWA approximations. The approach for the Fuel Cell (FC) is equivalent to the electrolyser, which results in the relationship given by Equation 2.20, where the same notation as for the electrolyser is used, P_{FC} is the fuel cell output electric power, $\dot{m}_{\text{H}_2,\text{FC}}$ is the input hydrogen mass flow to the fuel cell, and $\dot{m}_{\text{H}_2,\text{FC}}^{\max}$ is the maximum hydrogen mass flow that can pass through the fuel cell. The output power of the fuel cell is indirectly constrained by the maximum hydrogen mass flow, as shown in Equation 2.21.

$$\frac{P_{\text{FC}}(t)}{\dot{m}_{\text{H}_2,\text{FC}}^{\max}\text{HHV}_{\text{H}_2}} \leq \alpha_{\text{FC},j} + \beta_{\text{FC},j} \frac{\dot{m}_{\text{H}_2,\text{FC}}(t)}{\dot{m}_{\text{H}_2,\text{FC}}^{\max}}, \quad \forall j \in [1, n + 1] \quad (2.20)$$

$$0 \leq \dot{m}_{\text{H}_2,\text{FC}}(t) \leq \dot{m}_{\text{H}_2,\text{FC}}^{\max} \quad (2.21)$$

¹Throughout this work, the HHV is consistently used as the energy content of hydrogen. As mentioned in literature [16], using the Lower Heating Value (LHV) would lead to an overestimation of the heat recovery potential.

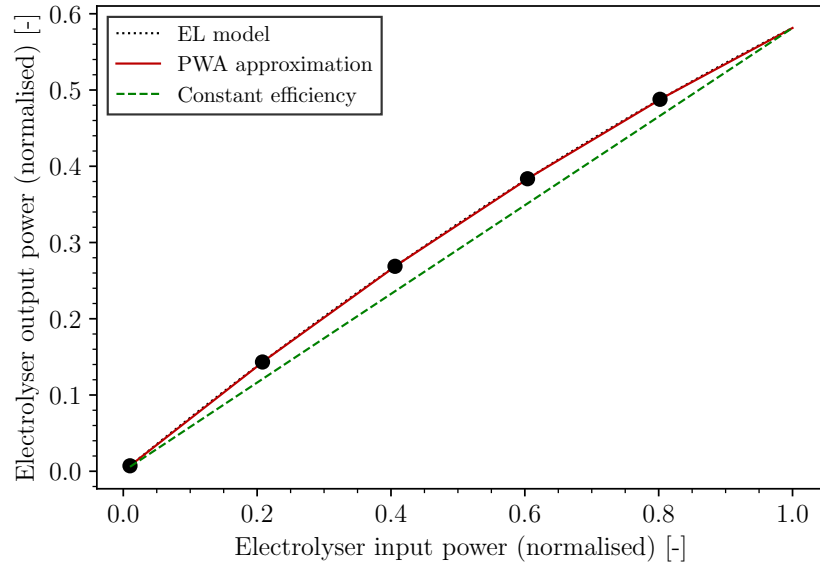


Figure 2.5: A normalised piecewise affine (PWA) approximation (with $n = 4$ breakpoints) of electrolyser output power, indicating the detailed electrolyser model and the constant efficiency approach.

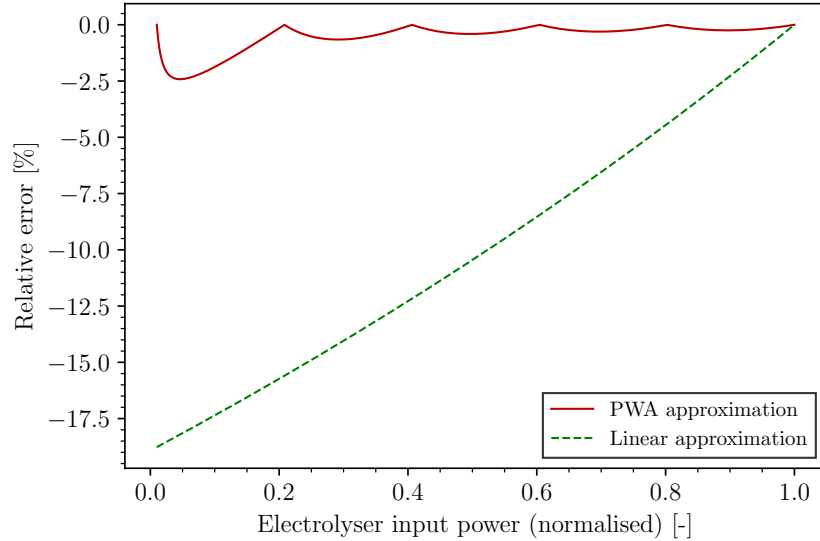


Figure 2.6: A comparison of the relative error between a linear and a PWA approximation (with $n = 4$ breakpoints) of the output power of a PEM electrolyser.

Waste heat recovery

Following the energy conservation principle, the excess heat released by the electrolyser, $Q_{\text{EL, total}}$, and fuel cell, $Q_{\text{FC, total}}$, is determined by the difference between the input and output power corresponding to each technology. This difference represents the total heat loss by the system. From this heat loss, a fraction can be recovered. The ratio between the recoverable heat and the total heat loss of the system, defined as the thermal efficiency η_{th} , depends on multiple parameters, such as the operating temperature and current density of the device [16]. For this study, however, this ratio is assumed to be

constant throughout the different loads on the device. Therefore, the total recoverable heat from the electrolyser and the fuel cell is linearly proportional to the total heat loss, by a constant thermal efficiency $\eta_{\text{EL,th}}$ and $\eta_{\text{FC,th}}$, as shown in Equation 2.22 and Equation 2.23, respectively.

$$Q_{\text{EL,total}}(t) = [P_{\text{EL}}(t) - \dot{m}_{\text{H}_2,\text{lp}}(t)\text{HHV}_{\text{H}_2}] \eta_{\text{EL,th}} \quad (2.22)$$

$$Q_{\text{FC,total}}(t) = [\dot{m}_{\text{H}_2,\text{FC}}(t)\text{HHV}_{\text{H}_2} - P_{\text{FC}}(t)] \eta_{\text{FC,th}} \quad (2.23)$$

The heat recovered from each component can either be transferred to the thermal network of the district, Q_{used} , or it can be dumped through the separate cooling system, Q_{waste} . This heat balance of the electrolyser and fuel cell is shown in Equations 2.24 and 2.25.

$$Q_{\text{EL,total}}(t) = Q_{\text{EL,used}}(t) + Q_{\text{EL,waste}}(t) \quad (2.24)$$

$$Q_{\text{FC,total}}(t) = Q_{\text{FC,used}}(t) + Q_{\text{FC,waste}}(t) \quad (2.25)$$

Hydrogen compressor

The hydrogen compression is modelled as an ideal adiabatic compression [22] [23] [20]. This relationship, shown in Equation 2.26, describes the power requirement, P_{CO} , for compressing hydrogen from an inlet pressure, P_{in} , to a desired outlet pressure, P_{out} , over time t . Here, R is the common gas constant, T_{in} is the inlet temperature, γ is the heat capacity ratio of hydrogen, M_{H_2} is the molar mass of hydrogen, η_{CO} is the compressor efficiency (assumed to be constant), and $\dot{m}_{\text{H}_2,\text{lp}}$ represents the mass flow rate of hydrogen into the compressor.

$$P_{\text{CO}}(t) = \frac{RT_{\text{in}}\gamma}{M_{\text{H}_2}(\gamma - 1)\eta_{\text{CO}}} \left(\left(\frac{P_{\text{out}}}{P_{\text{in}}} \right)^{\frac{\gamma-1}{\gamma}} - 1 \right) \dot{m}_{\text{H}_2,\text{lp}}(t) \quad (2.26)$$

An alternative approach to modelling hydrogen compression would be to assume an isothermal compression, which would result in the relationship shown in Equation 2.27. However, this approach underestimates the amount of work required to reach a certain compression ratio, since it assumes that all heat generated in the system is allowed to flow out of the system. The difference in the required compression power for these two different approaches is shown in Figure 2.7.

$$P_{\text{CO}}^{\text{iso}}(t) = \frac{RT}{M_{\text{H}_2}} \ln \left(\frac{P_{\text{out}}}{P_{\text{in}}} \right) \frac{1}{\eta_{\text{CO}}} \dot{m}_{\text{H}_2,\text{lp}}(t) \quad (2.27)$$

Hydrogen storage tank

The hydrogen stored in the pressure tank, $m_{\text{H}_2,\text{sto}}$, at every timestep t is given by the relation shown in Equation 2.28, where $\eta_{\text{H}_2,\text{sto}}$ is the storage efficiency, assumed to be constant. In addition, the hydrogen stored at every time step is constrained by the

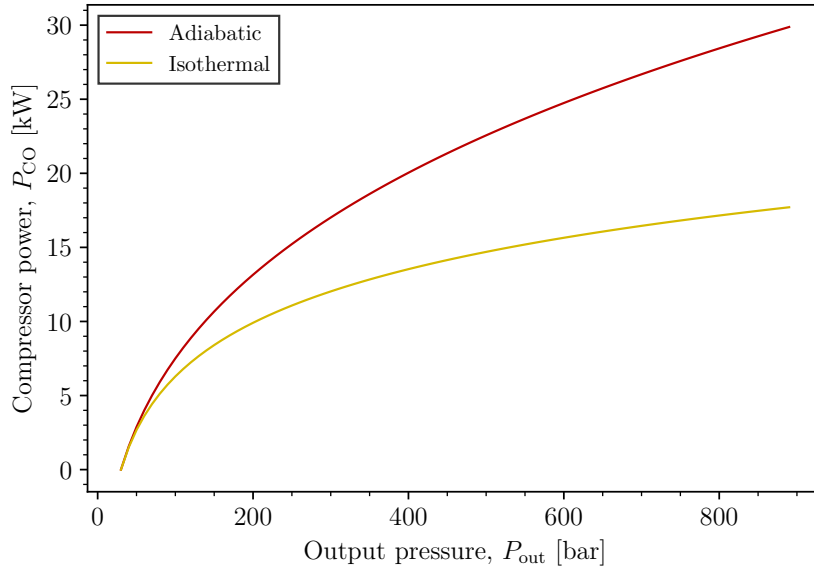


Figure 2.7: A comparison of the required compression power of hydrogen, under adiabatic and isothermal conditions, for different output pressures.

maximum storage capacity $m_{\text{H}_2,\text{sto}}^{\max}$, which in turn is given by the volume of each tank, $V_{\text{H}_2,\text{sto}}$, the number of tanks, n_{tanks} , and additional parameters, such as the pressure, $P_{\text{H}_2,\text{sto}}$, and temperature, $T_{\text{H}_2,\text{sto}}$, inside each tank, as shown in Equation 2.29.

$$m_{\text{H}_2,\text{sto}}(t) = m_{\text{H}_2,\text{sto}}(t-1) + \eta_{\text{H}_2,\text{sto}} \Delta t (\dot{m}_{\text{H}_2,\text{hp}}(t) + \dot{m}_{\text{H}_2,\text{imp}}(t)) - \frac{\Delta t}{\eta_{\text{H}_2,\text{sto}}} (\dot{m}_{\text{H}_2,\text{exp}}(t) + \dot{m}_{\text{H}_2,\text{FC}}(t)) \quad (2.28)$$

$$m_{\text{H}_2,\text{sto}}^{\max} = n_{\text{tanks}} \frac{P_{\text{H}_2,\text{sto}} M_{\text{H}_2} V_{\text{H}_2,\text{sto}}}{1e^3 R T_{\text{H}_2,\text{sto}}} \quad (2.29)$$

$$m_{\text{H}_2,\text{sto}}(t) \leq m_{\text{H}_2,\text{sto}}^{\max} \quad (2.30)$$

External connections

The energy system consists of two external connections, one to the power grid and one to a H₂ supply. Each of these connections allow for import and export of each energy carrier. Electricity is imported, P_{imp} , at price $p_{\text{imp}}^{\text{E}}$ and exported, P_{exp} , at price $p_{\text{exp}}^{\text{E}}$. Similarly, hydrogen is imported, $\dot{m}_{\text{H}_2,\text{imp}}$, at price $p_{\text{imp}}^{\text{H}_2}$ and exported, $\dot{m}_{\text{H}_2,\text{exp}}$, at price $p_{\text{exp}}^{\text{H}_2}$.

2.2 Centralised optimisation

The centralised optimisation problem for the multi-energy community corresponds to the optimal dispatch of energy technologies to supply the total energy demand. This section formulates the objective function and mentions the constraints required from the perspective of a centralised operator with complete information of the energy system's components.

2.2.1 Objective function

The goal of the multi-energy community is to minimise the total net operational costs, J_{op} , over the modelling period, \mathcal{T} , where the net costs are composed of all expenses and revenues of the system, as shown in Equation 2.31.

$$J_{\text{op}} = \sum_{t \in \mathcal{T}} (\text{expenses}(t) - \text{revenues}(t)) \quad (2.31)$$

Assuming that the operational costs consist of only the energy imported, x_{imp}^v , and energy exported, x_{exp}^v , of different energy carriers $v \in \mathcal{V}$, and given the corresponding import and export prices p_{imp}^v and p_{exp}^v , the net operational costs of the energy community can be expressed as shown in Equation 2.32.

$$J_{\text{op}} = \sum_{t \in \mathcal{T}} \sum_{v \in \mathcal{V}} (p_{\text{imp}}^v(t)x_{\text{imp}}^v(t) - p_{\text{exp}}^v(t)x_{\text{exp}}^v(t)) \quad (2.32)$$

The optimisation problem is then to minimise the objective cost function, where the set of decision variables Ω is composed of the control variables of all the energy components within the energy system. The resulting formulation of the centralised optimisation is represented in Equation 2.33. In practice, however, additional penalty terms may need to be added to the objective function of the optimisation problem, in order to achieve different objectives, such as the relaxation of constraints by using slack variables.

$$\underset{\Omega}{\text{minimize}} \quad J_{\text{op}} \quad (2.33)$$

2.2.2 Constraints

The constraints of the optimisation problem mainly consist of energy balance constraints and system feasibility constraints. These two categories are further explained in the following paragraphs.

Energy balance constraints

The energy balance constraints refer to the total district energy balance that must be achieved throughout the modelled period, i.e. energy production must equal energy consumption at every time step t of the modelling period. Note that *production* in this context includes any form of adding an energy carrier in the system (imports or self-production), and *consumption* includes any form of removing an energy carrier (exports or self-consumption). These balance constraints apply to every energy carrier, v , modelled in the system. Applying this to electricity and heat results in the constraints shown in Equation 2.34 and Equation 2.35, respectively.

$$P_{\text{prod}}(t) = P_{\text{cons}}(t), \quad : \lambda^E(t) \quad (2.34)$$

$$Q_{\text{prod}}(t) = Q_{\text{cons}}(t), \quad : \lambda^H(t) \quad (2.35)$$

The terms λ^E and λ^H are referred to as the *dual variables* or *Lagrange multipliers* of the respective constraints. These dual variables tell us the *sensitivity* of the value of objective function to a change in the specific constraint, i.e. the *marginal cost* of energy at time t , also referred to as the *shadow price*. The economic interpretation of these variables, in the context of an energy system, is the value of an additional unit of energy at timestep t . If the value is high, there is a high operational cost to supply energy at that period. Conversely, if the value is low or even zero, there is little or no impact of the energy demand in the operational cost of the system.

System feasibility constraints

System feasibility constraints refer to all constraints that reflect: the modelling of the components in the energy system, the limits imposed on external connections, and boundary conditions of the system. The component modelling applied to the energy system investigated in this work was already described in subsection 2.1.2. The complete formulation of the centralised optimisation problem applied to the energy system studied in the thesis can be found in section A.1.

2.3 Distributed optimisation

The previous section 2.2 formulated the optimisation problem from the perspective of a central coordinator and operator of the energy district. Such a traditional centralised optimisation method would rely on a single controller with access to all of the system information, including households, energy conversion technologies, and energy storage devices. However, as energy systems grow larger and integrate diverse participants, this method may become infeasible due to privacy and scalability issues. A distributed optimisation approach allows such a system to be decomposed into multiple, local, optimisation problems managed by individual agents which then coordinate to achieve the global optimum. This enables energy communities to reach their global objective, while preserving the privacy of individual agents, allowing to solve for large scale systems, and allowing for a flexible optimisation in dynamic environments.

Multiple distributed algorithm alternatives have been explored in literature for application in energy systems [24] [25] [18]. In this work, *Alternating Direction Method of Multipliers (ADMM)* is used as the distributed optimisation algorithm that coordinates multiple energy agents in the production and consumption within a multi-energy community. This method will be further described in the following section. After that, the application of the method to a multi-energy community will be formulated.

2.3.1 Alternating Direction Method of Multipliers (ADMM)

ADMM is an algorithm that consists of *decomposing* the global optimisation problem into subproblems and *coordinating* the solution to these local subproblems to find the global

optimal solution [26]. This section attempts to explain the steps taken to formulate an optimisation problem for the ADMM algorithm, to then apply it to an energy system.

General formulation

Take an optimisation problem such as the one proposed in Equation 2.36, where $\mathbf{x} \in \mathbb{R}^n$ and $\mathbf{y} \in \mathbb{R}^m$ are decision variables corresponding to two different agents, where $\mathbf{A} \in \mathbb{R}^{p \times n}$, $\mathbf{B} \in \mathbb{R}^{p \times m}$, $\mathbf{c} \in \mathbb{R}^p$, where $f : \mathbb{R}^n \rightarrow \mathbb{R}$ and $g : \mathbb{R}^m \rightarrow \mathbb{R}$ are the cost functions of both agents, and where $\boldsymbol{\lambda} \in \mathbb{R}^p$ is the dual variable associated with the equality constraint.

$$\begin{aligned} & \text{minimize} && f(\mathbf{x}) + g(\mathbf{y}) \\ & \text{subject to} && \mathbf{Ax} + \mathbf{By} = \mathbf{c}, \quad : \boldsymbol{\lambda} \end{aligned} \tag{2.36}$$

To be able to decompose this optimisation problem by each agent, we must first apply a *Lagrangian relaxation* of the complicating equality constraint. The (unaugmented) Lagrangian of the problem is shown in Equation 2.37.

$$\mathcal{L}(\mathbf{x}, \mathbf{y}, \boldsymbol{\lambda}) = f(\mathbf{x}) + g(\mathbf{y}) + \boldsymbol{\lambda}^T (\mathbf{Ax} + \mathbf{By} - \mathbf{c}) \tag{2.37}$$

For ADMM, however, an *augmented Lagrangian* is used instead. Thus ensuring the convergence of the algorithm without additional assumptions, such as the strict convexity of f and g . In ADMM, we formulate the augmented Lagrangian with a quadratic penalty term on the constraint violation, associated with a penalty parameter $\rho > 0$. This term encourages the agent's optimisations to satisfy the feasibility constraint and smoothens the path to convergence. This is especially important in problems with affine objective functions, such as the one formulated in this thesis. The augmented Lagrangian of the problem is shown in Equation 2.38.

$$\mathcal{L}_\rho(\mathbf{x}, \mathbf{y}, \boldsymbol{\lambda}) = f(\mathbf{x}) + g(\mathbf{y}) + \boldsymbol{\lambda}^T (\mathbf{Ax} + \mathbf{By} - \mathbf{c}) + \rho/2 \|\mathbf{Ax} + \mathbf{By} - \mathbf{c}\|_2^2 \tag{2.38}$$

It results apparent now that although Equation 2.37 was separable into the variables \mathbf{x} and \mathbf{y} , by adding the quadratic term in Equation 2.38, we can no longer separate the expression. This is solved, however, by optimising over each variable in an *alternating* fashion, i.e. first optimising the function for \mathbf{x} while \mathbf{y} is a fixed parameter, and then optimising the function for \mathbf{y} while \mathbf{x} is a fixed parameter. After the optimisation of the problem over each decision variable is solved over one iteration, the value of the dual variable $\boldsymbol{\lambda}$ is updated, and the subproblem associated to each decision variable is re-optimised with the updated dual variable. The dual variable update uses a step size equal to the augmented Lagrangian parameter ρ , since this ensures consistency between the primal and dual updates, increasing reliability and stability of convergence. The primal and dual update functions of iteration k of ADMM are outlined in Equations 2.39, 2.40, and 2.41.

$$\mathbf{x}^{k+1} := \underset{\mathbf{x}}{\operatorname{argmin}} \mathcal{L}_\rho(\mathbf{x}, \mathbf{y}^k, \boldsymbol{\lambda}^k) \tag{2.39}$$

$$\mathbf{y}^{k+1} := \underset{\mathbf{y}}{\operatorname{argmin}} \mathcal{L}_\rho(\mathbf{x}^{k+1}, \mathbf{y}, \boldsymbol{\lambda}^k) \tag{2.40}$$

$$\boldsymbol{\lambda}^{k+1} := \boldsymbol{\lambda}^k + \rho (\mathbf{Ax}^{k+1} + \mathbf{By}^{k+1} - \mathbf{c}) \tag{2.41}$$

Convergence

The following assumptions allow to make a series of statements about convergence.

1. the functions f and g are closed, proper and convex. This ensures that the subproblems for the \mathbf{x} -update and \mathbf{y} -update are *solvable* and can be minimised.
2. the unaugmented Lagrangian \mathcal{L} has a saddle point.

Under assumptions 1 and 2 ADMM is proven to satisfy the following convergence criteria:

- *Residual convergence.* $\mathbf{r}^k \rightarrow 0$ as $k \rightarrow \infty$, where $\mathbf{r}^k = \mathbf{A}\mathbf{x}^k + \mathbf{B}\mathbf{y}^k - \mathbf{c}$ is the *primal residual*.
- *Objective convergence.* $f(\mathbf{x}^k) + g(\mathbf{y}^k) \rightarrow \theta^*$ as $k \rightarrow \infty$, where θ^* is the optimal objective function value.
- *Dual variable convergence.* $\boldsymbol{\lambda}^k \rightarrow \boldsymbol{\lambda}^*$ as $k \rightarrow \infty$, where $\boldsymbol{\lambda}^*$ is a dual optimal point.

Optimality and stopping criteria

The sufficient optimality conditions for the ADMM algorithm is to reach *primal feasibility* (Equation 2.42) and *dual feasibility* (Equation 2.43, Equation 2.44).

$$\mathbf{A}\mathbf{x}^* + \mathbf{B}\mathbf{y}^* - \mathbf{c} = \mathbf{0} \quad (2.42)$$

$$\mathbf{0} \in \partial f(\mathbf{x}^*) + \mathbf{A}^T \boldsymbol{\lambda}^* \quad (2.43)$$

$$\mathbf{0} \in \partial g(\mathbf{y}^*) + \mathbf{B}^T \boldsymbol{\lambda}^* \quad (2.44)$$

For this reason, to decide to stop the iterations, a reasonable termination criteria is whether these residuals are met within allowable feasibility tolerances $\epsilon^{\text{pri}} > 0$ and $\epsilon^{\text{dual}} > 0$, as shown in Equation 2.45 and Equation 2.46.

$$\|\mathbf{r}^k\|_2 \leq \epsilon^{\text{pri}} \quad (2.45)$$

$$\|\mathbf{s}^k\|_2 \leq \epsilon^{\text{dual}} \quad (2.46)$$

The *dual residual*, \mathbf{s}^k , can be understood as the change in the dual feasibility condition, which is directly linked to the change in the primal variables from one iteration to the next. This indicates whether the value of the dual variable is stabilising over the iterations. Therefore, a small dual residual means that the solution is reaching near-optimality. The calculation of the dual residual is as shown in Equation 2.47. Meanwhile, the primal residual measures directly constraint feasibility. Note that although there is a dual residual corresponding to each primal variable, we only need the dual residual of \mathbf{y} since \mathbf{y}^{k+1} by definition in Equation 2.40 minimises $\mathcal{L}_\rho(\mathbf{x}^{k+1}, \mathbf{y}, \boldsymbol{\lambda}^k)$.

$$\mathbf{s}^{k+1} = \rho \mathbf{A}^T \mathbf{B} (\mathbf{y}^{k+1} - \mathbf{y}^k) \quad (2.47)$$

Exchange ADMM

So far, the standard structure of ADMM was used to explain the algorithm. However, for an application in multi-agent distributed optimisation cases, it is more practical to use an alternative formulation, known as *Exchange ADMM*. The generalised formulation for N agents is shown in Equation 2.48. Here, $\mathbf{x}_i \in \mathbb{R}^n, i = 1, \dots, N$ represents the decision variable vector for each agent i , where n is the number of decision variables for each agent, $f_i : \mathbb{R}^n \rightarrow \mathbb{R}$ represents the cost function of each agent, and $\boldsymbol{\lambda} \in \mathbb{R}^n$ represents the dual variable vector associated with the equality constraint. The components of each vector variable \mathbf{x}_i represent quantities exchanged among agents, and the *equilibrium constraint* enforces that these resources reach a balance.

$$\begin{aligned} & \text{minimize}_{\mathbf{x}_i} \quad \sum_{i=1}^N f_i(\mathbf{x}_i) \\ & \text{subject to} \quad \sum_{i=1}^N \mathbf{x}_i = 0, \quad : \boldsymbol{\lambda} \end{aligned} \tag{2.48}$$

From this new formulation, the following algorithm steps can be derived:

$$\mathbf{x}_i^{k+1} := \underset{\mathbf{x}_i}{\operatorname{argmin}} \left(f_i(\mathbf{x}_i) + (\boldsymbol{\lambda}^k)^T \mathbf{x}_i + \rho/2 \|N\bar{\mathbf{x}}^k - \mathbf{x}_i^k + \mathbf{x}_i\|_2^2 \right) \tag{2.49}$$

$$\boldsymbol{\lambda}^{k+1} := \boldsymbol{\lambda}^k + \rho \sum_{i=1}^N \mathbf{x}_i^{k+1} \tag{2.50}$$

This new formulation, which can be understood as a *resource allocation* problem, gives rise to an interpretation of the dual variable $\boldsymbol{\lambda}$ as a *price signal* which is shared with each agent over each iteration. After each iteration, each agent proceeds to re-optimise their *contribution* to the system, denoted by \mathbf{x}_i . For the \mathbf{x} -update of each agent, the total deviation of the balance constraint from the system must be known by each agent. To maintain privacy and reduce the amount of information shared to and from each agent, the average contribution of the agents $\bar{\mathbf{x}}$ and the number of agents N in the system is broadcast instead. This procedure resembles an auction process, where the price $\boldsymbol{\lambda}$ is constantly adjusted to reach a market equilibrium, i.e. increasing the price to incentivise supply and decreasing the price to incentivise demand. This formulation results practical to be applied to a distributed energy system, such as the one discussed in this thesis.

2.3.2 ADMM in a multi-energy community

To implement ADMM in a multi-energy community, we start from the objective function formulated previously in Equation 2.32. Since a multi-energy community can count with multiple energy carriers used by sector-coupling technologies, this results in multiple energy balance constraints, one for each energy carrier $v = v_1, \dots, v_f \in \mathcal{V}$. Each balance

constraint is associated with a dual variable $\lambda^v \in \mathbb{R}$ which indicates the marginal cost of that energy carrier at that timestep t . This formulation is shown in Equation 2.51, where $x_{\text{prod}}^v \in \mathbb{R}$ and $x_{\text{cons}}^v \in \mathbb{R}$ refer to the total energy produced and consumed by the energy system, corresponding to energy carrier v .

$$\begin{aligned} & \text{minimize} && \sum_{v \in \mathcal{V}} \sum_{t \in \mathcal{T}} (p_{\text{imp}}^v(t)x_{\text{imp}}^v(t) - p_{\text{exp}}^v(t)x_{\text{exp}}^v(t)) \\ & \text{subject to} && x_{\text{prod}}^v(t) = x_{\text{cons}}^v(t), \quad : \lambda^v(t), \quad \forall t, \quad \forall v \end{aligned} \quad (2.51)$$

Defining the cost function shown in Equation 2.51 as J_{op} , the augmented Lagrangian required for ADMM can be formulated as shown in Equation 2.52. Note that for the sake of conciseness, the notation from this equation onwards changed from a scalar to a vectorial representation of the variables, where $\mathbf{x}_{\text{prod}}^v \in \mathbb{R}^{t_{\text{tot}}}$ and $\mathbf{x}_{\text{cons}}^v \in \mathbb{R}^{t_{\text{tot}}}$ now represent the time vectors of energy production and consumption, $\boldsymbol{\lambda}^v \in \mathbb{R}^{t_{\text{tot}}}$ represents the dual variable vector corresponding to the energy balance constraint of energy carrier v , and where t_{tot} is the total number of timesteps considered in the time set $\mathcal{T} = \{1, \dots, t_{\text{tot}}\}$.

$$\mathcal{L}_\rho = J_{\text{op}} + \sum_{v \in \mathcal{V}} \left((\boldsymbol{\lambda}^v)^T (\mathbf{x}_{\text{cons}}^v - \mathbf{x}_{\text{prod}}^v) + \frac{\rho^v}{2} \|\mathbf{x}_{\text{cons}}^v - \mathbf{x}_{\text{prod}}^v\|_2^2 \right) \quad (2.52)$$

This expression can then be expressed in terms of the different agents variables. Where $\mathbf{x}_{\text{cons}}^v = \sum_{i=1}^N \mathbf{x}_{\text{cons},i}^v$, $\mathbf{x}_{\text{prod}}^v = \sum_{i=1}^N \mathbf{x}_{\text{prod},i}^v$. The augmented Lagrangian term over which each agent i optimises their prosumption is given in Equation 2.53.

$$\begin{aligned} \mathcal{L}_{\rho,i} = J_{\text{op},i} + \sum_{v \in \mathcal{V}} & ((\boldsymbol{\lambda}^{v,k})^T (\mathbf{x}_{\text{cons},i}^v - \mathbf{x}_{\text{prod},i}^v)) + \\ & \sum_{v \in \mathcal{V}} \left(\frac{\rho^v}{2} \left\| N \bar{\mathbf{x}}^{v,k} - (\mathbf{x}_{\text{cons},i}^{v,k} - \mathbf{x}_{\text{prod},i}^{v,k}) + \mathbf{x}_{\text{cons},i}^v - \mathbf{x}_{\text{prod},i}^v \right\|_2^2 \right) \end{aligned} \quad (2.53)$$

In order to further condense the notation, the consumption and production of each energy carrier v for each agent i can be expressed as the net value: $\mathbf{x}_i^v = \mathbf{x}_{\text{cons},i}^v - \mathbf{x}_{\text{prod},i}^v$.

$$\mathcal{L}_{\rho,i} = J_{\text{op},i} + \sum_{v \in \mathcal{V}} (\boldsymbol{\lambda}^{v,k})^T \mathbf{x}_i^v + \sum_{v \in \mathcal{V}} \frac{\rho^v}{2} \left\| N \bar{\mathbf{x}}^{v,k} - \mathbf{x}_i^{v,k} + \mathbf{x}_i^v \right\|_2^2 \quad (2.54)$$

This results in the following ADMM algorithm:

$$\mathbf{x}_1^{v_1,k+1}, \dots, \mathbf{x}_1^{v_f,k+1} := \underset{\mathbf{x}_1^{v_1}, \dots, \mathbf{x}_1^{v_f}}{\operatorname{argmin}} \mathcal{L}_{\rho,1} \quad (2.55)$$

⋮

$$\mathbf{x}_N^{v_1,k+1}, \dots, \mathbf{x}_N^{v_f,k+1} := \underset{\mathbf{x}_N^{v_1}, \dots, \mathbf{x}_N^{v_f}}{\operatorname{argmin}} \mathcal{L}_{\rho,N} \quad (2.56)$$

$$\boldsymbol{\lambda}^{v,k+1} := \boldsymbol{\lambda}^{v,k} + \rho^v \sum_{i=1}^N \mathbf{x}_i^{v,k+1} \quad \forall v \quad (2.57)$$

A flowchart of the ADMM algorithm applied for a multi-agent, multi-energy system is outlined in Figure 2.8. Furthermore, the complete formulation of the distributed optimisation problem, with the optimisation problem solved by each energy agent and the coordinator update, applied to the energy system shown in Figure 2.2, can be found in section A.2.

In a real setting, however, each of optimisation problem would be solved independently by each prosumer agent, and their planned dispatch would be shared with a central coordinator, who would then separately update the value of the dual variables, primal residuals, and dual residuals and broadcast them with the prosumers in the system. A visualisation of the calculations carried out by each agent i over iteration k , and the information shared from each energy agent to the central coordinator, and from the central coordinator to each agent is shown in Figure 2.9.

2.4 Economic assessment

To have a comprehensive assessment of the economic impacts of energy technologies and measures in an energy community, this section outlines the methodology used to allocate the operational cost savings contributions fairly and to prioritise capital investments.

2.4.1 Operational cost savings

In a multi-energy system, there are multiple ways of lowering the operational costs to meet its energy demand, such as adding new technologies in the system, or taking energy measures. For instance, adding a battery system provides the flexibility of displacing the electricity consumption from peak electricity prices to instances of lower electricity prices. Another example is adding a PV system, which allows the system to produce its own electricity, reducing the electricity imports from the grid. Alternatively, lower operational costs may also be reached by taking a measure in the system, for example, the temperature set-point in a household can be lowered, which would reduce its heating demand. An energy community may have multiple alternatives to reduce their operational

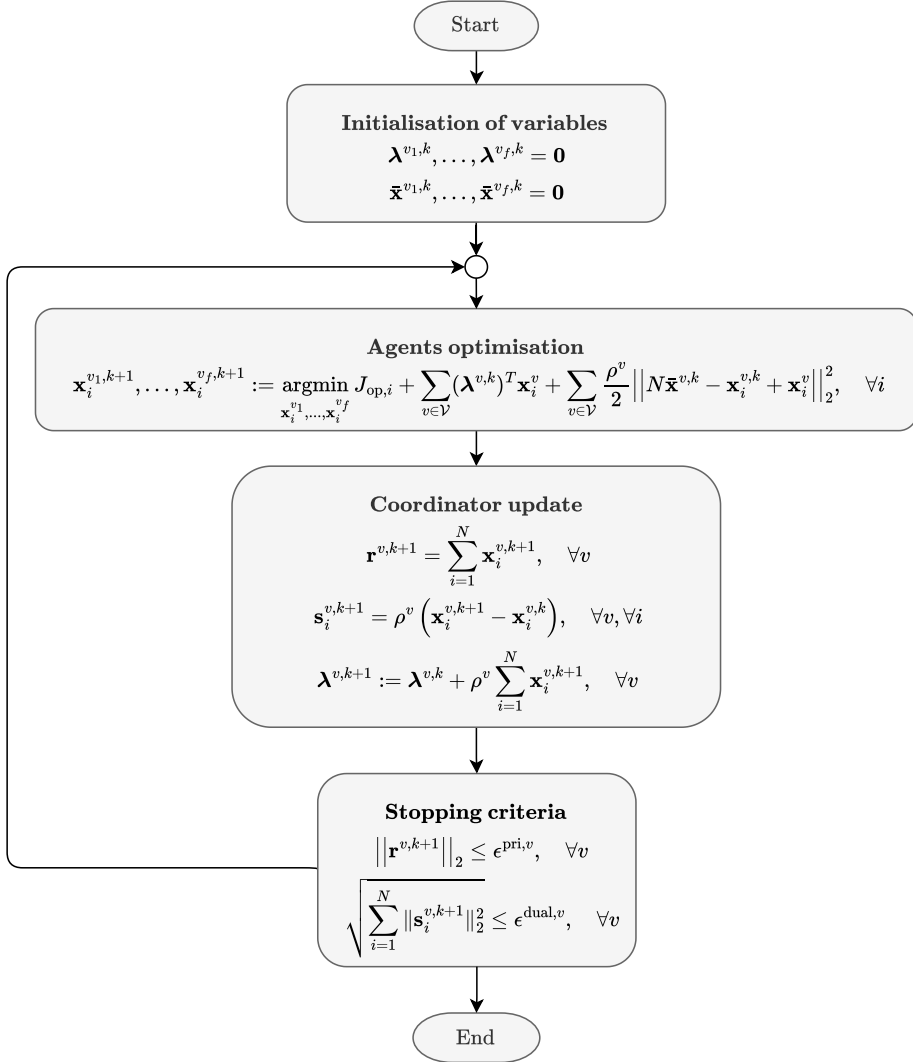


Figure 2.8: Flowchart of the Exchange ADMM algorithm applied to a multi-agent, multi-energy community.

costs, which raises the question of how to quantify the cost savings that different *energy players*² may contribute in an energy system.

Marginal contribution

A simple approach to quantify the benefit of adding a player to a system is to calculate its *marginal contribution*. The marginal contribution, ξ , that a player s provides to an existing *coalition*, \mathcal{S} , of energy players, where $s \notin \mathcal{S}$ is defined as the difference between the value of the coalition including s and the value of the coalition without this player. This calculation is shown in Equation 2.58.

$$\xi(s) = v(\mathcal{S} \cup \{s\}) - v(\mathcal{S}) \quad (2.58)$$

²*Energy players* in this context refers to either energy technologies or energy measures that may contribute to a change in the operational costs of an energy system to meet the energy demands.

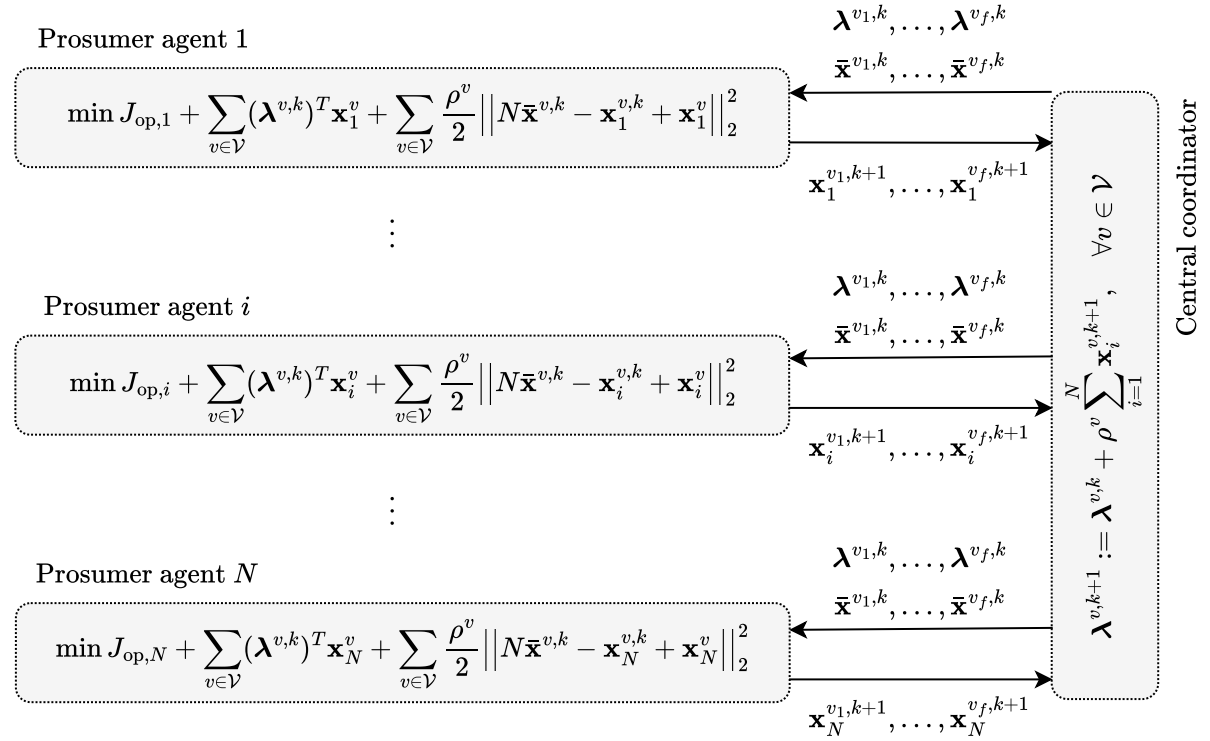


Figure 2.9: Schematic representation of the computation carried out by each prosumer agent $i = 1, \dots, N$ and the central coordinator, indicating the information exchanged between the agents over each iteration k under the Exchange ADMM algorithm.

Where v is the function that defines the *coalition value*. In this work, the coalition value is defined as the total operational cost saved by the coalition compared to a baseline. For instance, defining $J_{\text{op}}^*(\emptyset)$ as the optimal operational cost of an energy system with no energy players (the *baseline scenario*), the value of coalition \mathcal{S} will be given as shown in Equation 2.59, where $J_{\text{op}}^*(\mathcal{S})$ is the total optimal operational cost of an energy system with all energy players $\{s\} \in \mathcal{S}$.

$$v(\mathcal{S}) = J_{\text{op}}^*(\emptyset) - J_{\text{op}}^*(\mathcal{S}) \quad (2.59)$$

However, although the marginal contribution approach can capture part of the value provided by a player, it fails to attribute the fair contributions of each player by not taking into the interactions or synergies among players. It does not capture the different ways in which a coalition can be formed, and as such, can give a result which may over- or under-estimate the value that a player brings to a coalition. To address the shortcoming of this approach, a quantification method based on the *Shapley value* is used instead to assess the *fair* contribution of each energy player. This approach is explained and discussed in the following paragraphs.

Fair Operational Cost Savings (FOCS) value

The Shapley value, a concept originating from cooperative game theory, provides a solution to the problem of fairly allocating the surplus generated by a collection of agents in

a coalition. In term of an energy system, it can solve the problem of fairly distributing the value created by multiple energy players in a system, particularly when their contributions might interact in complex ways. Unlike the marginal contribution approach, the Shapley value considers every possible coalition arrangement to capture the full spectrum of contributions a player might make within different groupings. This is particularly useful in multi-energy systems where the interactions between energy players can give rise to synergies and influence each other's value.

The Shapley value, $\phi(s)$, of a player s is calculated as an average of all possible marginal contributions that s makes across the different coalition arrangements. For each possible coalition \mathcal{S} , which does not contain s , the marginal contribution $\xi(s)$ is calculated, and the Shapley value is determined as the weighted sum of these contributions across all coalitions, as shown in Equation 2.60.

$$\phi(s) = \sum_{\mathcal{S} \subseteq N \setminus \{s\}} \frac{|\mathcal{S}|!(|N| - |\mathcal{S}| - 1)!}{|N|!} (v(\mathcal{S} \cup \{s\}) - v(\mathcal{S})) \quad (2.60)$$

where N is the set of all players, $|\mathcal{S}|$ is the size of coalition \mathcal{S} , and $v(\mathcal{S})$ represents the coalition value, defined previously in Equation 2.59. The weighting factor ensures that each coalition arrangement is considered proportionally, resulting in a fair allocation of the total value across players based on their individual and synergistic contributions.

Therefore, when the value of the coalition is calculated as indicated in Equation 2.59, the Shapley value becomes the *Fair Operational Cost Savings (FOCS)* value of an energy player, which provides a fair estimation of the economic surplus that each player brings to the energy coalition, compared to a baseline scenario. As such, the Shapley value, and variants, is often proposed as an alternative as a revenue sharing method in energy communities [27] [28]. This is particularly important in a distributed energy system, where different energy agents can be incentivised to invest or behave in a way as to reduce the overall energy system costs of the community. To avoid ambiguity, in this work, we refer to the Shapley values that use the operational cost reduction as the coalition value as the FOCS values, since it is a more accurate naming that already reflects how a coalition value is calculated, and they are represented by the symbol $\phi^{\text{FOCS}}(s)$.

2.4.2 Investment prioritisation

A relevant subject for an energy community is the prioritisation of investments into energy technologies. Different metrics can be used to evaluate the economic feasibility of such investments from the investor's point of view. Some of the most used metrics are: the Net Present Value (NPV), which calculates the difference between the discounted incoming and outgoing cash flows over a period of time T ; the Return on Investment (ROI), which measures the total return obtained in relation to the investment; the Internal Rate of Return (IRR), which calculates the growth an investment is expected to generate; the payback period, which calculates the amount of time required to recover the initial costs; among others.

The NPV is a well-known metric which is often used to analyse investments, since it considers the time preference of investors to receive payments earlier rather than later.

The formula, shown in Equation 2.61, considers the incoming cash flows, C_{in} , i.e. revenues, the outgoing cash flows, C_{out} , i.e. expenses, and the discount rate, r . The selection of the discount rate can have a significant impact on the resulting profitability of the investment. Typical values used for the discount factor are the *risk-adjusted discount-rate*, which states that the expected discount rate should capture the risk of the investment, and the *Weighted Average Cost of Capital (WACC)*, which is the cost of accessing capital for an investor, differentiating between equity and debt capital.

$$\text{NPV} = \sum_{t=0}^T \frac{C_{\text{in}}(t) - C_{\text{out}}(t)}{(1+r)^t} \quad (2.61)$$

The investment prioritisation in this work is assessed with the NPV of different energy technologies. The revenues for each investment are assumed to be proportional to the *fair contribution* that an energy player brings to the energy community, which is calculated with the approach discussed previously in subsection 2.4.1. The expenses taken into account are the initial capital investment, and the operational and maintenance costs associated with the technology. With the calculation of the NPV of different energy investment options and their comparison, the investment for an energy community, from the economic perspective, can be prioritised.

Chapter 3

Case study

This chapter presents the case study used to implement the methodology developed in the previous chapter. Section 3.1 presents a high level description of the energy community modelled. Then, section 3.2 presents all the required inputs to model the energy system: boundary conditions, energy demands, and techno-economic parameters. Lastly, section 3.3 presents a description of the main scenarios modelled, which will then provide a point of comparison for the results discussed in the next chapter.

3.1 Energy community

The energy community modelled in this work is based on the *nanoverbund* pilot project [6] which sets out to demonstrate the potential of shared energy resources in a set of residential households. The pilot project consists of a set of three thermally connected terraced houses located in the city of Basel, Switzerland. Energy-related data is constantly being collected from these three households which makes it a suitable case study. However, the set of technologies modelled in the energy system in this work are different from the ones of the pilot project. The technologies, energy demands, external connections, and energy flows modelled for the multi-energy community in this work were previously illustrated in Figure 2.2.

3.2 Inputs

There are three sets of inputs that are relevant to model the energy community: (a) boundary conditions, (b) energy demands, (c) techno-economic parameters. Each of these three inputs are discussed in the following subsections.

3.2.1 Boundary Conditions

The boundary conditions required for the case study are ambient temperature, solar irradiance, electricity prices, and hydrogen prices. The time horizon used throughout

this work is of one year. The boundary conditions correspond to data gathered for the year of 2023. The time resolution is of one hour, therefore, all yearly data consists of 8'760 time steps. The inputs for ambient temperature and solar irradiance are taken from historical data for 2023 collected in the city of Basel [29] and the plots are shown in Figure 3.1 and Figure 3.2, respectively.

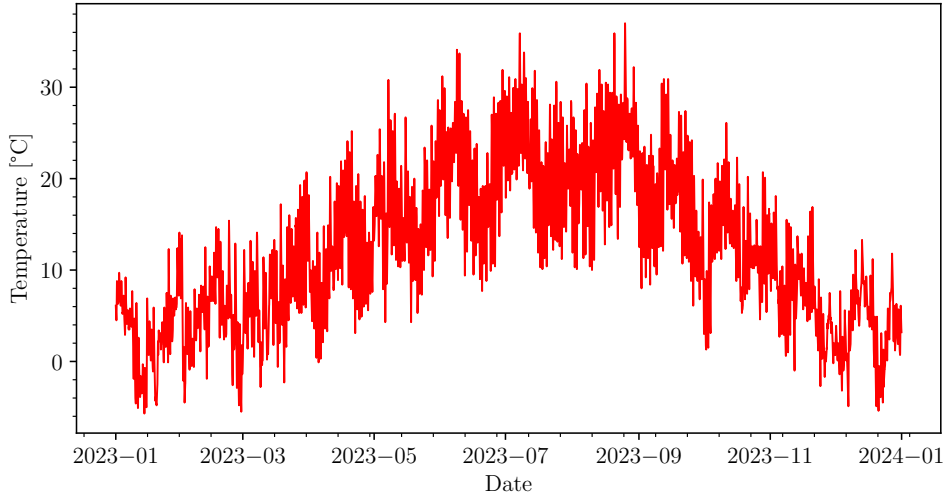


Figure 3.1: Ambient temperature in the city of Basel over the modelled period (year 2023).

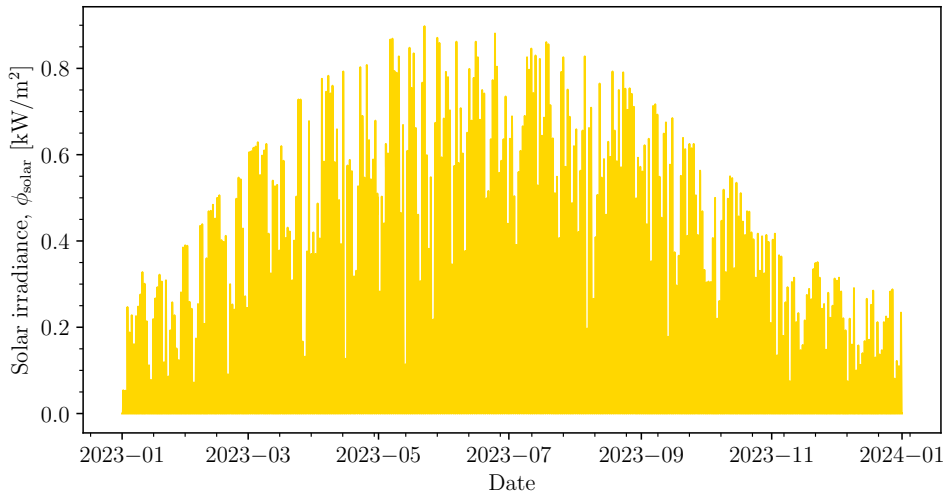


Figure 3.2: Solar irradiance in the city of Basel over the modelled period (year 2023).

There are two sets of electricity prices relevant to the energy system modelled. One is the electricity import price, which in this case is the electricity tariff from IWB for the year of 2023 [30]. This work uses the double tariff which applies to households with a fuse size up to 100 A, an annual consumption of up to 13 MWh (*IWB Strom small*) and includes all network tariffs, cantonal and federal taxes. The resulting electricity tariffs for the low and high tariff periods are $p_{\text{imp}}^{\text{E,low}} = 0.2748 \text{ CHF/kWh}$ and $p_{\text{imp}}^{\text{E,high}} = 0.3665 \text{ CHF/kWh}$, respectively. The high tariff period applies in the system from 6 am to 8 pm from Monday to Friday, the low tariff applies the remaining of the time. The electricity

export prices, which are used to remunerate the surplus electricity of the energy system, are given by the prices from the spot ("day ahead") market in Switzerland for the year 2023 [31]. Figure 3.3 shows both electricity prices over the modelled period.

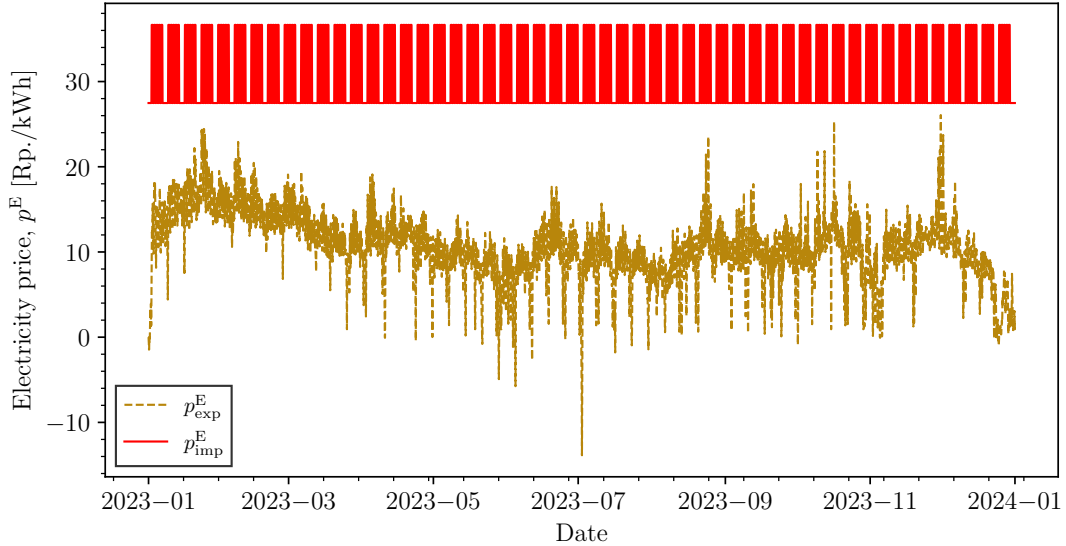


Figure 3.3: Import and export electricity prices in the city of Basel over the modelled period (year 2023).

Since there is no standard hydrogen market price, a set of different hydrogen price scenarios is used. Each of these hydrogen prices are assumed to remain constant throughout the modelled period. The name and value of these three price scenarios are shown in Table 3.1.

Table 3.1: Values of hydrogen prices for different scenarios.

| Price scenario | Current [32] | High forecast [33] | Low forecast [33] |
|---------------------------|--------------|--------------------|-------------------|
| Hydrogen price, p^{H_2} | 10 CHF/kg | 6 CHF/kg | 2 CHF/kg |

3.2.2 Energy community demands

There are two energy demands taken into account for the energy community: electricity demand and heat demand. These demands are determined with an hourly resolution for the modelled period of one year. Each of these demands is modelled differently, the electricity demand follows a fixed hourly profile, while the heat demand is modelled as a flexible demand which is subject to a set of temperature constraints and temperature responses. The modelling of each demand is described in the following paragraphs.

Electricity demand

As previously mentioned, the electricity demand for each household is modelled with a fixed consumption profile. The electricity consumption profiles takes into account two

different demands: lighting and electric appliances [34]. These profiles estimate the hourly electricity demand for each application as a percentage of the yearly electricity demand for the respective application. The demand profiles differentiate between weekdays and weekends, and between the four seasons in the year. To scale the total electricity demand by each household, the data collected from the *nanoverbund* pilot case was used. Each of the three households in the *nanoverbund* pilot has on average an electricity end-demand of 5'000 kWh/year [35]. From this, 90% (4'500 kWh) is assumed to be used for electric appliances and 10% (500 kWh) to cover the lighting consumption in each household. Figure 3.4 shows examples of demand profiles as a percentage of the yearly electricity demand for a weekday during summer and a weekend during winter. In this figures the different consumption profile can be compared.

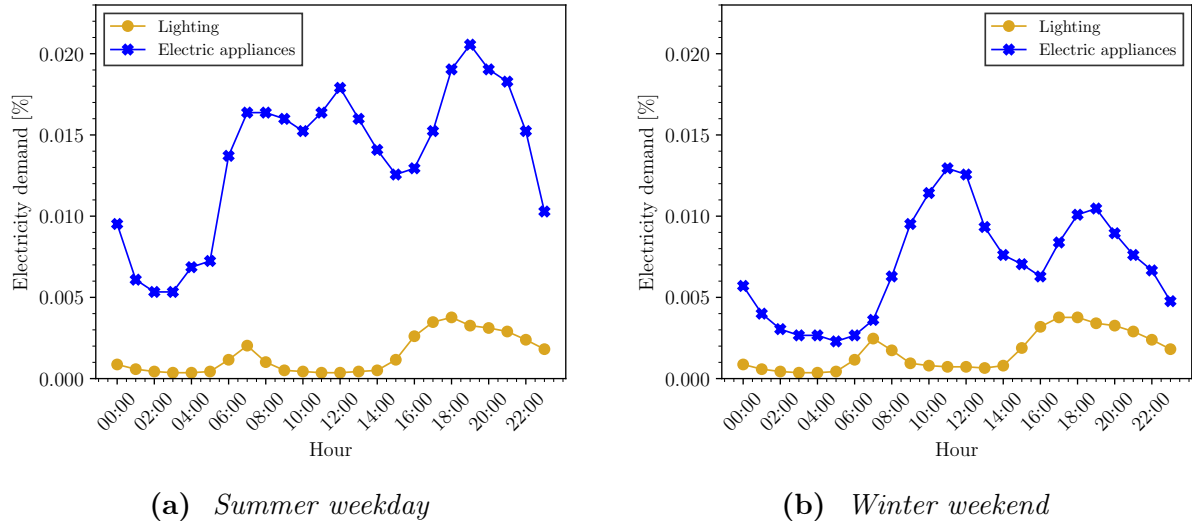


Figure 3.4: Electricity demand profiles for lighting and electric appliances as a percentage of total yearly electricity demand for a (a) summer weekday and (b) winter weekend.

Heat demand

The heat demand, in contrast to the electricity demand, is a flexible demand which arises from setting constraints on the desired indoor temperature range and modelling the change in indoor temperature as a function of the input heat from the heat network, the solar irradiation and the ambient temperature (as seen in subsection 2.1.2).

There are two different scenarios modelled for the allowed indoor temperature. The values for these scenarios are shown in Table 3.2. The flexible temperature range values are selected based on the european standard for the design and assessment of energy performance of buildings [36]. The inflexible demand aims to maintain an almost fixed temperature set-point that is selected in order to maintain the same average indoor temperature throughout the modelled period, in order to make the results from both scenarios comparable.

The thermal inertia parameters for the household consist of the thermal resistivity and the thermal capacitance of the buildings. The thermal capacitance was obtained from

Table 3.2: Temperature ranges used for different scenarios.

| Scenario | Flexible demand [36] | Inflexible demand |
|-------------------------------|---|---|
| Temperature range, ΔT | $5^\circ \text{C} (20 - 25^\circ \text{C})$ | $0.1^\circ \text{C} (20.3 - 20.4^\circ \text{C})$ |

previous calculations based on the building's dimensions, internal and external surface areas, and their respective specific heats [35]. These resulted in a total heat capacitance for each household of $14.71 \text{ kWh}/^\circ\text{C}$. The solar irradiance surface area for each building was obtained from their dimensions, and is assumed to have a constant area of approximately 40 m^2 perpendicular to the irradiance direction. The absorptivity of the household's irradiated area and the thermal resistance of the building were fine-tuned such that the total heat demand and maximum temperature during the summer months that result as outputs from the simulation match the values from the data collected from *nanoverbund*. The total heat demand for each household is on average approximately $11.5 \text{ MWh}/\text{year}$ and the maximum temperature reached throughout the modelled period is of 28.6°C . This results in a thermal resistance of $5.6 [\text{C}/\text{kW}]$ and an absorptivity of $0.04 [-]$. The values of these parameters are summarised in Table 3.3

Table 3.3: Parameters to model the heat demand of households.

| Parameter | Value | Units |
|--|-------|----------------------------|
| Thermal capacitance of building, C_c | 14.71 | kWh/K |
| Thermal resistance of building, R_c | 5.6 | $^\circ\text{C}/\text{kW}$ |
| Area of solar irradiance, $A_{\text{irr},c}$ | 40 | m^2 |
| Absorptivity, α_c | 0.04 | - |

3.2.3 Techno-economic parameters

The technical parameters used for the technologies modelled in the system are summarised in Table B.2, in Appendix B. For the hydrogen technologies, this table indicates the nominal efficiency, which is the efficiency at which these components operate when they are at their nominal capacity. However, as mentioned in Chapter 2, these technologies are modelled with a PWA approximation of their output curves. The *real* curves are obtained from operational data of a fuel cell [37] and an electrolyser [38] and are then approximated with quadratic functions. The quadratic curves approximating the normalised output power, p_{out} , as a function of the normalised input power, p_{in} , for an electrolyser and a fuel cell are shown in Equation 3.1 and Equation 3.2, respectively. These curves are then interpolated by the desired number of breakpoints to generate the PWA approximation. The investment and O&M costs are summarised in Table B.1, which is also found in Appendix B.

$$p_{\text{out},\text{EL}} = -0.1357 p_{\text{in},\text{EL}}^2 + 0.7171 p_{\text{in},\text{EL}} - 0.0088 \quad (3.1)$$

$$p_{\text{out},\text{FC}} = -0.2377 p_{\text{in},\text{FC}}^2 + 0.6744 p_{\text{in},\text{FC}} - 0.0095 \quad (3.2)$$

3.3 Scenarios

To gain insights into the operation and value of different technologies, various technology scenarios are considered. Each scenario includes a distinct set of energy technologies within the multi-energy community. These scenarios are:

1. *Baseline scenario*: This scenario includes only a heat pump.
2. *Hydrogen system scenario*: This scenario adds the complete hydrogen system (which consists of a PEM electrolyser, a PEM fuel cell, hydrogen storage, a hydrogen connection, and WHR for both electrochemical devices) to the baseline scenario's energy system.
3. *Complete system scenario*: This scenario considers the complete energy system illustrated in Figure 2.2, adding a TES, BES, and PV to the hydrogen system scenario's energy system.

Within each of these technology scenarios, various sub-scenarios are also considered. A schematic representation of the main scenarios examined in this work is found in Figure 3.5.

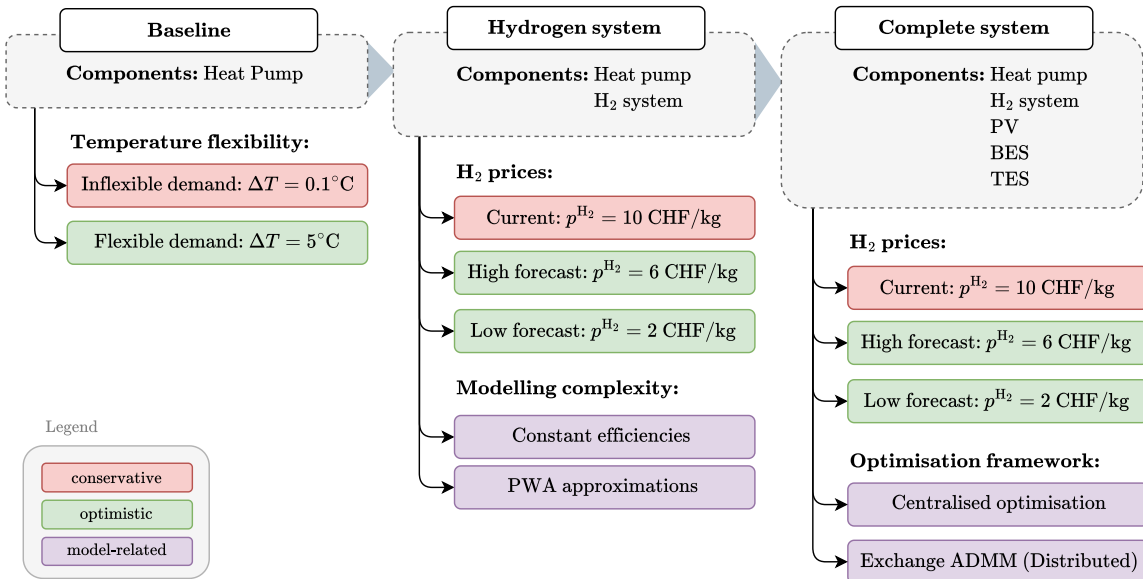


Figure 3.5: Schematic representation of the three energy system scenarios modelled, and the corresponding sub-scenarios that were modelled for each configuration.

Chapter 4

Results

section 4.1 in this chapter begins with the results related to the optimal operation of an energy system under various scenarios, delving into the optimal operation of hydrogen technologies and their relation to energy values. Then section 4.2 presents the convergence results obtained using distributed optimisation to reach the optimal solution for the multi-energy community. Finally, section 4.3 presents the results from the economic assessment of the energy technologies as part of the energy system.

4.1 Optimal operation and energy values

To analyse and interpret the optimisation problem results, three energy system scenarios are considered, each incorporating an increasing number of energy technologies. The energy system configurations for these scenarios were previously shown, and are depicted in Figure 3.5. This section begins by presenting the results for the *baseline scenario*, followed by those for the *hydrogen system scenario*, and concludes with the results for the *complete system scenario*, which includes all the energy technologies.

4.1.1 Baseline scenario

As Figure 3.5 shows, in the *baseline scenario* the only energy technology in the system is a heat pump without energy storage or generation technology. In this scenario, the only source of demand flexibility is the building's thermal inertia. Additionally, the community's electricity demand can only be met by electricity imports and the heat demand can only be covered by the heat pump.

The resulting cumulative energy demands of the community in the *baseline scenario* are shown in Figure 4.1. Both demand requirements are satisfied by importing electricity from the grid, subject to electricity import prices. This scenario results in annual electricity imports of 24.2 MWh, out of which 15 MWh (62%) are used to supply electricity end-demand and the remaining 9.2 MWh (38%) are consumed by the heat pump to supply space heating demand. At the dual-tariff electricity prices mentioned in Chapter 3, this scenario results in yearly operating costs of 7'417 CHF, all spent to import electricity.

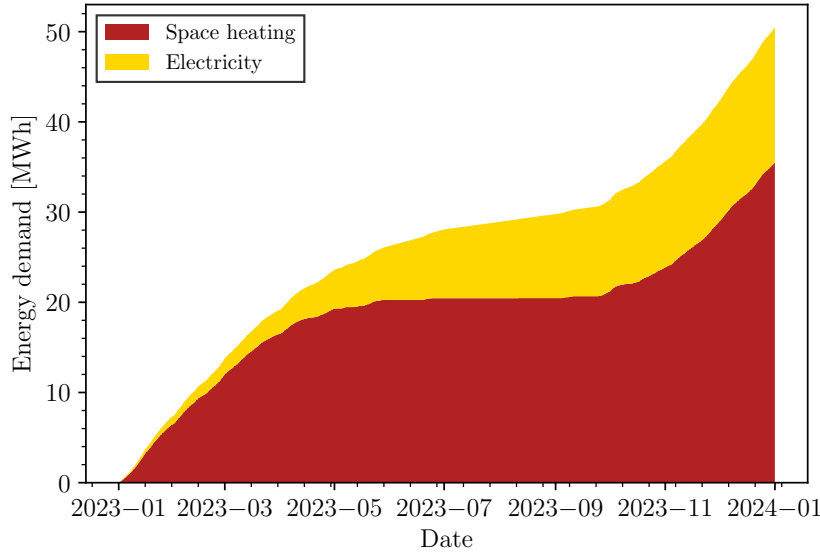


Figure 4.1: Cumulative space heating and electricity demands of energy community over one year in the baseline scenario.

As previously shown in Figure 2.4, the only heat transfers are the heat consumed from the thermal network Q_{cons} , the solar heat absorbed Q_{solar} , and the exchanged heat with the ambient Q_{amb} . Therefore, the heat demand is inflexible to the outdoor temperature when the ambient temperature is low. Additionally, the direct coupling of power-to-heat in the system, with no energy storage alternative (besides the thermal inertia of the building) leads to a high correlation between the electricity import prices and the derived heat value in the community. These characteristics highlight two main properties of the energy system in this scenario: **(a) low demand temporal flexibility** and **(b) high correlation between the heat value and electricity prices**. Both of these characteristics are further discussed in the following paragraphs.

Low demand temporal flexibility

In an energy system without electricity or heat storage, the boundary conditions directly determine the energy imports to satisfy the energy demands with little to no temporal flexibility. In the *baseline scenario*, the electricity imports are directly coupled to the electricity demand, which follows an inflexible demand profile, as mentioned in Chapter 3. Similarly, the heat demanded from the decentralised DHN is inflexible to the ambient temperature and the heat gained from solar radiation. The demand flexibility in the system stems from the allowable temperature range, ΔT , of the buildings with thermal inertia parametrised as discussed in subsection 2.1.2.

Figure 4.2 visualises the impact of ΔT on heat pump's operational flexibility. As seen in the plot, the standard temperature range of 5°C allows the heat pump to operate over the full range of partial loads at all ambient temperatures. This allows the system to benefit from the electricity price differences between low-tariff and high-tariff periods, thus resulting in lower operational costs. Additionally, the system's operation under a narrow

temperature range of 0.1°C is modelled to display the effect of tightening this constraint. The range is $[T_c^{\min} = 20.3^\circ\text{C}, T_c^{\max} = 20.4^\circ\text{C}]$, which is selected to maintain the same average consumer temperature as the one obtained with the standard temperature range of $[T_c^{\min} = 20^\circ\text{C}, T_c^{\max} = 25^\circ\text{C}]$. As shown in Figure 4.2, now the heat pump operates under narrower upper and lower limits at different ambient temperatures. The upper power limit is determined by the fact that a higher heat pump power would result in an indoor temperature larger than T_c^{\max} . Conversely, the lower power limit is determined by the fact that the indoor temperature would otherwise fall below T_c^{\min} , thus not maintained within the allowable temperature range. This shows how the advantage of the thermal inertia of the building is limited when the allowable temperature range is tightened.

A comparison of the main results obtained between the scenario of $\Delta T = 5^\circ\text{C}$ and $\Delta T = 0.1^\circ\text{C}$ is shown in Table 4.1. As can be seen in the table, the total electricity imports for space heating increase by 0.7% for the inflexible scenario. At the same time, the electricity imports for space heating only account for 38% of the total imports for the energy system. Since the electricity end-demand remains the same, this results in total electricity imports increasing by 0.2%. Despite the slight increase in total electricity imports, operating costs rise by 2.5%. This is because, in the inflexible scenario, electricity consumption during high-tariff periods cannot be shifted to low-tariff periods due to the narrow temperature range.

Table 4.1: Comparison of main results for the baseline scenario between an allowable temperature range of 5°C and 0.1°C . The percentages indicate their relative difference.

| Metric | Baseline scenario | | Units |
|--|------------------------------|--------------------------------|---------|
| | $\Delta T = 5^\circ\text{C}$ | $\Delta T = 0.1^\circ\text{C}$ | |
| total operating cost, J_{op} | 7'417 | 7'604 (+2.5%) | CHF/y |
| <i>Electricity results</i> | | | |
| electricity end-demand | 15.0 | 15.0 (+0.0%) | kWh/y |
| space heating demand | 9.22 | 9.28 (+0.7%) | kWh/y |
| total electricity imports | 24.22 | 24.28 (+0.2%) | kWh/y |
| <i>Dual variables</i> | | | |
| avg electricity value, $\bar{\lambda}^E$ | 31.8 | 31.8 (+0.0%) | Rp./kWh |
| avg heat value, $\bar{\lambda}^H$ | 7.87 | 7.92 (+0.6%) | Rp./kWh |

High correlation between heat value and electricity prices

As previously mentioned, in the baseline scenario the heat demanded by the thermal network and the electricity imports are directly coupled. This means that when the heat demand is positive, i.e. $Q_{\text{cons},\text{total}}(t) > 0$, at timestep t , a proportional amount of electricity is imported, i.e. $P_{\text{imp}}(t) \propto Q_{\text{cons},\text{total}}(t)$. In addition, as previously mentioned, the system has low heat demand flexibility in relation to the ambient temperature. This results in a heat value strongly correlated to the price of electricity imported from the grid.

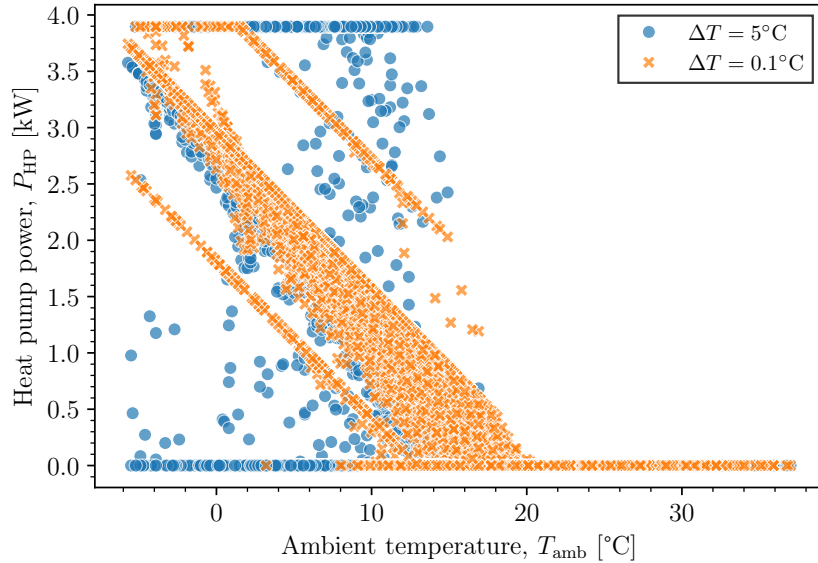


Figure 4.2: Scatter plot of heat pump power consumption at different ambient temperatures for different allowable indoor temperature ranges.

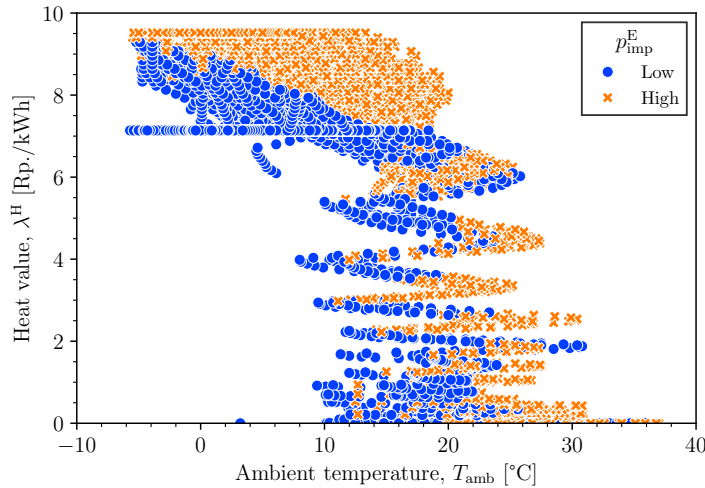
Figure 4.3a displays the heat value in the system over the ambient temperature, distinguishing between periods of low and high electricity import tariffs. The maximum heat value over the modelled period is of $\lambda^{H,\max} = 9.52 \text{ Rp./kWh}$, which is achieved at the high electricity tariff of $p_{\text{imp}}^{E,\text{high}} = 36.65 \text{ Rp./kWh}$. This is related to the COP of the heat pump of 3.85, i.e. $\lambda^{H,\max} = p_{\text{imp}}^{E,\text{high}}/\text{COP}$.

To understand the relation to the minimum heat value, Figure 4.3b filters out non-heating periods and focuses on periods where there is a heat demand in the system, i.e. $Q_{\text{cons},\text{total}} > 0$. Here, the minimum heat value at which the system produces heat can be observed. In this scenario, the minimum heat production cost is reached during periods of low-tariff, with a cost equal to the low electricity tariff prices scaled by the COP of the heat pump. Therefore whenever the heat value in the system is lower than this minimum cost of heat production $\lambda^{H,\min} = p_{\text{imp}}^{E,\text{low}}/\text{COP} = 7.14 \text{ Rp./kWh}$, the system decides not to produce heat, since the marginal benefit of the cost function would be lower than the increase in the cost function by the marginal cost of heat production. However, adding alternative energy technologies can provide further operational flexibility. The next section explores this potential from hydrogen technologies with WHR.

4.1.2 Hydrogen system scenario

The addition of hydrogen technologies in the energy system has the potential to provide it with additional sources of flexibility. Specifically, the following capabilities from each component can be leveraged by the energy system:

- **PEM electrolyser** enables power-to-H₂ conversion, which can provide additional sources of revenue to the system by exporting H₂.
- **Hydrogen storage** gives an energy storage option to the system, providing additional flexibility.



(a) Unfiltered, includes all time periods.

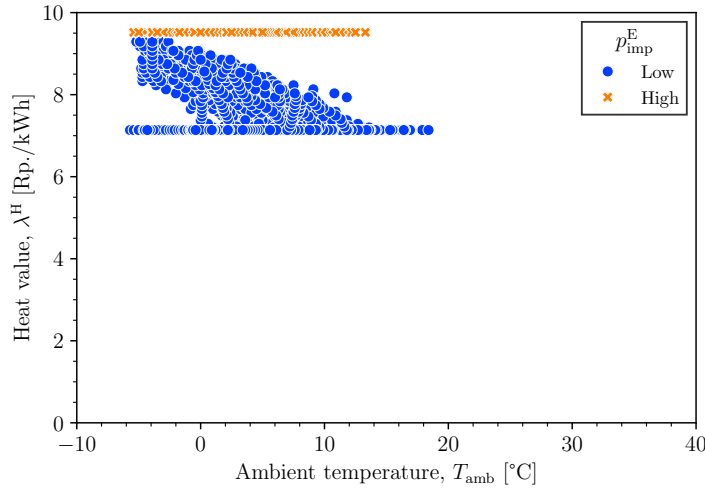
(b) Filtered, includes only periods when $Q_{\text{cons},\text{total}}(t) > 0$.

Figure 4.3: Heat value over ambient temperature, indicating periods with low and high electricity import tariffs. Subfigure (a) displays all periods, while subfigure (b) filters out periods with no heat demand.

- **PEM fuel cell** enables H₂-to-power conversion, which allows exporting electricity at a revenue and/or supplying the community's electricity demand.
- **WHR system** allows supplying the community's space heating demand through the operation of either the electrolyser or the fuel cell, which can lead to reducing the reliance of the energy system on alternative heating solutions.

The utilisation of H₂ technologies, however, is subject to them being cost-optimal for the community. For this to be the case, the cost to supply the energy end-demands through H₂ technologies must be cheaper than the production cost of existing alternatives. The price of hydrogen, denoted as p^{H_2} , is a key factor in determining this outcome. To evaluate the impact of the hydrogen price in the utilisation of hydrogen technologies, the three hydrogen price scenarios mentioned in Table 3.1 are considered.

Figure 4.4 compares the share of total heat generation by each technology for the *baseline scenario* and the three *hydrogen scenarios*. As can be seen in the figure, there is no difference in terms of the heat production technology used between the scenario with no H_2 system and with the *current* hydrogen price of 10 CHF/kg. All of the heat generated in both of these scenarios comes from the heat pump. In fact, when the hydrogen price is 10 CHF/kg, all of the hydrogen technologies remain unused throughout the modelled period. This means that at this p^{H_2} , none of the energy conversion capabilities by the hydrogen system is cost-optimal.

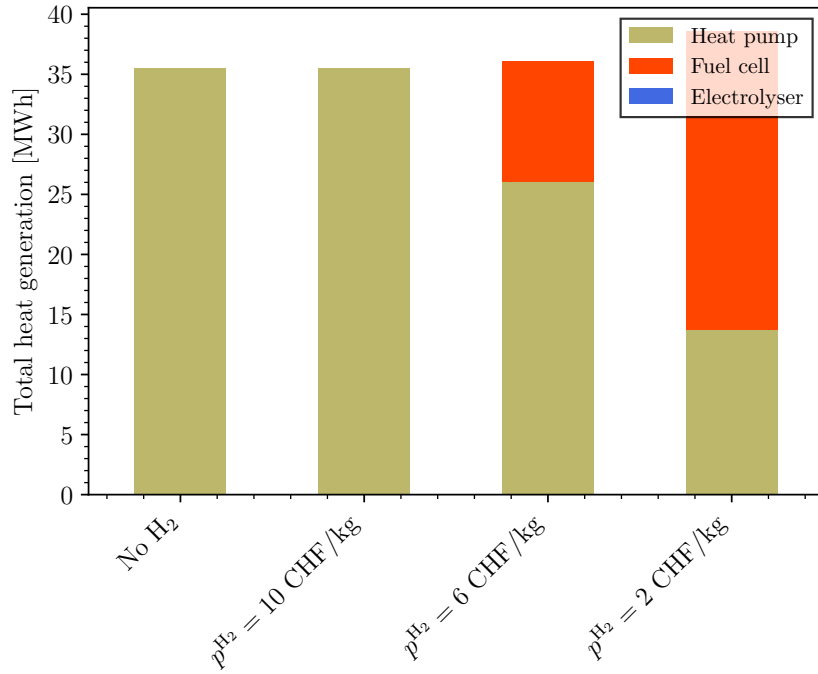


Figure 4.4: Comparison of total heat generation by technology for the baseline and hydrogen scenarios with different prices.

However, Figure 4.4 also shows that when hydrogen prices are reduced, part of the heat demanded is supplied by the fuel cell, as can be seen for the scenarios with a high ($p^{H_2} = 6 \text{ CHF/kg}$) and low price forecast ($p^{H_2} = 2 \text{ CHF/kg}$), where the heat supplied by the fuel cell covers 28% and 69% of the total energy demanded each scenario, respectively. This indicates that operating the fuel cell with WHR has a lower net cost than importing electricity to operate the heat pump to supply the heat demand during certain periods. The total operating cost of the energy system is decreased in both instances of lower hydrogen prices.

Since the fuel cell enables H_2 -to-power and H_2 -to-heat conversion, there are three reasons why operating the fuel cell may lead to lower operating costs for the system:

1. **reduced electricity imports:** the energy system can now use electricity generated by the fuel cell instead of importing electricity from the grid. This electricity can cover any electricity demand in the system.

2. **electricity exports:** in the case of surplus electricity in the system there will be net exports to the grid, which are remunerated as explained in Chapter 3, providing an additional revenue source to the system.
3. **alternative heat production:** since the heat from operating the fuel cell is recovered, this can reduce the consumption of heating alternatives, such as the heat pump, thus further reducing the electricity imported.

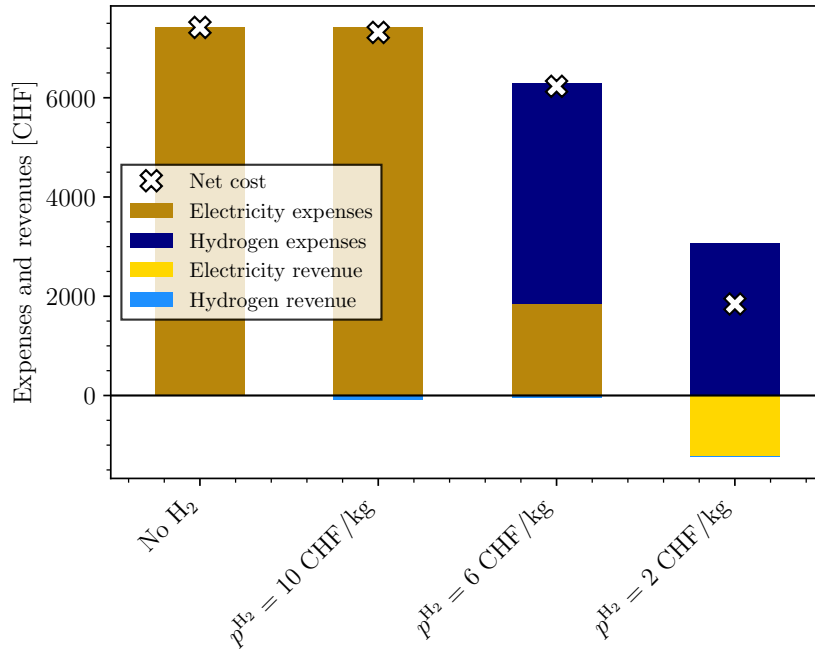


Figure 4.5: Comparison of expenses and revenues of the energy system for the baseline scenario and hydrogen scenarios with different hydrogen prices, indicating the net yearly operating costs.

Since there is an electricity price difference between imports and exports, the former being higher than the latter, as described in Chapter 3, the system is expected to first benefit from reducing the reliance on electricity imports and exporting electricity if there is a surplus. This can be observed in Figure 4.5, which breaks down the expenses and revenues for each scenario. As expected, the cost breakdown of the scenario with no H_2 import and the scenario with a $p^{H_2} = 10 \text{ CHF/kg}$ remains unchanged¹. All the results discussed in this section are summarised in Table 4.2.

In the high-price forecast scenario, a decrease in electricity imports of 73% is observed. At the same time, total electricity consumption is reduced by 15%. This is because the heating demand is partly covered by the WHR system from the fuel cell. As illustrated in Figure 4.4, around 28% of the total space heating demand from the energy community is covered by the excess heat of the fuel cell in this scenario. This reduces the reliance on the power-to-heat conversion by the heat pump, reducing total electricity consumption. Overall, in the high-price scenario, total operating costs are reduced by 16% compared

¹The hydrogen revenue of 100 CHF in the hydrogen scenario with current prices is a result from export of 10 kg of hydrogen, which is added in the formulation of the constraints of the problem as an initial and final value, as seen in section A.1.

Table 4.2: Comparison of the main results obtained for the baseline scenario and hydrogen scenarios with three different prices for hydrogen. The percentages indicate the relative difference to the baseline scenario.

| Metric | Baseline No H ₂ | Hydrogen scenarios | | | Units |
|--|-------------------------------|----------------------|---------------------------|--------------------------|--------------|
| | | Current 10 CHF/kg | High forecast 6 CHF/kg | Low forecast 2 CHF/kg | |
| <i>Cost breakdown</i> | | | | | |
| electricity expenses | 7'417 | 7'417 | 1'853 | 0 | CHF/y |
| electricity revenues | 0 | 0 | 0 | 1'218 | CHF/y |
| H ₂ expenses | 0 | 0 | 4'437 | 3'082 | CHF/y |
| H ₂ revenues | 0 | 100 | 60 | 20 | CHF/y |
| total operating cost, J_{op} | 7'417 | 7'317 (-1.3%) | 6'230 (-16.0%) | 1'844 (-75.1%) | CHF/y |
| <i>Consumer costs</i> | | | | | |
| electricity end-demand | 1'592 | 1'592 (-0.0%) | 1'440 (-9.5%) | 604 (-62.0%) | CHF/(cons·y) |
| space heating demand | 931 | 931 (-0.0%) | 835 (-10.3%) | 347 (-62.7%) | CHF/(cons·y) |
| <i>Electricity results</i> | | | | | |
| consumption | 24.2 | 24.2 | 21.8 | 18.6 | MWh/y |
| production | 0 | 5.0 | 15.0 | 27.2 | MWh/y |
| imports | 24.2 | 24.2 | 6.7 | 0 | MWh/y |
| exports | 0 | 0 | 0 | 8.7 | MWh/y |
| <i>Heating results</i> | | | | | |
| heat pump production | 35.5 | 35.5 | 26.1 | 13.7 | MWh/y |
| electrolyser production | 0 | 0 | 0 | 0 | MWh/y |
| fuel cell production | 0 | 0 | 10.1 | 24.9 | MWh/y |
| <i>Hydrogen results</i> | | | | | |
| consumption | 0 | 0 | 651 | 1'356 | kg/y |
| production | 0 | 0 | 0 | 0 | kg/y |
| imports | 0 | 0 | 740 | 1'541 | kg/y |
| exports | 0 | 10 | 10 | 10 | kg/y |
| <i>Dual variables</i> | | | | | |
| avg electricity value, $\bar{\lambda}^E$ | 31.30 | 31.30 (-0.0%) | 28.30 (-9.5%) | 12.09 (-61.4%) | Rp./kWh |
| avg heat value, $\bar{\lambda}^H$ | 7.87 | 7.87 (-0.0%) | 7.07 (-10.2%) | 2.86 (-63.7%) | Rp./kWh |

to the baseline scenario. From the consumer's perspective, the total costs to cover their electricity and space heating demand decrease by around 10% compared to the baseline scenario. In this scenario, however, the energy system is still a net importer of electricity.

As for the low forecast scenario, there are no electricity imports from the grid. Instead, 32% of the electricity generated by the fuel cell is exported. This is because at a purchase price of hydrogen of 2 CHF/kg, the conversion and export of electricity become profitable during high electricity export prices. This additional source of revenue, in addition to the total self-reliance in terms of electricity imports, leads the low forecast scenario to have a total operating cost 75% lower than the baseline scenario. From each consumer's perspective, their costs to cover electricity and space heating demand are reduced by 62%.

This is also reflected in the lower average² electricity and heat values, with a decrease of 61% and 64%, respectively.

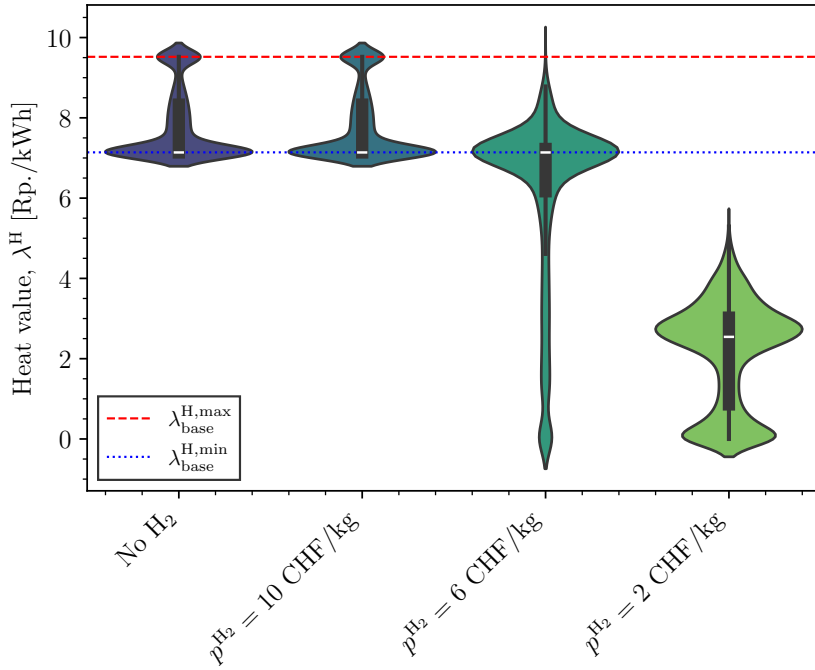


Figure 4.6: Comparison of the heat value distributions for the baseline and hydrogen scenarios with different hydrogen prices. The dashed and dotted lines represent the heat values associated with producing heat with the heat pump with electricity imported during the high and low tariff periods, respectively. The heat values only correspond to periods when there is heat demand.

The distributions of the heat values over the modelled period for each of the four scenarios are shown in the violin plots of Figure 4.6. This figure also shows the maximum and minimum heat values at which the energy system can generate heat in the baseline scenario (when it only counts with a heat pump), $\lambda_{\text{base}}^{\text{H},\text{max}}$ and $\lambda_{\text{base}}^{\text{H},\text{min}}$, respectively. These two lines represent the cost of producing heat by importing electricity from the grid using the heat pump. Heat values concentrated around either of these two lines indicate a direct correlation to the electricity import prices. As can be seen in the figure, the heat value distributions of the baseline and current hydrogen price scenarios are identical and concentrated around both lines. This behaviour was also visible in the previously shown Figure 4.3b.

For the high-price scenario, there are no heat values at $\lambda_{\text{base}}^{\text{H},\text{max}}$, which indicates that the heat supply is no longer subject to electricity imports during high tariff periods. There is still, however, heat values distributed around $\lambda_{\text{base}}^{\text{H},\text{min}}$. As seen in the figure, around 50% of the periods when there is heat consumption, the heat value is higher than $\lambda_{\text{base}}^{\text{H},\text{min}}$.

However, this changes in the low price scenario, where now all of the heat values are below $\lambda_{\text{base}}^{\text{H},\text{min}}$. This indicates a complete decoupling of the heat value from the electricity

²The weighted average electricity and heat values are used, instead of the simple average, to reflect the real costs incurred and provide a fair comparison across scenarios.

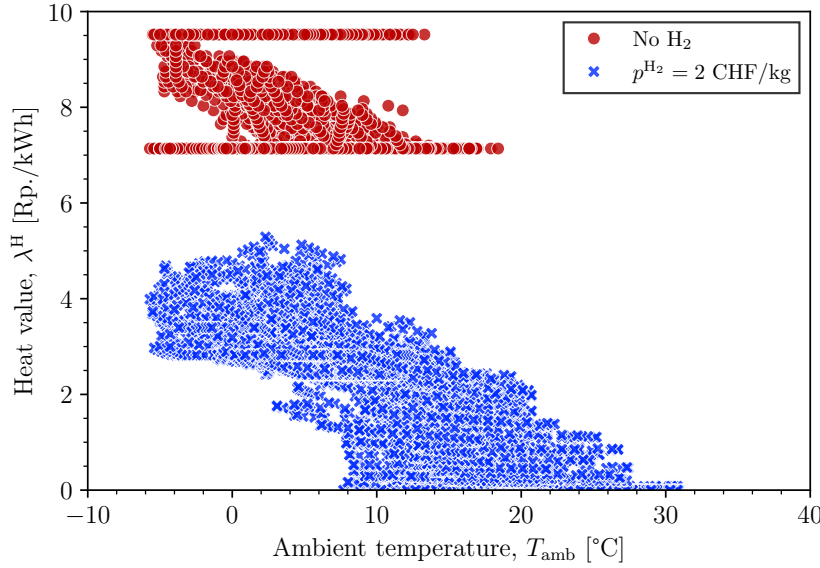


Figure 4.7: Scatter plot comparing the heat value vs ambient temperature for the baseline and hydrogen scenarios with low forecasted hydrogen prices. The heat values only correspond to periods when there is heat demand.

import prices for the low forecast scenario. This can also be inferred from the fact that in this scenario, there are no electricity imports, as seen in Table 4.2. To visualise the impact of low hydrogen prices, Figure 4.7 shows a comparison of the heat value against the ambient temperature for the baseline scenario and the low forecast scenario. This figure makes the considerably lower value of heat reached in the latter scenario more visible. It additionally shows the general trend of higher heat values at lower ambient temperatures.

Optimal operating region of hydrogen technologies

In the previous section, the results obtained for scenarios with three different hydrogen prices were explored. These results are intuitive: at a sufficiently low hydrogen price, the system finds it optimal to generate electricity from hydrogen instead of importing it from the grid. If the hydrogen price is even lower, it is optimal for the system to produce surplus electricity to export to the grid during high electricity prices. If the hydrogen price is not sufficiently low, however, the system does not utilise any hydrogen technology and relies on electricity imports.

Nevertheless, these observations can be interpreted more in-depth by analysing not only the hydrogen prices, but also looking at the hydrogen price-to-electricity price ratio. Since electricity and hydrogen are the only boundary conditions that determine prices in the system, their relation plays a fundamental role in establishing the merit order of technologies to supply the energy demands of the system. The operation of the electrolyser and the fuel cell is subject to the energy values that derive from the system's boundary conditions. To explain the relation between the price ratio and the operation of energy



Figure 4.8: Schematic representation of the electrolyser and fuel cell with the energy flows and the corresponding price or value associated with it.

technologies, it is important to first understand under which condition it is *optimal* for a technology to be in operation.

To explain the optimal operation of hydrogen technologies, Figure 4.8 shows a schematic representation of an electrolyser and a fuel cell, with their corresponding energy flows and their price or value in the system. From these diagrams, the condition for an optimal operation of the technologies can be derived. These conditions are derived analytically and are shown for the electrolyser and the fuel cell in Equation 4.1 and Equation 4.2, respectively. A *state* of "on" means that operating the device is optimal, and a *state* of "off" means that operating the device is not optimal. These relations can be intuitively stated as follows: if the total output value of the device is larger than the total input value, it should be operated; if the opposite is true, the device should not be operated. It is important to state that this same expression could not be expressed by replacing λ^E with the electricity price since they are not the same. The **electricity price** only reflects the cost of electricity imported from the grid; the **electricity value** reflects the marginal cost to the global objective function for an additional unit of electricity, considering the time value of that unit of electricity. These values can be the same under certain conditions, but as soon as there are energy technologies that can generate, convert or store energy, their value might diverge.

$$state_{EL} = \begin{cases} \text{on}, & \text{if } \dot{m}_{H_2}p^{H_2} + Q_{EL}\lambda^H \geq P_{EL}\lambda^E \\ \text{off}, & \text{otherwise} \end{cases} \quad (4.1)$$

$$state_{FC} = \begin{cases} \text{on}, & \text{if } P_{FC}\lambda^E + Q_{FC}\lambda^H \geq \dot{m}_{H_2}p^{H_2} \\ \text{off}, & \text{otherwise} \end{cases} \quad (4.2)$$

The expressions for these conditionals can be further reduced by making use of the modelling of components explained in subsection 2.1.2³. This allows to represent these conditionals in terms of only constant parameters and the energy values in the system. The reduced expressions for the conditional operation of the electrolyser and the fuel cell are displayed in Equation 4.3 and Equation 4.4, respectively.

$$state_{EL} = \begin{cases} \text{on}, & \text{if } \frac{p^{H_2}}{HHV_{H_2}} + \left(\frac{1}{\eta_{EL}} - 1 \right) \eta_{EL,\text{th}}\lambda^H \geq \frac{1}{\eta_{EL}}\lambda^E \\ \text{off}, & \text{otherwise} \end{cases} \quad (4.3)$$

³For now, and to simplify the explanation, constant electrochemical conversion efficiencies are assumed for the electrolyser and fuel cell, instead of the PWA approximation used in the model. The impact of the modelling complexity is investigated in the next section.

$$state_{FC} = \begin{cases} \text{on}, & \text{if } \eta_{FC}\lambda^E + (1 - \eta_{FC})\eta_{FC,\text{th}}\lambda^H \geq \frac{p^{H_2}}{\text{HHV}_{H_2}} \\ \text{off}, & \text{otherwise} \end{cases} \quad (4.4)$$

These equations represent the *optimal frontiers* that ultimately determine whether operating the device will be optimal at time step t . Since in the new formulation, the only time-dependent variables are the electricity and heat values, λ^E and λ^H , the frontiers can be plotted with each of these variables on a separate axis. The expressions for the optimal frontiers of both technologies are shown in Equation 4.5 and Equation 4.6. When $\lambda^H(t) > \lambda_{OF}^H$ at time step t , then the optimisation will find it optimal to operate the technology, this region is referred to as the *optimal operating region* of the respective technology.

$$\text{Electrolyser optimal frontier: } \lambda_{OF}^H(\lambda^E) = \frac{\frac{1}{\eta_{EL}}\lambda^E(t) - \frac{p^{H_2}}{\text{HHV}_{H_2}}}{\left(\frac{1}{\eta_{EL}} - 1\right)\eta_{EL,\text{th}}} \quad (4.5)$$

$$\text{Fuel cell optimal frontier: } \lambda_{OF}^H(\lambda^E) = \frac{\frac{p^{H_2}}{\text{HHV}_{H_2}} - \eta_{FC}\lambda^E(t)}{(1 - \eta_{FC})\eta_{FC,\text{th}}} \quad (4.6)$$

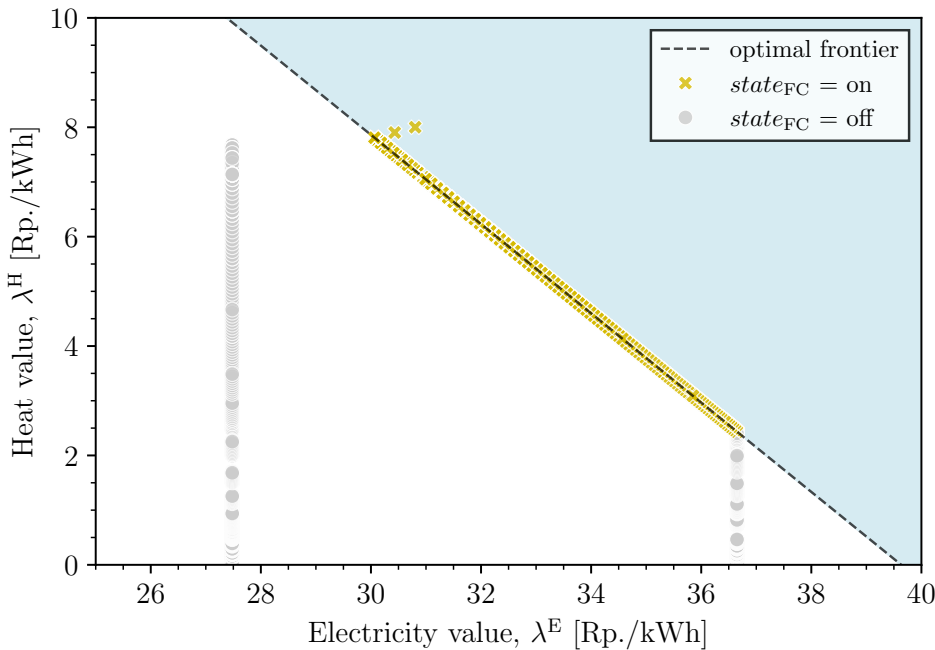


Figure 4.9: Scatter plot showing the relationship between the heat value and the electricity value for the hydrogen scenario with a high price forecast of 6 CHF/kg. The time periods from the optimisation results when the fuel cell is consuming hydrogen and producing electricity are indicated with a different marker. The black dashed line is obtained from the analytical optimal frontier function for the fuel cell. The optimal operating region is shaded in blue.

These equations can be verified with the results obtained from the scenarios investigated previously. Figure 4.9 shows the relationship between the heat value and the

electricity value for the high H₂ price forecast scenario. The scatter plot distinguishes between periods where the fuel cell is operational, i.e. $P_{FC}(t) > 0$, and when it is unused, i.e. $P_{FC}(t) = 0$. Additionally, the figure displays the optimal frontier, which follows the function shown in Equation 4.6. The region above the line, coloured in blue, represents the optimal operating region of the fuel cell, as indicated in Equation 4.4. The same

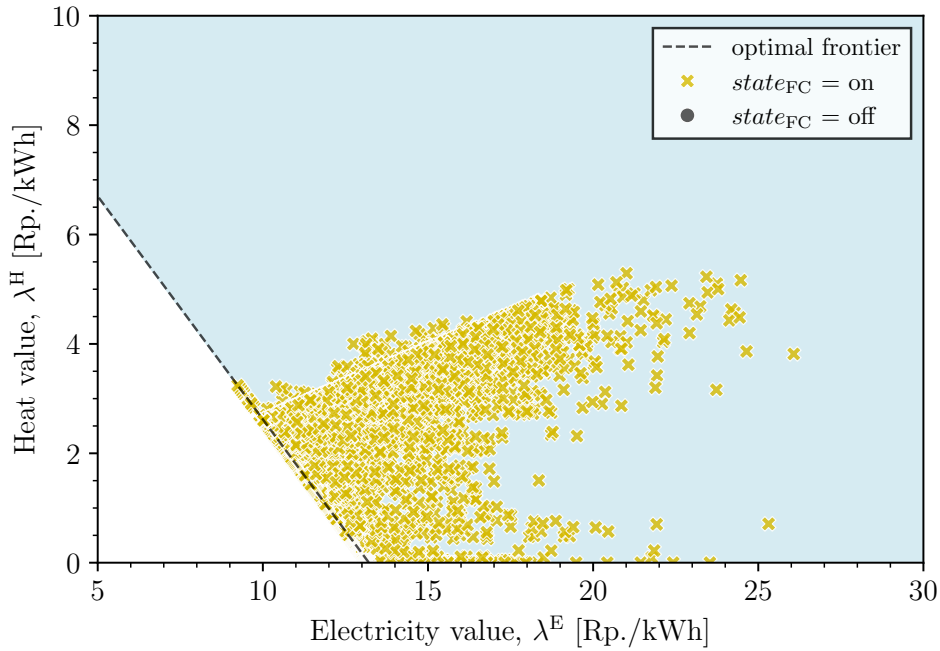


Figure 4.10: Scatter plot showing the relationship between the heat value and the electricity value for the hydrogen scenario with a low price forecast of 2 CHF/kg. The time periods from the optimisation results when the fuel cell is consuming hydrogen and producing electricity are indicated with a different marker. The black dashed line is obtained from the analytical optimal frontier function for the fuel cell. The optimal operating region is shaded in blue.

plot is made for the low H₂ price forecast scenario in Figure 4.10. As can be seen in this figure, once again the fuel cell is only operational in the blue region. Furthermore, in this scenario, the fuel cell is always operational. This is expected since there is electricity demanded by the consumers at all times, and as previously discussed, under this hydrogen price it is always beneficial to produce electricity rather than importing it. As seen in both figures, the periods in which the optimisation model decides to operate the fuel cell lie exactly on top or above this optimal frontier line, thus verifying the optimal frontier and optimal operating region formulations.

Determinants of the optimal operating region

From the frontiers indicated by Equations 4.5 and 4.6, it can be observed that the optimal operating region is a function of the hydrogen price p^{H_2} , the electrochemical efficiency of the device η_{EL}, η_{FC} , the recoverable heat from the device $\eta_{th,EL}, \eta_{th,FC}$, and the energy content of hydrogen as indicated by its HHV. A change in one of these parameters may

have a different impact on each of these technologies. For instance, a higher hydrogen price will make operating the electrolyser more attractive but will increase the costs of operating the fuel cell. For brevity, this section focuses on their impact on the optimal operating region of a fuel cell. The impact on the electrolyser is similar.

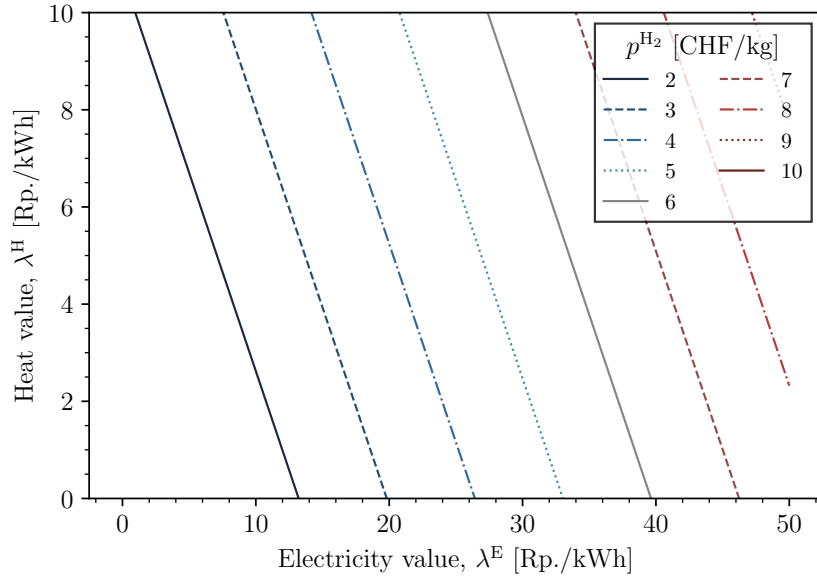


Figure 4.11: *Optimal frontiers of a fuel cell as a function of the heat and electricity values in an energy system at different hydrogen prices.*

Figure 4.11 shows the optimal frontiers for operating a fuel cell at different hydrogen prices, ranging from the price of the low forecast scenario to the current prices scenario. As seen in the figure, a higher hydrogen price shifts the optimal operating region outwards. This means that either heat, electricity or both must have a higher value in the energy system in order to justify operating the fuel cell when the hydrogen price is higher. This explains why the fuel cell is operated less when hydrogen prices are higher.

As observed so far, both the electricity and heat values in the system determine whether or not the fuel cell should be operated. The fact that the heat value has an impact is a direct consequence of having a WHR system. In other words, without WHR, there would be no heat utilised from the fuel cell, and thus the operation of the fuel cell would only be a function of the electricity value in the system. The slope in the optimal frontier indicates the ratio between the heat value and electricity value at which the fuel cell remains in the optimal operating region. This is determined by how much heat or electricity we can extract from the fuel cell when it is operating. This can also be understood as the elasticity⁴ of the optimal frontier of the fuel cell to a change in the heat or electricity value. For example, if 50% of the energy output of the fuel cell is electricity and 50% is recovered heat, this would result in a line with a slope of -1, i.e. 1 Rp./kWh of electricity value has the same impact on the optimal operating region as 1 Rp./kWh of heat value, or in other terms, the elasticity of the optimal frontier to the heat and electricity value is equal.

⁴Elasticity in this context refers to the *economic* interpretation, which in this case measures the responsiveness of the frontier to a change in the energy value.

However, when the output ratios are different for electricity and recovered heat, the slope in the frontier changes. The output ratio of electricity-to-recovered heat is mainly a function of the electrochemical efficiency of the fuel cell, η_{FC} . A lower η_{FC} means that there is more excess heat produced by the fuel cell, which makes the frontier less elastic to the electricity value, but at the same time increases the recovered heat from the fuel cell, which increases its elasticity to the heat value. Conversely, a higher η_{FC} leads to a change in slope in the opposite direction. Figure 4.12 illustrates the impact of a change in the electrochemical efficiency of the fuel cell on the optimal frontier. These plots correspond to fuel cells modelled with constant electrochemical efficiencies. However, when a fuel cell is modelled with different electrochemical efficiencies at different partial loads, the optimal frontier changes depending on the total load on the fuel cell. This is further explored in the next section.

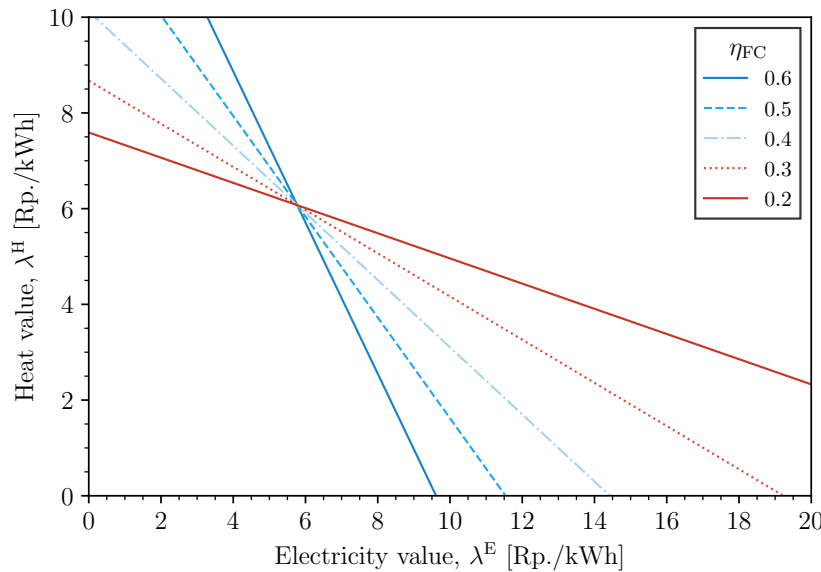


Figure 4.12: Optimal frontiers of a fuel cell as a function of the heat and electricity values in an energy system for different electrochemical efficiencies.

Impact of model fidelity on the optimal operating region

The previous sections explored the concept of an optimal operating region for H₂ technologies with a constant electrochemical efficiency. This simplification allowed the derivation of simple expressions for the optimal frontier, as shown in Equations 4.5 and Equation 4.6. However, as shown in the previous section, the frontier changes at different electrochemical efficiencies. In the energy community modelled in this work, a PWA approximation is used for the modelling of H₂ technologies, as shown in subsection 2.1.2. Therefore, there is a set of electrochemical efficiencies at which the electrolyser and the fuel cell can operate.

As seen previously in Equation 2.18 and Equation 2.20, the electrochemical efficiencies of these technologies are higher at low loading points. Therefore, it is expected that the fuel cell and electrolyser can operate profitably at a low load, even when increasing the

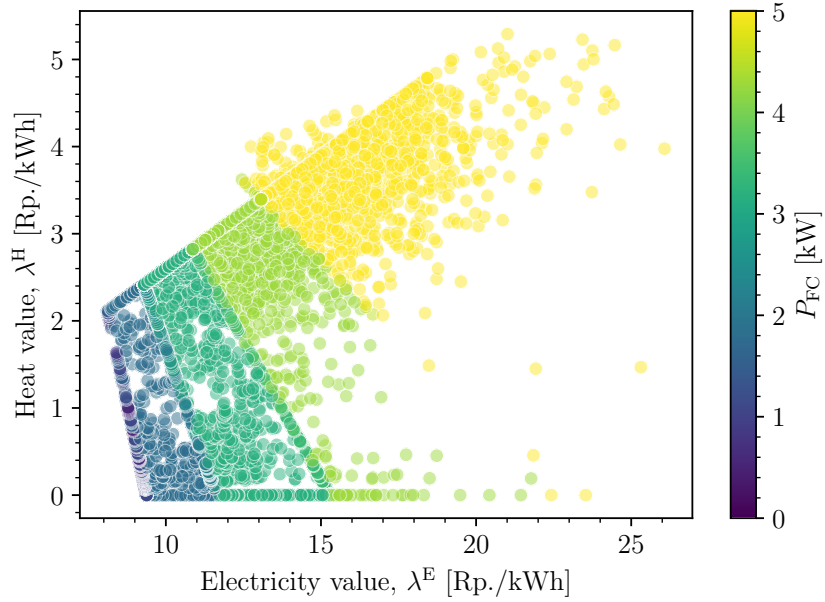


Figure 4.13: Scatter plot of the heat value vs the electricity value for the hydrogen scenario with low price forecast of 2 CHF/kg, modelling the fuel cell as a PWA function with 3 breakpoints, indicating with a hue the output power of the fuel cell.

load would decrease the profitability. In the specific case of the fuel cell, when the electricity value is low, it can operate at lower partial loads, and as the electricity value increases, operating at a higher load also starts to become profitable. This scenario modelled the fuel cell with a PWA approximation with three breakpoints ($n = 3$), thus splitting the operating region of the fuel cell into four different electrochemical efficiencies. This discrete set over four regions can be observed in Figure 4.13. This figure shows a scatter plot of different time steps of the modelled period, indicating the output power of the fuel cell at each time step with a hue. As seen in the figure, the optimal operating region of the fuel cell changes at different partial loads. For comparison, Figure 4.14 displays a plot of the same variables for the same scenario but modelling the fuel cell with a constant electrochemical efficiency.

By comparing Figure 4.13 with Figure 4.14, the following impacts of reducing the modelling complexity can be observed:

- **distortion of optimal operating frontier:** at low loads, the real electrochemical efficiency of a fuel cell is high, which means that generating electricity at low electricity values may be optimal. When the model is too simplified, it underestimates the electrochemical efficiency at low partial loads.
- **inflexible use of technology:** with a constant efficiency, once the combination of energy values lies above the single optimal frontier, the model always finds it optimal to operate the technology at its maximum capacity. This underrates the value of operating the technology at different loading points over the modelling period.

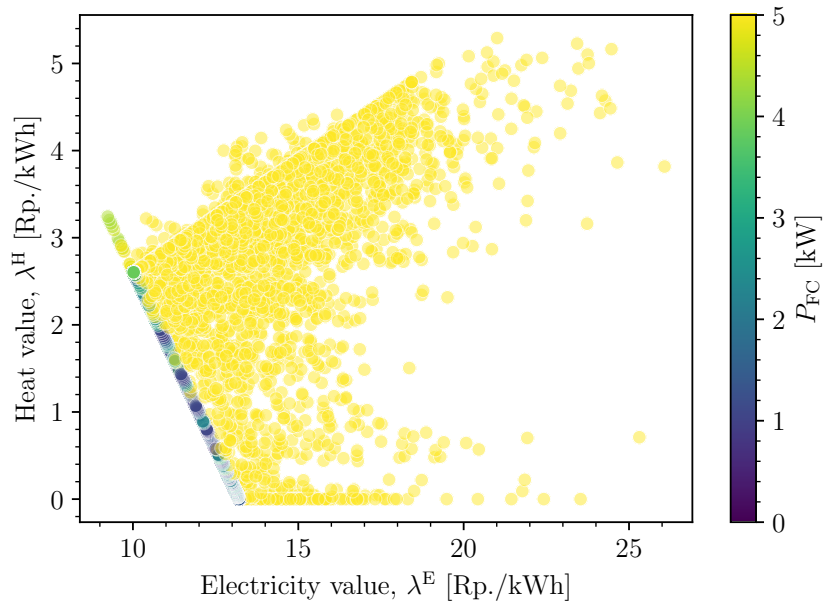


Figure 4.14: Scatter plot showing the relationship between the heat value and the electricity value for the hydrogen scenario with a low price forecast of 2 CHF/kg, modelling the fuel cell with a constant efficiency, indicating with a hue the output power of the fuel cell.

Approximation of optimal frontier for unknown energy values

So far, the optimal operating regions of an electrolyser and a fuel cell in a multi-energy community have been derived analytically and verified with the optimisation results of the modelled energy system. These optimal operating regions have been derived in terms of the electricity and heat values of the energy system. However, in a real application with no internal mechanism for determining energy values, these variables are unknown. As mentioned in section 2.2, these are the dual variables or *shadow prices* of their corresponding energy balance constraints and are obtained in an ex-post analysis, meaning that they can only be derived after solving the centralised optimisation problem. This property renders expressing the optimal operating region in terms of the dual variables impractical at the moment of deciding whether or not operating the technology⁵. This section focuses on developing an approximation of the optimal operating region for an electrolyser and a fuel cell based on the hydrogen and electricity prices instead of the dual variables.

A conservative approximation of the optimal operating region can be derived for an energy system with grid electricity prices. Here, the approximation can be expressed in terms of electricity prices, efficiency of power-to-heat conversion, and hydrogen prices. To do so, the conditional Equations 4.3 and 4.4 are expressed in terms of p^{H_2} . The resulting

⁵Here it is important to remark that when the distributed optimisation approach is used, these energy values *are known*, in fact as seen in section 2.3, these values are found iteratively and shared with all energy agents. Therefore, in that setting the derived expression for the optimal operating frontier is still valid and applicable.

conditional equations are shown in Equation 4.7 and Equation 4.8.

$$\text{electrolyser condition: } p^{\text{H}_2} \geq \text{HHV}_{\text{H}_2} \left(\frac{1}{\eta_{\text{EL}}} \lambda^{\text{E}}(t) - \left(\frac{1}{\eta_{\text{EL}}} - 1 \right) \eta_{\text{EL},\text{th}} \lambda^{\text{H}}(t) \right) \quad (4.7)$$

$$\text{fuel cell condition: } p^{\text{H}_2} \leq \text{HHV}_{\text{H}_2} \left(\eta_{\text{FC}} \lambda^{\text{E}}(t) + (1 - \eta_{\text{FC}}) \eta_{\text{FC},\text{th}} \lambda^{\text{H}}(t) \right) \quad (4.8)$$

Even when the heat and electricity values at time t are not known, the following statements can be made regarding the range of their values:

- **upper-bounded electricity value, $\lambda^{\text{E}}(t)$:** the value of electricity in the energy system can never be above the electricity tariff during period t , since importing electricity from the grid at this value is always possible:

$$\lambda^{\text{E}}(t) \leq p_{\text{imp}}^{\text{E}}(t), \quad \forall t$$

- **lower-bounded electricity value, $\lambda^{\text{E}}(t)$:** independently of the amount of surplus electricity in the system, as long as there is no bottleneck in the grid capacity, the electricity value can never be below the electricity export price, since an additional unit of electricity could always be sold at this price to the grid:

$$\lambda^{\text{E}}(t) \geq p_{\text{exp}}^{\text{E}}(t), \quad \forall t$$

- **upper-bounded heat value, $\lambda^{\text{H}}(t)$:** in an energy system with power-to-heat technology, the heat value remains upper-bounded by the electricity value and the corresponding conversion to heat coefficient. In the case of a heat pump this is represented by the coefficient of performance. Since the electricity value itself is bounded, this can be represented as follows:

$$\lambda^{\text{H}}(t) \leq p_{\text{imp}}^{\text{E}}(t)/\text{COP}_{\text{HP}}, \quad \forall t$$

- **lower-bounded heat value, $\lambda^{\text{H}}(t)$:** since the energy system modelled has no option of exporting heat at a set price, the value of heat can reach zero, e.g., when the ambient temperature regularly maintains the temperature of households above the minimum temperature, an additional unit of heat will have no impact in reducing the operational cost of the system. However, there is internal heat demand at time t , the value of heat can still be given a lower-bound:

$$\lambda^{\text{H}}(t) \geq p_{\text{exp}}^{\text{E}}(t)/\text{COP}_{\text{HP}} \quad \forall t$$

These upper and lower bounds on the electricity and heat value allow for the expression of an approximation of the optimal operating region of each technology as indicated in Equation 4.9 and Equation 4.10.

$$\text{Electrolyser approx: } p^{\text{H}_2} \geq \text{HHV}_{\text{H}_2} \left(\frac{1}{\eta_{\text{EL}}} p_{\text{imp}}^{\text{E}}(t) - \left(\frac{1}{\eta_{\text{EL}}} - 1 \right) \eta_{\text{EL},\text{th}} \frac{p_{\text{exp}}^{\text{E}}(t)}{\text{COP}_{\text{HP}}} \right) \quad (4.9)$$

$$\text{Fuel cell approx: } p^{\text{H}_2} \leq \text{HHV}_{\text{H}_2} \left(\eta_{\text{FC}} p_{\text{exp}}^{\text{E}}(t) + (1 - \eta_{\text{FC}}) \eta_{\text{FC},\text{th}} \frac{p_{\text{exp}}^{\text{E}}(t)}{\text{COP}_{\text{HP}}} \right) \quad (4.10)$$

If we apply these conditions to the *baseline scenario*, stronger assumptions regarding the heat and electricity values can be made. Since there are no electricity generation technologies in the system, $\lambda^E(t)$ inside the energy system is lower bounded by the import electricity price, i.e. $\lambda^E(t) \geq p_{\text{imp}}^E(t)$. Therefore, under the assumptions mentioned below, the approximated optimal operating region for the technologies can be expressed.

1. *Energy demand:* there is demand for electricity and heat in the energy system at time t .
2. *Energy technologies:* there are no additional electricity or heat generation technologies besides power-to-heat conversion, i.e. only imported electricity can cover the energy demands.

For simplicity, Φ_{EL} and Φ_{FC} are used to indicate the hydrogen-to-electricity price ratio that approximates the optimal operating region of the electrolyser and the fuel cell, respectively. These functions are shown in Equation 4.11 and Equation 4.12. With the parameters mentioned in Chapter 3, the numerical values of these ratios can be obtained, these are $\Phi_{\text{EL}} = 69.1 \left[\frac{\text{CHF/kg}}{\text{CHF/kWh}} \right]$ and $\Phi_{\text{FC}} = 20.0 \left[\frac{\text{CHF/kg}}{\text{CHF/kWh}} \right]$.

$$\frac{p^{\text{H}_2}}{p_{\text{imp}}^E(t)} \geq \Phi_{\text{EL}} = \text{HHV}_{\text{H}_2} \left(\frac{1}{\eta_{\text{EL}}} - \left(\frac{1}{\eta_{\text{EL}}} - 1 \right) \frac{\eta_{\text{EL},\text{th}}}{\text{COP}_{\text{HP}}} \right) \quad (4.11)$$

$$\frac{p^{\text{H}_2}}{p_{\text{imp}}^E(t)} \leq \Phi_{\text{FC}} = \text{HHV}_{\text{H}_2} \left(\eta_{\text{FC}} + (1 - \eta_{\text{FC}}) \frac{\eta_{\text{FC},\text{th}}}{\text{COP}_{\text{HP}}} \right) \quad (4.12)$$

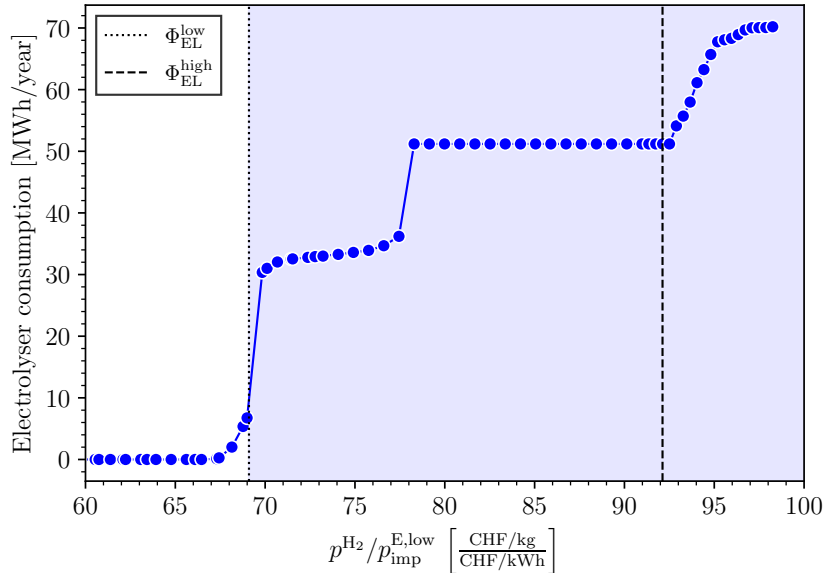


Figure 4.15: Optimal yearly electricity consumption of the electrolyser for multiple scenarios with different hydrogen-to-electricity price ratios, indicating the approximated optimal boundaries at low and high electricity tariffs. The shaded region represents an approximation of the optimal operating region.

To verify that these defined ratios approximate the boundaries for the optimal operating region of the devices, several optimisations were run with varying hydrogen-to-electricity import price ratios for the *hydrogen scenario*. From the results of each optimisation, the total electricity consumption from the electrolyser and the total hydrogen

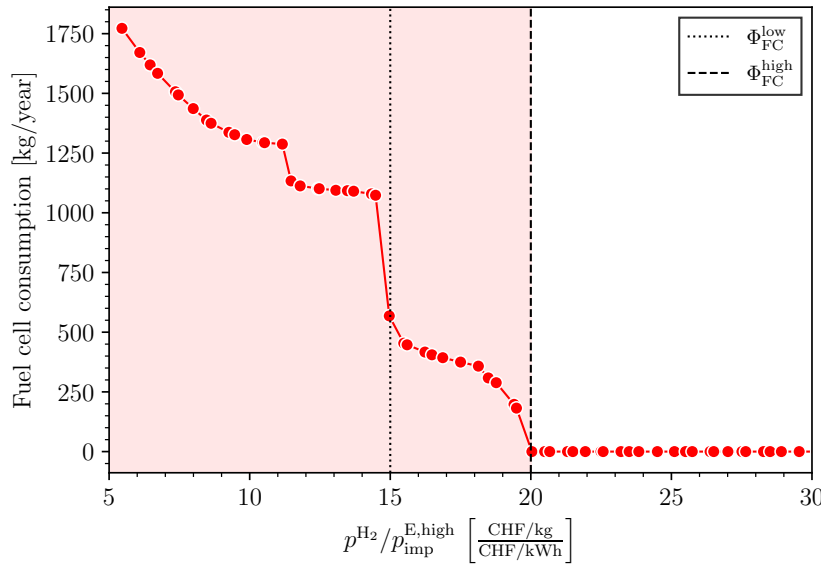


Figure 4.16: Optimal yearly hydrogen consumption of the fuel cell for multiple scenarios with different hydrogen-to-electricity price ratios, indicating the approximated optimal boundaries at low and high electricity tariffs. The shaded region represents an approximation of the optimal operating region.

consumption by the fuel cell were obtained. Figure 4.15 and Figure 4.16 display line plots of the electrolyser and fuel cell consumption as a function of the $p_{\text{H}_2}/p_{\text{imp}}^{\text{E},\text{low}}$ and $p_{\text{H}_2}/p_{\text{imp}}^{\text{E},\text{high}}$ ratios⁶, respectively. The vertical lines in the figures indicate the approximations of the optimal ratios using the high and low electricity import tariffs. The shaded regions indicate the approximation of the optimal operating region for each technology. It can be observed in both figures that Φ_{EL} and Φ_{FC} approximate the price ratios at which operating the devices starts to become optimal for the energy system. Furthermore, the impact of reaching a price ratio that falls within the region by both electricity tariffs ($\Phi_{\text{EL}}^{\text{low}}$ and $\Phi_{\text{FC}}^{\text{high}}$) can also be observed as a "step" in the consumption by each technology, which indicates that operating each technology now becomes optimal in more periods.

Impact of WHR in the operation of hydrogen technologies

Until now, the operating regions were formulated assuming that there is a WHR system that repurposes the excess heat from the operation of hydrogen technologies to cover space heating demand. This excess heat thus became valuable and made operating the technologies profitable at a less strict price ratio, Φ . If no waste heat is recovered, it is expected that the optimal operating region for each technology will be narrower. Equation 4.13 and Equation 4.14 formulate the price ratio at which operating each technology

⁶The electrolyser's plot uses the ratio with the low electricity tariff because for its operation the lowest electricity price is most important. The fuel cell's plot, on the other hand, uses the ratio with the high electricity tariff, since reducing electricity imports in the high tariff period determines when the operation of the fuel cell becomes valuable

becomes valuable when there is no WHR.

$$\frac{p^{\text{H}_2}}{p_{\text{imp}}^{\text{E}}(t)} \geq \Phi_{\text{EL,noWHR}} = \text{HHV}_{\text{H}_2} \left(\frac{1}{\eta_{\text{EL}}} \right) = 77.0 \quad (4.13)$$

$$\frac{p^{\text{H}_2}}{p_{\text{imp}}^{\text{E}}(t)} \leq \Phi_{\text{FC,noWHR}} = \text{HHV}_{\text{H}_2} (\eta_{\text{FC}}) = 15.1 \quad (4.14)$$

These boundaries are also verified by running several optimisations over a range of price ratios, where now the hydrogen technologies are modelled without their waste heat being recovered. The results of these scenarios are overlaid on the previous results, and the more constraining price ratios with no WHR are shown in Figure 4.17 and Figure 4.18. As seen in the figures, the operation of the technology only becomes optimal at a higher Φ for the electrolyser and at a lower Φ for the fuel cell. This means that these technologies require a more pronounced price difference to become economically viable.

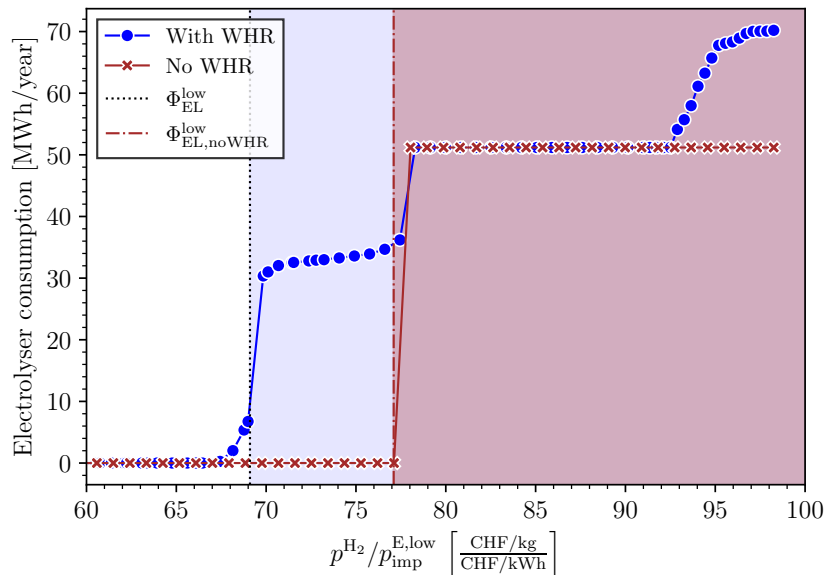


Figure 4.17: Comparison of the optimal yearly electricity consumption of the electrolyser for multiple scenarios with different hydrogen-to-electricity price ratios, with and without a WHR system to reutilise heat. The shaded regions represent an approximation of the optimal operating region in both cases.

Remarks on hydrogen-to-electricity price ratios in the future

The analysis thus far showed that boundary conditions such as the cost of hydrogen and value of heat and electricity determine whether hydrogen technologies are valuable for an energy community. As mentioned, operating a fuel cell becomes valuable at low hydrogen-to-electricity price ratios, conversely, operating an electrolyser becomes valuable at high price ratios. To assess the long-term value of these technologies, however, it is also important to reflect on whether either of these price ratio conditions could be sustained in reality for a period of time long enough to make such investments viable in the long term.

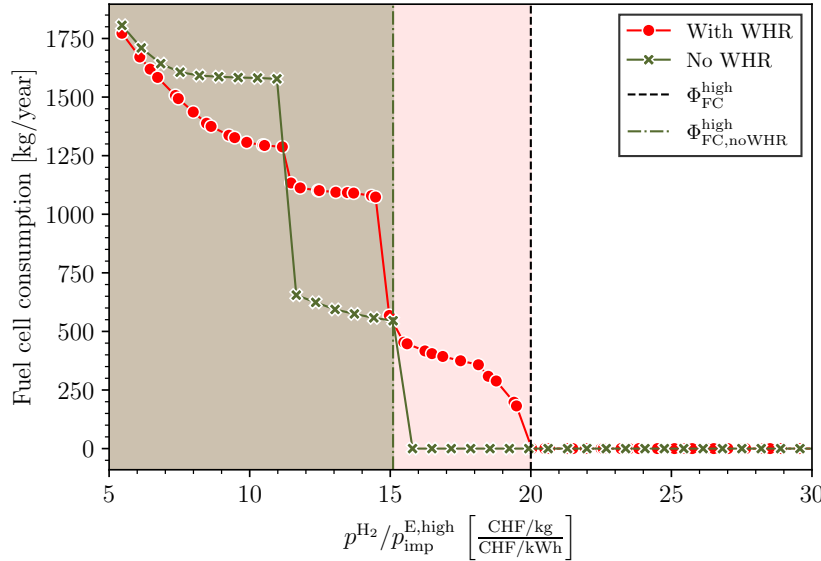


Figure 4.18: Optimal yearly hydrogen consumption of the fuel cell for multiple scenarios with different hydrogen-to-electricity price ratios, with and without a WHR system to reutilise heat. The shaded regions represent an approximation of the optimal operating region in both cases.

The price dynamics of these energy resources in an energy community is a consequence of existing technologies that can either be a part of the energy system or be able to supply the system externally. For example, if there is a large PV installation, these would be a source of low cost electricity, which could increase the value of an electrolyser. On the other hand, if an energy community relies on a grid with high electricity tariffs to cover their electricity demands, fuel cell investments might increase in value. At the same time, the existence of energy technologies is also determined in the long run by the value of energy resources. For instance, a region with electricity tariffs might invest in technologies that have lower costs of production, reducing prices in the region. This could make investments which initially seemed profitable, yield lower returns than anticipated in the long run.

As an example, consider a scenario where an energy community has access to low-cost electricity and the opportunity to sell hydrogen for a price that makes an electrolyser a profitable investment. The attractiveness of this investment could spark additional investment into electrolyzers, increasing the value of electricity for the community and thus reducing the profitability of investing. Alternatively, if an energy community has access to low-cost hydrogen, but has a high value on electricity, increasing the installed capacity of fuel cells in the system would increase demand for hydrogen, potentially leading to higher local prices, and increasing low-cost electricity, ultimately reducing the profitability of a fuel cell investment. The reason for the susceptibility of the profitability of hydrogen technologies to installed local energy technologies, is that it relies on local energy resource values.

This work investigates the value of hydrogen technologies in the presence of additional energy technologies. However, analysing the influence of the long-term variations in the

energy system configuration, the impact on the value of energy resources in an energy community, and the feasibility of reaching and maintaining boundary condition scenarios that make operating hydrogen technologies profitable remains outside the scope of this thesis.

4.1.3 Complete energy community

The previous sections modelled only a subset of all the energy technologies indicated in Figure 2.2. This section presents the optimisation results when the full set of technologies shown are included. As indicated in Figure 3.5, the optimisation of the complete system is evaluated at three hydrogen price scenarios. Table 4.3 presents the main results obtained for the complete system, comparing the value to those obtained for the baseline scenario.

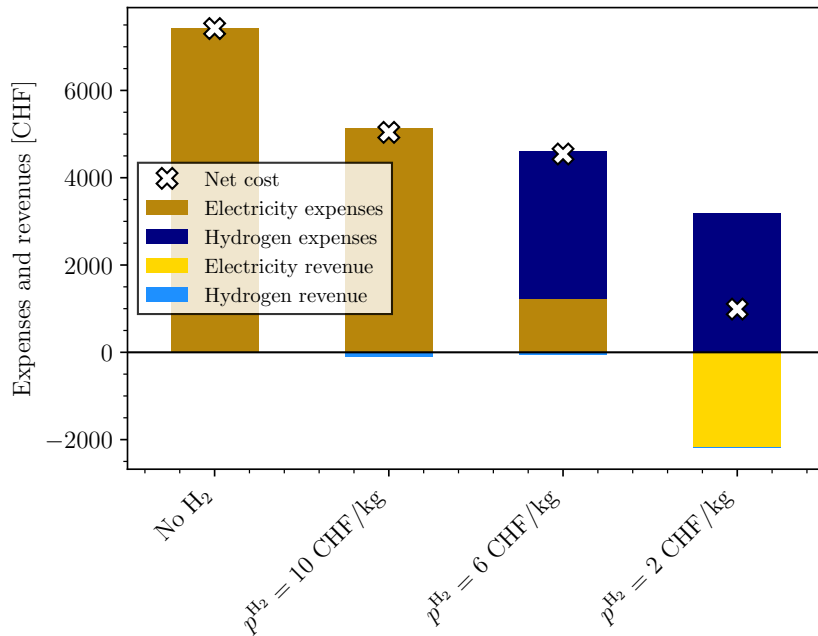


Figure 4.19: Comparison of expenses and revenues of the energy system for the baseline scenario and complete system scenario with different hydrogen prices, indicating the net yearly operating costs.

As can be seen in the results, in the *current scenario* there is a substantial decrease in the total operating cost of the system of 32% compared to the baseline. This cost decrease can be observed in Figure 4.19. The reason for this decrease is the reduced electricity imports. The total electricity import expenses are reduced by 2'278 CHF. This is also the same difference in electricity expenses between the *hydrogen scenario with current H₂ prices* and *complete system scenario with current H₂ prices*, since in the former one there was no difference in total electricity imported. This is in line with the addition of a PV system to the energy community.

The total production from PV is equivalent to 26% of the total electricity consumption. Therefore, by leveraging the BES, the PV production can be stored for consumption during high electricity tariff periods, leading to a further decrease in costs. The electricity

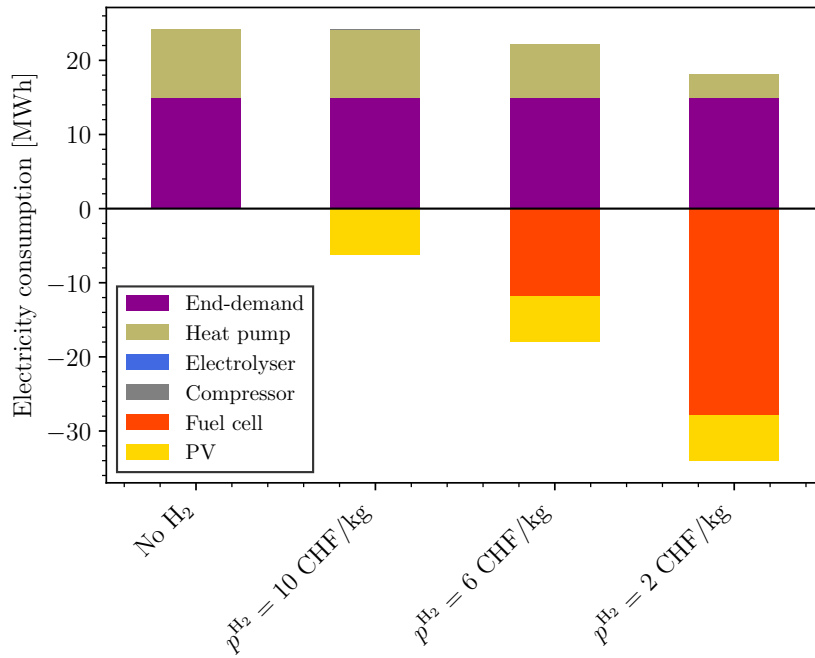


Figure 4.20: Comparison of total electricity consumption (positive) and generation (negative) by technology for the baseline scenario and complete system scenario with different hydrogen prices.

consumption (positive) and generation (negative) by each technology are observed in Figure 4.20. This reduced reliance on electricity imports is reflected in the average electricity value and consumer costs to cover their electricity end-demand, both of which are reduced by 9% compared to the baseline. As can be seen in the figure, the electricity production by the PV is not exported, and is instead only used to cover the electricity demands of the energy system. This is because even with the losses incurred in the BES, the price difference between electricity imports and electricity exports make it more profitable to reduce electricity imported rather than exporting electricity.

In the *high price forecast scenario* the fuel cell starts producing electricity and heat, covering 53% and 21% of their total consumption, respectively. The heat pump, however still remains the main source for space heating, covering the remaining 79% of the total demand. In this scenario hydrogen imports become the largest expense for the energy community, with a share of 74% of the total operating yearly costs. Nevertheless, the total operating cost is reduced by 39% compared to the baseline scenario.

In the *low price forecast scenario*, the total operating costs are further reduced, being 87% lower than the baseline. As mentioned in subsection 4.1.2, this is because at this hydrogen price, it becomes profitable to export electricity at some time periods. Thus becoming the only scenario in which electricity is exported and substantial revenues are received by the energy community, which are 68% of the total expenses of the community. The costs for the consumers reflect the lower operating costs, with the total cost to cover the electricity end-demand and space heating demand are reduced by 62% and 61% compared to the baseline.

Table 4.3: Comparison of the main results obtained for the baseline and complete system with three different prices for hydrogen. The percentages indicate the relative difference to the baseline scenario.

| Metric | Baseline | | | Complete system | | Units |
|--|-------------------|----------------|----------------|-----------------|--------------|-------|
| | No H ₂ | Current | High forecast | Low forecast | | |
| | 10 CHF/kg | 6 CHF/kg | 2 CHF/kg | | | |
| <i>Cost breakdown</i> | | | | | | |
| electricity expenses | 7'417 | 5'139 | 1'225 | 0 | CHF/y | |
| electricity revenues | 0 | 0 | 4 | 2'177 | CHF/y | |
| H ₂ expenses | 0 | 0 | 3'382 | 3'187 | CHF/y | |
| H ₂ revenues | 0 | 100 | 60 | 20 | CHF/y | |
| total operating cost, J_{op} | 7'417 | 5'039 (-32.1%) | 4'543 (-38.8%) | 990 (-86.6%) | CHF/y | |
| <i>Consumer costs</i> | | | | | | |
| electricity end-demand | 1'592 | 1'450 (-8.9%) | 1'329 (-16.6%) | 598 (-62.4%) | CHF/(cons·y) | |
| space heating demand | 931 | 910 (-2.2%) | 822 (-11.7%) | 367 (-60.6%) | CHF/(cons·y) | |
| <i>Electricity results</i> | | | | | | |
| consumption | 24.2 | 24.2 | 22.2 | 18.2 | MWh/y | |
| fuel cell production | 0.0 | 0.0 | 11.7 | 27.9 | MWh/y | |
| PV production | 0.0 | 6.2 | 6.2 | 6.2 | MWh/y | |
| imports | 24.2 | 18.4 | 4.5 | 0.0 | MWh/y | |
| exports | 0.0 | 0 | 0 | 15.1 | MWh/y | |
| <i>Heating results</i> | | | | | | |
| total heat demand | 35.5 | 35.2 | 34.8 | 35.8 | MWh/y | |
| heat pump production | 35.5 | 35.2 | 27.6 | 12.2 | MWh/y | |
| fuel cell production | 0.0 | 0.0 | 7.4 | 26.0 | MWh/y | |
| <i>Hydrogen results</i> | | | | | | |
| consumption | 0 | 0 | 496 | 1'402 | kg/y | |
| production | 0 | 0 | 0 | 0 | kg/y | |
| imports | 0 | 0 | 564 | 1'594 | kg/y | |
| exports | 0 | 10 | 10 | 10 | kg/y | |
| <i>Dual variables</i> | | | | | | |
| avg electricity value, $\bar{\lambda}^E$ | 31.85 | 29.00 (-9.0%) | 26.58 (-16.5%) | 11.96 (-62.5%) | Rp./kWh | |
| avg heat value, $\bar{\lambda}^H$ | 7.87 | 7.76 (-1.4%) | 7.08 (-10.0%) | 3.07 (-61.0%) | Rp./kWh | |

A further point of comparison, is between the hydrogen system scenario and complete system scenario for the hydrogen prices. Using the definition of coalition value developed in section 2.4, the operational cost reductions compared to the baseline scenario for each of these scenarios are shown in Table 4.4. From these coalition values, the marginal contribution ξ of adding a PV, TES, and BES to the hydrogen system scenario can be obtained for each hydrogen price. As can be seen in the table, the marginal contribution that these energy technologies provide the energy community reduces as a function of the hydrogen price. This is expected, since a lower hydrogen price makes the hydrogen system price competitive to alternative technologies. This estimation, however, is limited in providing an accurate representation of the value of each technology. A fair assessment of the value of each technology is further developed upon in section 4.3.

Table 4.4: Coalition values of the hydrogen system and complete system scenarios at three different hydrogen prices. Indicating the marginal contribution of having the complete energy system in addition to the hydrogen system.

| p^{H_2} [CHF/kg] | $v(\text{H}_2)$ | $v(\text{H}_2 \cup \{\text{TES}, \text{BES}, \text{PV}\})$ | \parallel | $\xi(\text{TES}, \text{BES}, \text{PV})$ |
|---------------------------|-----------------|--|-------------|--|
| current: 10 | 0 | 2,278 | | 2,278 |
| high forecast: 6 | 1,187 | 2,874 | | 1,687 |
| low forecast: 2 | 5,573 | 6,427 | | 854 |

4.2 Multi-agent distributed coordination

The last section presented the results for the optimal operation of the complete energy system, consisting of three energy consumers and multiple energy technologies, as indicated in Figure 2.2. The results from the previous section were obtained using a centralised optimisation formulation, which assumes that a centralised controller has all the information from the different agents' constraints and costs. This assumption, however, implies that there is no privacy preserved by any energy agent, which in a real application may be either infeasible or undesirable. For this reason, section 2.3 formulated a distributed optimisation in which energy agents in a multi-energy community are able to maintain their privacy and a central coordinator continuously updates internal energy values to reach a feasible and near-optimal solution. In this way an electricity and heat market are internally developed in the multi-energy community. However, under a distributed optimisation limited by the information received by the central coordinator, the iterative approach of finding the optimal energy values to reach a feasible and optimal solution means that we can only *approximate* the global optimum that is obtained with the centralised optimisation.

This section presents how the distributed optimisation algorithm converges towards the optimal and feasible solution of the previous section. For this, the *complete system scenario* is modelled and solved with the methodology presented in subsection 2.3.2, which applies the Exchange ADMM algorithm to a multi-energy community.

4.2.1 Convergence to a feasible solution

The most important criteria for reaching convergence is that the solution is feasible. In this setting, feasibility means that the energy balance constraints are satisfied for all time steps t . This can be verified by observing the value of the primal residuals \mathbf{r}^E and \mathbf{r}^H over iterations. As mentioned in the methodology, the convergence of the ADMM algorithm greatly depends on the penalty parameter ρ . To explore the impact of the penalty parameters, multiple optimisations are solved, with different values and combinations of ρ^E and ρ^H .

Figure 4.21 and Figure 4.22 present the ℓ_1 -norm of the electricity and heat primal residuals, respectively. The ℓ_1 -norm of the primal residuals represents the cumulative absolute deviation over one year in the respective energy balance constraints. The shaded

regions indicate when the stopping criteria for the primal residual have been met, i.e. $\|\mathbf{r}^v\|_1 \leq \epsilon^{\text{pri}} = 10$, which means that over the 8'760 periods, there is a cumulative deviation of 10 kWh. Comparing this value to the electricity and heat consumptions shown in previous sections, this represents around a 0.01-0.05% deviation from the total yearly demand. As seen in both figures, this criterion is met by some penalty parameter combinations at around iteration $k = 30$. In fact, for the (ρ^H, ρ^E) combination (0.1, 0.1), this criteria is satisfied for both primal residuals by iteration $k = 29$.

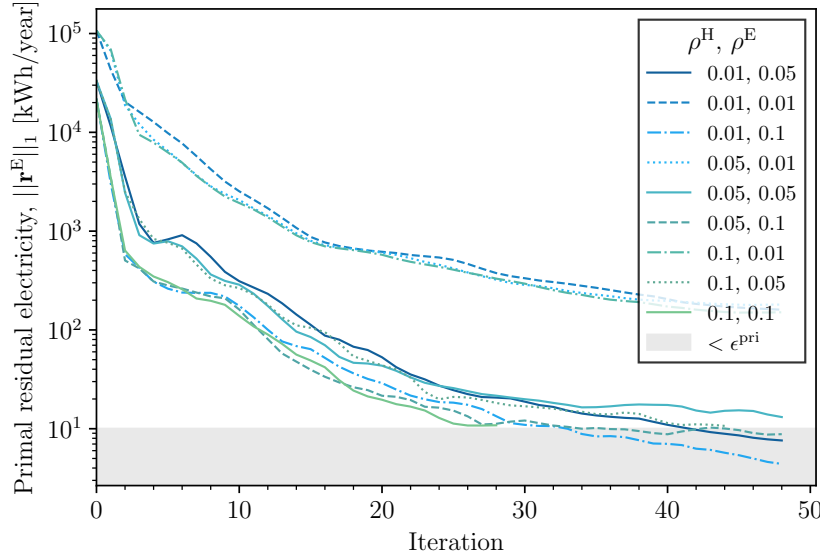


Figure 4.21: Plot of the convergence of ℓ_1 -norm of the electricity primal residual over multiple iterations for the complete energy system scenario, for various combinations of heat and electricity penalty parameters.

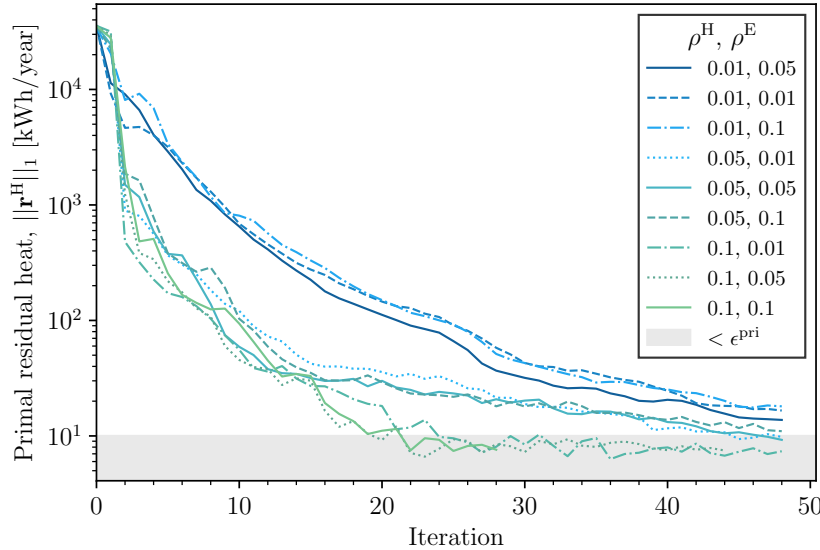


Figure 4.22: Plot of the convergence of ℓ_1 -norm of the heat primal residual over multiple iterations for the complete energy system scenario, for various combinations of heat and electricity penalty parameters.

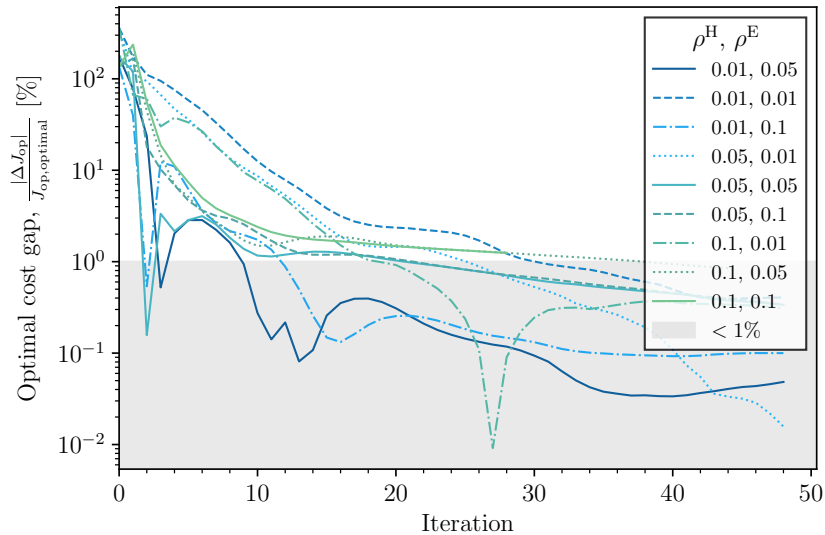


Figure 4.23: Plot of the optimal cost gap, comparing the relative difference in the operational cost from the distributed optimisations at different penalty parameters over the iterations.

4.2.2 Convergence to an optimal solution

In addition to the solution being feasible, it must also approximate the globally optimal solution. To verify the approximation to an optimal solution, Figure 4.23 presents the relative difference in percentage terms between the yearly operational cost estimated by the distributed optimisation and the one obtained from the centralised approach $J_{\text{op,optimal}}$. As is shown in the figure, most of the penalty parameter combinations fall within 1% difference from the optimal solution before reaching $k = 30$ iterations, with some of them reaching 0.1% by that same number of iterations.

Remarks on the optimal operating region with a local energy market

In section 4.1, the optimal operating regions for hydrogen technologies were analysed and verified with the results obtained. Furthermore, the optimal operating regions were approximated based on the hydrogen-to-electricity price ratio Φ . This approximation was necessary because the internal energy values for a multi-energy community are unknown when solving the problem with a centralised approach. However, in a setting where local energy markets are formed, the internal energy values become explicit, as they are broadcast by the central coordinator over each iteration to all energy agents. Therefore, the optimal operating region expressed in terms of the electricity and heat values can now provide the operators of hydrogen technologies with a viable mechanism for deciding whether or not to operate their devices and at which load (if the efficiencies at partial loads are known).

Computational time

An important indicator of the applicability of the presented distributed optimisation as a viable algorithm to be used in real applications is the computational burden. The CPU execution time to solve the *complete system scenario* with the centralised optimisation approach was of 28 seconds. In comparison, the total CPU execution time to reach the allowable tolerances for the distributed approach with $(\rho^H, \rho^E) = (0.1, 0.1)$ was of 455 seconds. However, each agent's optimisation was solved sequentially using one machine in this case. In a real application, each agent's optimisation would be solved in parallel, which implies that the total time to reach convergence would be shorter⁷. In this scenario, there are 8 agents. Therefore, the CPU execution time per agent for the distributed optimisation approach is 57 seconds, comparable to the time to solve the centralised optimisation.

A standard modification in the ADMM algorithm to improve the convergence and computational time, and to reduce the reliance on the initial choice of a penalty parameter, is to implement a dynamic penalty parameter that updates its value over each iteration [39] [40]. This direction was also explored in this work, implementing the simple update mechanism shown in Equation 4.15 [26]. However, the convergence results of this algorithm did not yield an improved convergence compared to the constant penalty parameters. For this reason, these results are excluded from this work. A refined hyper-parameter choice or a different update mechanism could improve this.

$$\rho^{v,k+1} := \begin{cases} \tau\rho^{v,k}, & \text{if } \|\mathbf{r}^k\|_2 > \mu\|\mathbf{s}^k\|_2 \\ \rho^{v,k}/\tau, & \text{if } \|\mathbf{s}^k\|_2 > \mu\|\mathbf{r}^k\|_2 \\ \rho^{v,k}, & \text{otherwise} \end{cases} \quad (4.15)$$

All optimisation scenarios and simulations were solved using Gurobi as a solver, with the CVXPY package for Python, in a MacBook Air with the M2 chip (8-core CPU, 16 GB of RAM).

4.3 Economics assessment results

This section presents the results regarding the economic assessment for the energy technologies modelled in the multi-energy community. As mentioned in Chapter 2, the FOCS value of an energy technology provides a fair estimation of its contribution towards the operational cost savings that the technology provides to a multi-energy community.

4.3.1 FOCS values

The FOCS values for the technologies in the complete energy system for the three different hydrogen price scenarios are shown in Figure 4.24. The numerical results including the

⁷Some additional time might be spent for additional processes, such as communication across devices. However, this analysis falls beyond the scope of this work.

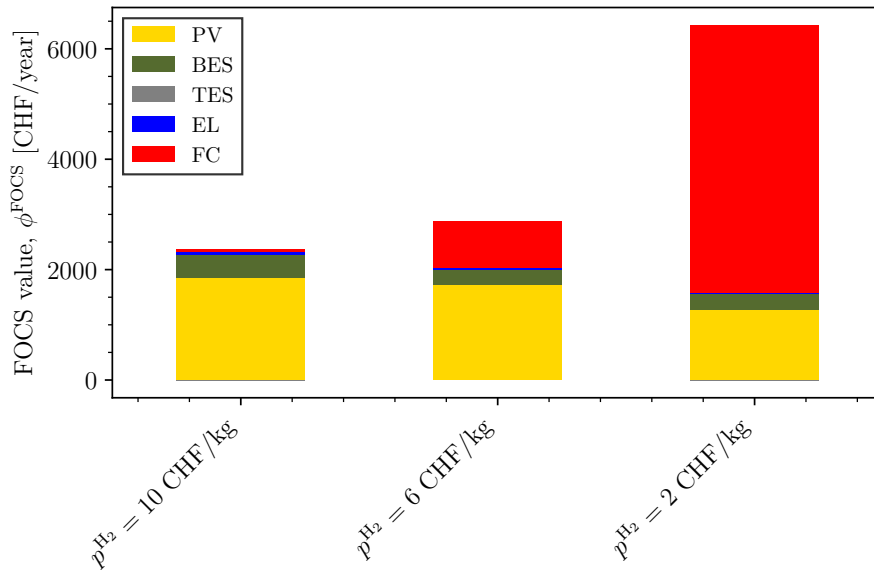


Figure 4.24: Comparison of the fair operational cost savings of each technology for the different hydrogen prices scenarios.

absolute FOCS values of the technologies and their values in specific terms are shown in Table 4.5. At the current hydrogen prices, PV provides the highest contribution to cost reduction of the energy technologies, with a value of 78% of the total cost savings. At the lowest hydrogen price, however, the FC becomes the technology with the highest contribution, with 78% of the total cost savings.

The specific FOCS value of a technology is its absolute FOCS values normalised by its total installed capacity in the system. These value is useful to understand what is the estimated value of a unit of capacity of the technology, e.g. how much is a squared meter of PV worth to the energy community?

Impact of H_2 prices

As could already be observed in the results shown in Table 4.5, the FOCS value of each technology changes at different hydrogen prices. Figure 4.25 shows the FOCS value of each technology as a function of the hydrogen-to-electricity price ratio (using the low tariff electricity price). As expected, the fuel cell becomes increasingly valuable at low ratios, since it is now profitable to convert hydrogen to electricity for self-consumption and eventually exports. In contrast, the value of PV decreases at these low price ratios. This negative correlation can be interpreted as a *negative synergy* between these technologies. As the fuel cell is able to cover the electricity demands of the energy community at lower costs, the addition of a PV system becomes less valuable for a community. The understanding of such negative synergies is relevant at the moment of making investment decisions, since it might impact the revenue share of a technology and thus the long-term profitability of the investment. In this case, at the low forecast scenario the value of the PV system is 32% lower compared to its value in the current prices scenario. Similarly,

Table 4.5: Comparison of the FOCS values obtained for each technology under the complete system scenario with three different prices for hydrogen. The values are presented in absolute and in percentage term. The percentages in parenthesis indicate the relative difference to the baseline scenario.

| Technology | Complete system scenario | | | Units |
|---|--------------------------|----------------|----------------|----------------------------|
| | Current | High forecast | Low forecast | |
| | 10 CHF/kg | 6 CHF/kg | 2 CHF/kg | |
| <i>Absolute values</i> | | | | |
| PV | 1'854 | 1'722 | 1'261 | CHF/y |
| BES | 410 | 274 | 307 | CHF/y |
| TES | 0 | 0 | 0 | CHF/y |
| EL | 63 | 34 | 10 | CHF/y |
| FC | 51 | 843 | 4'849 | CHF/y |
| Total cost savings ΔJ_{op} | 2'378 (-32.1%) | 2'874 (-38.8%) | 6'427 (-86.6%) | CHF/y |
| <i>Specific values</i> | | | | |
| PV | 61.8 | 57.4 | 42.0 | CHF/(y·m ²) |
| BES | 13.7 | 9.1 | 10.2 | CHF/(y·kWh) |
| TES | 0.0 | 0.0 | 0.0 | CHF/(y·kWh) |
| EL | 6.3 | 3.4 | 1.0 | CHF/(y·kW _{in}) |
| FC | 10.1 | 168.6 | 969.8 | CHF/(y·kW _{out}) |

the BES also becomes less valuable as the price of hydrogen decreases, reduced by 25% of its original value.

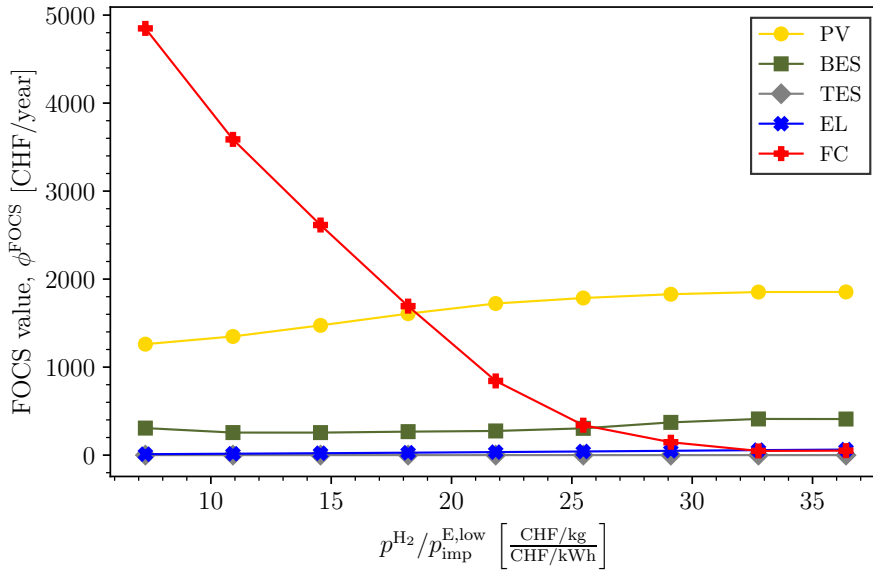


Figure 4.25: Plot of the fair operational cost saving values for each technology in the complete system scenario at different hydrogen-to-electricity import prices.

Impact of PV capacity

Another important design parameter with a large impact on the FOCS values of technologies, is the PV installed capacity. First of all, it is expected that there are decreasing marginal returns on the continuous expansion of the PV area for the value of PV. This is because as the PV area becomes larger, there are lower opportunities for cost savings. An inverse relationship can be expected in the FOCS value of the BES. As there is the PV capacity increases, an additional capacity of BES becomes more valuable, since there is additional zero marginal cost electricity that can be leveraged with the temporal flexibility a battery provides.

To evaluate this impact, the FOCS values of all technologies were evaluated at a range of increasing PV capacities. Figure 4.26 shows the specific FOCS values of PV and of the BES as a function of this increase in PV capacity. As can be observed, when the PV capacity is doubled from the 30 m^2 to 60 m^2 , the specific PV FOCS value decreases by 13%, meaning that a m^2 of PV is now 13% less valuable on average. In contrast, the specific FOCS value of BES increased by 20% as the PV capacity doubled.

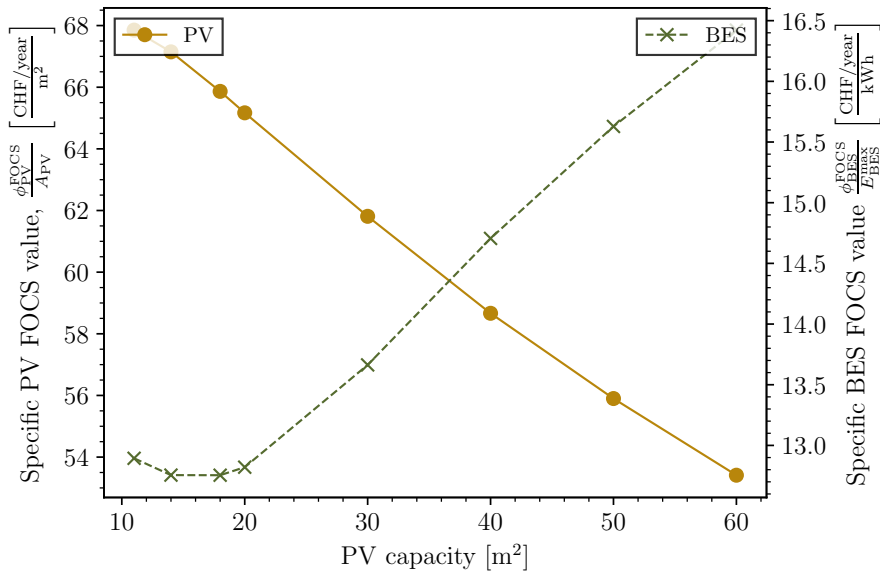


Figure 4.26: Plot of the specific fair operational cost saving values for PV and BES for different PV installed capacities.

Energy storage alternatives

An interesting observation in the results provided so far, is that the TES seems to provide no value to the community in terms of cost reduction. As this technology mainly provides an option for temporal flexibility, a reason for this could be that in the current setting, other energy storage alternatives provide the energy system with more valuable flexibility than *outcompetes* the TES alternative. To verify this claim the FOCS values of the TES and BES were calculated in combinations of the BES being excluded from the system $\mathcal{S} \setminus \{BES\}$, BES being included in the system $\mathcal{S} \cup \{BES\}$, inflexible temperature range

from consumers $\Delta T = 0.1^\circ\text{C}$ (as explored in section 4.1), and the normal temperature range $\Delta T = 5^\circ\text{C}$. The results for both the BES and the TES in terms of their specific FOCS values for the combination of these scenarios are shown in Table 4.6. As can be seen from the results, the value of TES remains zero even when the battery is removed. The only scenario where the TES provides value to the system is when the flexibility of the heating demand from consumers is further constrained by $\Delta T = 0.1^\circ\text{C}$. In this setting, the exclusion of the BES increases the value of TES by 55%, reaching 1.4 CHF/kWh.

Table 4.6: *Specific fair operational cost saving values for BES and TES for combinations of inflexible and flexible heating demand, and an energy system excluding and including a BES.*

| | | $\Delta T = 0.1^\circ\text{C}$ | $\Delta T = 5^\circ\text{C}$ |
|---|--|--------------------------------|------------------------------|
| $\frac{\phi_{\text{BES}}^{\text{FOCS}}}{E_{\text{BES}}^{\max}}$ | $\mathcal{S} \setminus \{\text{BES}\}$ | (0, 1.4) | (0, 0) |
| $\frac{\phi_{\text{TES}}^{\text{FOCS}}}{E_{\text{TES}}^{\max}}$ | $\mathcal{S} \cup \{\text{BES}\}$ | (14.5, 0.9) | (13.6, 0) |

4.3.2 Investment prioritisation

The economic assessment thus far focuses on the operational cost savings of the energy technologies. While this provides valuable insights, it does not encompass all economically relevant factors. For a multi-energy community, practical guidance is better achieved by prioritising capital investments that yield the greatest overall economic benefits. To this end, it is essential to consider not only operational cost savings but also the investment costs, operation and maintenance (O&M) costs, and the expected lifetime of each technology. The analysis incorporates these factors by calculating the NPV and IRR for each technology under different hydrogen price scenarios, with the results presented in Table 4.7⁸.

The results show that the PV system remains a profitable investment across all three scenarios, although its NPV decreases by 77% in the low hydrogen price scenario compared to the current price scenario. The BES and EL remain unprofitable investments throughout all three scenarios. Meanwhile, the fuel cell becomes a profitable investment in the low hydrogen price scenario, with a substantial IRR of 55%. However, in the high price forecast scenario, the fuel cell is unprofitable, even though, as noted in previous sections, it significantly contributes to reducing electricity imports. This underscores the importance of an economic assessment that includes the additional costs of technologies. Despite their potential to substantially reduce costs for a multi-energy community, their investment and O&M costs might render these ventures unprofitable.

Furthermore, the economic viability of these technologies is assessed across three scenarios of installed photovoltaic capacity—10, 30, and 60 m²—to explore the impact of system design choices. The corresponding results are summarised in Table 4.8. As expected, the NPV of PV increases with a larger installed capacity, however, the IRR

⁸TES is excluded from the analysis since the FOCS values calculated are zero for all scenarios.

Table 4.7: Comparison of net present values and internal rates of return of multiple energy technologies for three different hydrogen price scenarios. IRR values for some technologies are missing because their FOCS values are too low to compute an internal rate of return.

| Technology | Complete system scenario | | |
|---------------------------------|--------------------------|---------------------------|--------------------------|
| | Current 10 CHF/kg | High forecast 6 CHF/kg | Low forecast 2 CHF/kg |
| | 10 CHF/kg | 6 CHF/kg | 2 CHF/kg |
| <i>Net present values</i> | | | |
| PV | 9'868 | 8'182 | 2'279 |
| BES | -6'006 | -7'560 | -7'186 |
| TES (<i>excluded</i>) | - | - | - |
| EL | -17'427 | -17'757 | -18'029 |
| FC | -10'924 | -3'559 | 33'676 |
| <i>Internal rates of return</i> | | | |
| PV | 13% | 12% | 8% |
| BES | -6% | -12% | -10% |
| TES (<i>excluded</i>) | - | - | - |
| EL | - | - | - |
| FC | - | -2% | 54% |

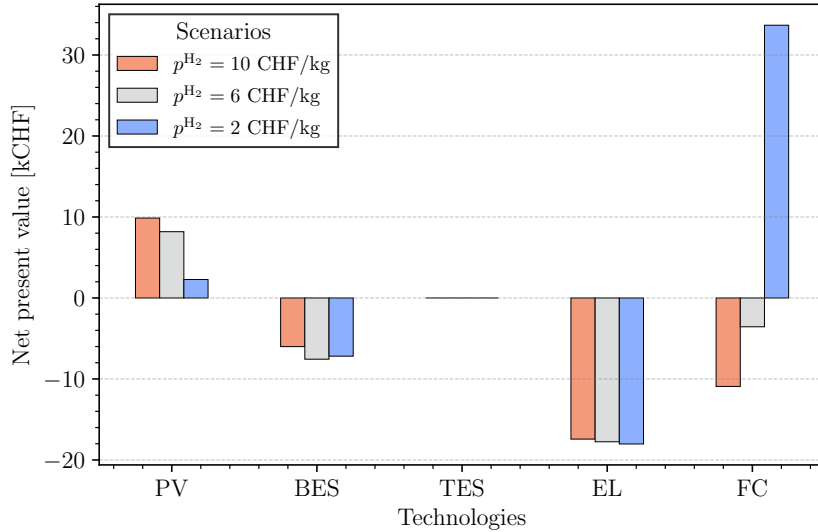


Figure 4.27: Net present value of investments into different energy technologies for different hydrogen price scenarios.

decreases, which reflects the decreasing marginal value of additional PV capacity as seen in Figure 4.26. All other technologies remain unprofitable throughout the modelled scenarios.

Table 4.8: Comparison of net present values and internal rates of return of multiple energy technologies for three different PV installed capacities. IRR values for some technologies are missing because their FOCS values are too low to compute an internal rate of return.

| Technology | PV Capacity | | |
|---------------------------------|---------------------------|---------------------------|---------------------------|
| | $A_{PV} = 10 \text{ m}^2$ | $A_{PV} = 30 \text{ m}^2$ | $A_{PV} = 60 \text{ m}^2$ |
| <i>Net present values</i> | | | |
| PV | 4'264 | 9'868 | 14'290 |
| BES | -6'271 | -6'006 | -5'057 |
| TES (<i>excluded</i>) | - | - | - |
| EL | -17'574 | -17'427 | -16'642 |
| FC | -10'926 | -10'924 | -10'917 |
| <i>Internal rates of return</i> | | | |
| PV | 15% | 13% | 11% |
| BES | -6% | -6% | -3% |
| TES (<i>excluded</i>) | - | - | - |
| EL | - | - | - |
| FC | - | - | - |

Chapter 5

Conclusion & Discussion

The final chapter of this report begins by presenting the main conclusions in relation to the research questions and develops on the main contributions of this thesis. Lastly, it discusses this work's limitations and suggests further research directions.

5.1 Conclusions

Energy communities are gaining prominence as key players in the energy transition, offering opportunities for localised energy management that enhances efficiency and reduces costs. These communities, which enable citizens to manage their energy production and consumption, also offer flexibility to energy suppliers. Additionally, decentralised DHNs are a promising solution for decarbonising the heating sector by integrating renewable heat sources, and allowing the reutilisation of waste heat. Moreover, introducing hydrogen technologies with WHR into energy communities with a decentralised DHN can further reduce energy costs when certain conditions are met. This thesis has addressed several aspects of energy communities and the integration of waste heat from hydrogen technologies, contributing to a deeper understanding of their potential within the energy transition.

Through the exploration of key research questions, the work has investigated the dynamic valuation of heat, the economic potential of hydrogen waste heat recovery, optimal coordination in multi-agent, multi-energy communities, and the comparative economic benefits of different energy technologies. For this exploration, a model was developed of a multi-energy community with multiple energy technologies. Their operation was optimised for a one year period such as to satisfy the community's energy demands. Multiple different scenarios were simulated with varying parameters, boundary conditions, and system configurations. In a simple energy system which only consists of a heat pump to satisfy the heat demand, the results underscore two significant characteristics: low demand flexibility and a high correlation between the heat value and electricity prices. The inflexibility of demand, especially under strict temperature range constraints, leads to higher operational costs. Additionally, the heat value is lower bounded by electricity prices, limiting the cost reduction potential. However, adding a hydrogen system with

WHR has the potential to increase the system's flexibility and reduce operational cost under certain conditions.

Hydrogen technologies become optimal to operate when the energy values in an energy system are within their *optimal operating regions*. These regions are determined by external and internal factors such as hydrogen prices and electrochemical efficiencies, which determine the energy values achieved by the systems. Conversely, with the energy values of an energy system one can evaluate whether operating hydrogen technologies is optimal at a certain period. The optimal frontiers that define these optimal operating regions determine the energy values that can be achieved in a multi-energy community which can further reduce operational costs. As an alternative to energy values, the hydrogen-to-electricity price ratios can be used as an approximation of the boundary that determines when a hydrogen technology becomes optimal to operate. It was found that the presence of a WHR system broadens the optimal operating region, making it easier for the hydrogen technologies to become economically viable. In contrast, when no WHR is available, the operating regions become more constrained, requiring a higher price ratio for the electrolyser and a lower one for the fuel cell, reducing the economic potential of hydrogen technologies for an energy community.

In a multi-agent, multi-energy community reaching the globally optimal solution with a centralised optimisation assumes complete information sharing among agents, which may be undesirable in practical applications. Additionally, adding new energy agents to the optimisation may bring computational challenges and requires the reformulation of an optimisation problem. To address this, a distributed optimisation approach using the exchange ADMM algorithm was formulated, where energy agents maintain privacy while a central coordinator updates internal energy values iteratively to achieve a feasible and near-optimal solution. The results demonstrate that the distributed optimisation approach converges to the globally optimal solution in comparable computational time to the centralised approach. Additionally, the distributed optimisation allows for the explicit determination of internal energy values, simulating a dual, local energy market for heat and electricity which is solved in tandem. Making the internal energy values transparent to energy agents enables them to make informed decisions with knowledge about the optimal operation of energy technologies.

To quantify the value that an energy technology provides to an energy community, a fair estimation based on the Shapley value is developed, referred to as the Fair Operational Cost Savings (FOCS) value. The analysis explores the change in value of technologies over varying boundary conditions. For instance, PV contributes the most to cost reduction under current hydrogen prices, while the fuel cell becomes more valuable as hydrogen prices decrease. The study also highlights synergies across technologies and the impact of system design choices, such as the capacity of PV installations, on the economic value of each technology; for example, as PV capacity increases, the value of a battery energy storage system rises due to the increased availability of low-cost electricity. With a fair quantification of the operational cost value of energy technologies and information regarding their investment costs, the study assesses the profitability of investment alternatives and the impact by different boundary conditions.

In conclusion, the primary contributions of this thesis include the development of a model for assessing the dynamic value of heat and its integration with waste heat, a comprehensive analysis of hydrogen technologies' operational dynamics, the formulation of a distributed, optimal coordination mechanism for multi-agent energy systems, and the quantification of operational cost savings across multiple energy agents. These findings offer valuable insights into the design and operation of more efficient and sustainable distributed energy systems, highlighting the role of local resources and the potential for energy communities to drive the decarbonisation of heating and electricity supply.

5.2 Limitations & future work

This work examined the impact on the value of heat in an energy community when hydrogen technologies with waste heat recovery are integrated into the energy system. However, there are multiple sources of excess heat with the potential to meet a significant share of heating demand, such as energy-intensive industries and data centres, which generate heat through server cooling. The economic feasibility of incorporating these technologies within a multi-energy community could provide an additional basis for comparing the value of waste heat recovery from hydrogen technologies. Furthermore, the optimal operating regions of energy technologies beyond hydrogen technologies could be defined in terms of energy values within a multi-energy community, potentially leading to the formulation of an energy value region over which the system can operate.

The modelled scenarios could also be extended beyond the assumption of constant hydrogen prices. Alternative boundary conditions, such as variable hydrogen prices or hourly and sub-hourly electricity import tariffs, could significantly influence the economic value of flexibility-enabling technologies within the system. Additionally, other sources of revenue for an energy community could be explored, such as remuneration from grid operators for providing ancillary services or establishing external connections, for example, to a larger district heating network beyond the community's boundaries.

Furthermore, this work formulated and examined the boundary conditions and internal energy values that make hydrogen technologies valuable and a profitable investment. However, this work did not investigate the feasibility of reaching these conditions in a multi-energy community. Further work could look at the long-term evaluation of the value of these technologies considering an energy system configuration that responds to energy prices. Additionally, a probabilistic assessment could shed a light on the impact of the uncertainty in energy prices in the value of hydrogen technologies in the future.

The agent-based distributed optimisation simulating a local energy market could be further developed in several directions. For instance, the exploration of optimal penalty parameters in this work was restricted to constant parameter combinations; however, dynamic penalty parameters may improve convergence performance. Moreover, this study assumes all energy agents include a penalty term in their optimisation functions to achieve convergence, but this may not always be enforceable. This raises the question of how uncooperative agents could impact the system. Additionally, this work did not investigate

the implementation of such a coordination mechanism in a real-world setting, which presents another avenue for future research.

Further analysis of the economic assessment of technologies based on their fair operational cost savings is also warranted. As noted, numerous factors can influence the valuation of a technology, such as energy prices, system configurations, and technical parameters. While this study focused on varying hydrogen-to-electricity price ratios and the capacities of specific technologies, it did not account for other factors, such as learning curves. More comprehensive sensitivity analyses incorporating these elements could provide a deeper understanding of the economic potential of energy technologies in future scenarios.

Bibliography

- [1] IEA. Empowering people – the role of local energy communities in clean energy transitions, 2023.
- [2] European Commission. Energy communities, 2024.
- [3] Hans Christian Gils. Assessment of the theoretical demand response potential in Europe. *Energy*, 67, 2014.
- [4] Inês Campos and Esther Marín-González. People in transitions: Energy citizenship, prosumerism and social movements in Europe. *Energy Research and Social Science*, 69, 2020.
- [5] Federal Statistical Office. Households and climate from the perspective of environmental accounts. Technical report, BFS, Neuchatel, 2 2022.
- [6] Hanmin Cai, Philipp Heer, Philipp Schütz, Lucas Miehé, Gabriela Hug, Carlo Tajoli, Dominik Born, and Julien Marquant. Nanoverbund. Technical report, Swiss Federal Office of Energy, Bern, 6 2024.
- [7] Swiss Federal Office of Energy. Federal act on a secure electricity supply.
- [8] Ieva Pakere, Dagnija Blumberga, Anna Volkova, Kertu Lepiksaar, and Agate Zirne. Valorisation of Waste Heat in Existing and Future District Heating Systems. *Energies*, 16(19), 2023.
- [9] Hailong Li, Qie Sun, Qi Zhang, and Fredrik Wallin. A review of the pricing mechanisms for district heating systems. *Renewable and Sustainable Energy Reviews*, 42:56–65, 2 2015.
- [10] Lisa Brange, Jessica Englund, and Patrick Lauenburg. Prosumers in district heating networks – A Swedish case study. *Applied Energy*, 164:492–500, 2 2016.
- [11] Linde Frölke, Ida Marie Palm, and Jalal Kazempour. Market integration of excess heat. *Electric Power Systems Research*, 212:108459, 11 2022.
- [12] Tabbi Wilberforce, A. G. Olabi, Imran Muhammad, Abed Alaswad, Enas Taha Sayed, Ahmed G. Abo-Khalil, Hussein M. Maghrabie, Khaled Elsaid, and Mohammad Ali Abdelkareem. Recovery of waste heat from proton exchange membrane fuel cells – A review. *International Journal of Hydrogen Energy*, 52:933–972, 1 2024.

- [13] Ana María Villarreal Vives, Ruiqi Wang, Sumit Roy, and Andrew Smallbone. Techno-economic analysis of large-scale green hydrogen production and storage. *Applied Energy*, 346:121333, 9 2023.
- [14] Harikishan R. Ellamla, Iain Staffell, Piotr Bujlo, Bruno G. Pollet, and Sivakumar Pasupathi. Current status of fuel cell based combined heat and power systems for residential sector. *Journal of Power Sources*, 293:312–328, 10 2015.
- [15] N. Briguglio, M. Ferraro, G. Brunaccini, and V. Antonucci. Evaluation of a low temperature fuel cell system for residential CHP. *International Journal of Hydrogen Energy*, 36(13):8023–8029, 7 2011.
- [16] W J Tiktak. Heat Management of PEM Electrolysis, 2021.
- [17] Els van der Roest, Ron Bol, Theo Fens, and Ad van Wijk. Utilisation of waste heat from PEM electrolyzers – Unlocking local optimisation. *International Journal of Hydrogen Energy*, 48(72):27872–27891, 8 2023.
- [18] Qiwei Qin and Louis Gosselin. Community-based transactive energy market concept for 5th generation district heating and cooling through distributed optimization. *Applied Energy*, 371:123666, 10 2024.
- [19] Paolo Gabrielli, Ben Flamm, Annika Eichler, Matteo Gazzani, John Lygeros, and Marco Mazzotti. Modeling for optimal operation of PEM fuel cells and electrolyzers. In *EEEIC 2016 - International Conference on Environment and Electrical Engineering*, 2016.
- [20] Manuel Tobias Baumhof, Enrica Raheli, Andrea Gloppen Johnsen, and Jalal Kazem-pour. Optimization of Hybrid Power Plants: When is a Detailed Electrolyzer Model Necessary? In *2023 IEEE Belgrade PowerTech, PowerTech 2023*, 2023.
- [21] Feras Alshehri, Víctor García Suárez, José L. Rueda Torres, Arcadio Perilla, and M. A.M.M. van der Meijden. Modelling and evaluation of PEM hydrogen technologies for frequency ancillary services in future multi-energy sustainable power systems. *Heliyon*, 5(4):e01396, 4 2019.
- [22] M. Minutillo, A. Perna, A. Forcina, S. Di Micco, and E. Jannelli. Analyzing the levelized cost of hydrogen in refueling stations with on-site hydrogen production via water electrolysis in the Italian scenario. *International Journal of Hydrogen Energy*, 46(26):13667–13677, 4 2021.
- [23] Yi Zheng, Shi You, Henrik W. Bindner, and Marie Münster. Optimal day-ahead dispatch of an alkaline electrolyser system concerning thermal–electric properties and state-transitional dynamics. *Applied Energy*, 307:118091, 2 2022.
- [24] Alexander Engelmann, Sungho Shin, François Pacaud, and Victor Zavala. Scalable Primal Decomposition Schemes for Large-Scale Infrastructure Networks. 4 2023.
- [25] Hanmin Cai, Shi You, and Jianzhong Wu. Agent-based distributed demand response in district heating systems. *Applied Energy*, 262:114403, 3 2020.

- [26] Stephen Boyd, Neal Parikh, Eric Chu, Borja Peleato, and Jonathan Eckstein. Distributed Optimization and Statistical Learning via the Alternating Direction Method of Multipliers. *Foundations and Trends in Machine Learning*, 3:1–122, 12 2011.
- [27] Raquel Alonso Pedrero, Paolo Pisciella, and Pedro Crespo del Granado. Fair investment strategies in large energy communities: A scalable Shapley value approach. *Energy*, 295:131033, 5 2024.
- [28] Sho Cremers, Valentin Robu, Peter Zhang, Merlinda Andoni, Sonam Norbu, and David Flynn. Efficient methods for approximating the Shapley value for asset sharing in energy communities. *Applied Energy*, 331, 2023.
- [29] Linda K Lawrie and B Crawley Drury. Development of Global Typical Meteorological Years (TMYx). 2022.
- [30] IWB. Strom Tarif- und Preisübersicht, 2023.
- [31] ENTSO-E. ENTSO-E Transparency Platform, 2024.
- [32] G Humbert. H2districts – WP4 - Milestone MS4: Techno-economic cases to be investigated. 2024.
- [33] Marius Schwarz, Matthieu Boubat, Arijit Upadhyay, Pascal Geistlich, Jared Garrison, Christian Schaffner, and Jonas Savelsberg. The role of synthetic fuels in a net-zero emission electricity system in Switzerland. Technical report, ETH Zurich, Zurich, 3 2024.
- [34] Evangelos Panos and Kannan Ramachandran. Space heating, process heat, water heating, air conditioning and other electric appliances (e.g. refrigerators, ovens, information&communication technologies, washers and dryers,etc.) hourly profile by typical day and sector - Assumption in STEM model, 2 2019.
- [35] Bernadino Bernadino. Economic and Environmental Assessment of Heat Prosumer Communities. Technical report, ETH Zurich, Zurich, 2023.
- [36] European Standard. EN 15251: Indoor environmental input parameters for design and assessment of energy performance of buildings addressing indoor air quality, thermal environment, lighting and acoustics. Technical report, 2006.
- [37] Paolo Marocco, Domenico Ferrero, Emanuele Martelli, Massimo Santarelli, and Andrea Lanzini. An MILP approach for the optimal design of renewable battery-hydrogen energy systems for off-grid insular communities. *Energy Conversion and Management*, 245:114564, 10 2021.
- [38] EMPA. Data from MOVE demonstrator, 2024.
- [39] P. M.R. Bento, S. J.P.S. Mariano, M. R.A. Calado, and L. A.F.M. Ferreira. A novel lagrangian multiplier update algorithm for short-term hydro-thermal coordination †. *Energies*, 13(24), 2020.

- [40] N. Jiménez Redondo and A. J. Conejo. Short-term hydro-thermal coordination by lagrangian relaxation: solution of the dual problem. *IEEE Transactions on Power Systems*, 14(1), 1999.
- [41] Christian Holzner, Martin Michel, and Christian Schaffner. Grundlagen Energieversorgungssicherheit. Bericht zur Energiestrategie 2050. *Swiss Energy Strategy 2050*, 2012.
- [42] Ivalin Petkov and Paolo Gabrielli. Power-to-hydrogen as seasonal energy storage: an uncertainty analysis for optimal design of low-carbon multi-energy systems. *Applied Energy*, 274:115197, 9 2020.
- [43] Manuel Prinzing, Matthias Berthold, Stefan Bertsch, and Mick Eschmann. Feldmessungen von Wärmepumpen-Anlagen Heizsaison 2020/21. Technical report, 2021.
- [44] Thomas Marti, Matthias Sulzer, Martin Rüdisüli, Christian Opitz, Elliot Romano, Julien Marquant, Kristina Orehounig, Mashael Yazdanie, Michael Schuerle, Natasa Vulic, Philipp Heer, Robin Muttschler, Sven Eggimann, Youssef Sherif, and Urs Elber. ENERGIEVERSORGUNG DER SCHWEIZ BIS 2050 Zusammenfassung von Ergebnissen und Grundlagen. 12 2022.
- [45] Alicia Lerbinger, Ivalin Petkov, Georgios Mavromatidis, and Christof Knoeri. Optimal decarbonization strategies for existing districts considering energy systems and retrofits. *Applied Energy*, 352, 2023.

Appendix A

Optimisation problems

This chapter contains the centralised and distributed formulations of the optimisation problem to minimise total operational costs of a multi-energy community.

A.1 Centralised optimisation

This section of the appendix formulates the optimisation problem to minimise the total operational costs for a multi-energy community with a centralised approach. The first part expresses the objective function and the second part formulates the constraints.

A.1.1 Objective function

$$\underset{\mathcal{V}_{\text{tot}}, \mathcal{V}_{\text{slack}}}{\text{minimize}} \quad \mathcal{J}_{\text{tot}} + \mathcal{J}_{\text{slack}} \quad (\text{A.1})$$

$$\begin{aligned} J_{\text{tot}} &= \sum_{t \in \mathcal{T}} \left(P_{\text{imp}}(t) p_{\text{imp}}^{\text{E}}(t) + \dot{m}_{\text{H}_2, \text{imp}}(t) p^{\text{H}_2}(t) - P_{\text{exp}}(t) p_{\text{exp}}^{\text{E}}(t) - \dot{m}_{\text{H}_2, \text{exp}}(t) p^{\text{H}_2}(t) \right) \Delta t \\ J_{\text{slack}} &= \sum_{t \in \mathcal{T}} \left(\zeta_{\text{slack}} \sum_{c \in \mathcal{C}} T_{\text{slack},c}(t) \right) \end{aligned}$$

$$\mathcal{V}_{\text{tot}} = \{P_{\text{imp}}(t), P_{\text{exp}}(t), \dot{m}_{\text{H}_2, \text{imp}}(t), \dot{m}_{\text{H}_2, \text{exp}}(t)\} \quad \forall t$$

$$\mathcal{V}_{\text{slack}} = \{T_{\text{slack},c}(t)\} \quad \forall t, \forall c$$

A.1.2 Constraints

Energy balance

$$Q_{\text{HP}}(t) + Q_{\text{H}_2}(t) = Q_{\text{TES,net}}(t) + \sum_{c \in \mathcal{C}} Q_{\text{cons},c}(t) + Q_{\text{slack}}(t), \quad : \lambda^{\text{H}}(t), \quad \forall t$$

$$\begin{aligned} P_{\text{imp}}(t) + P_{\text{PV}}(t) + P_{\text{FC}}(t) + &= \\ P_{\text{exp}}(t) + P_{\text{H}_2}(t) + P_{\text{HP}}(t) + P_{\text{BES,net}}(t) + \sum_{c \in \mathcal{C}} P_{\text{cons},c}(t), & : \lambda^{\text{E}}(t) \quad \forall t \end{aligned}$$

Connection constraints

$$\begin{aligned} P_{\text{imp}}(t) &\leq P_{\text{imp}}^{\max}, & \forall t \\ P_{\text{exp}}(t) &\leq P_{\text{exp}}^{\max}, & \forall t \\ \dot{m}_{\text{H}_2,\text{imp}}(t) &\leq \dot{m}_{\text{H}_2,\text{imp}}^{\max}, & \forall t \\ \dot{m}_{\text{H}_2,\text{exp}}(t) &\leq \dot{m}_{\text{H}_2,\text{exp}}^{\max}, & \forall t \end{aligned}$$

Hydrogen system balance at nodes

$$\begin{aligned} P_{\text{H}_2}(t) &= P_{\text{EL}}(t) + P_{\text{CO}}(t), & \forall t \\ Q_{\text{H}_2}(t) &= Q_{\text{EL,used}}(t) + Q_{\text{FC,used}}(t), & \forall t \end{aligned}$$

Electrolyser constraints

$$\begin{aligned} P_{\text{EL}}(t) &\leq P_{\text{EL}}^{\max}, & \forall t \\ Q_{\text{EL,total}}(t) &= (P_{\text{EL}}(t) - \dot{m}_{\text{H}_2,\text{EK}}(t)\text{HHV}_{\text{H}_2}) \eta_{\text{EL,th}}, & \forall t \\ Q_{\text{EL,total}}(t) &= Q_{\text{EL,used}}(t) + Q_{\text{EL,waste}}(t), & \forall t \\ \frac{\dot{m}_{\text{H}_2,\text{EL}}(t)\text{HHV}_{\text{H}_2}}{P_{\text{EL}}^{\max}} &\leq \alpha_{\text{EL},j} + \beta_{\text{EL},j} \frac{P_{\text{EL}}(t)}{P_{\text{EL}}^{\max}}, & \forall j \in [1, n+1], \forall t \end{aligned}$$

Fuel cell constraints

$$\begin{aligned}
P_{\text{FC}}(t) &\leq P_{\text{FC}}^{\max}, & \forall t \\
\dot{m}_{\text{H}_2,\text{FC}}(t) &\leq \dot{m}_{\text{H}_2,\text{FC}}^{\max}, & \forall t \\
Q_{\text{FC},\text{total}}(t) &= (\dot{m}_{\text{H}_2,\text{FC}}(t)\text{HHV}_{\text{H}_2} - P_{\text{FC}}(t))\eta_{\text{FC},\text{th}}, & \forall t \\
Q_{\text{FC},\text{total}}(t) &= Q_{\text{FC},\text{used}}(t) + Q_{\text{FC},\text{waste}}(t), & \forall t \\
\frac{P_{\text{FC}}(t)}{\dot{m}_{\text{H}_2,\text{FC}}^{\max}\text{HHV}_{\text{H}_2}} &\leq \alpha_{\text{FC},j} + \beta_{\text{FC},j}\frac{\dot{m}_{\text{H}_2,\text{FC}}(t)}{\dot{m}_{\text{H}_2,\text{FC}}^{\max}}, & \forall j \in [1, n+1]
\end{aligned}$$

Compressor constraints

$$\begin{aligned}
P_{\text{CO}}(t) &= \frac{RT_{\text{in}}\gamma}{M_{\text{H}_2}(\gamma-1)\eta_{\text{CO}}} \left(\left(\frac{P_{\text{out}}}{P_{\text{in}}} \right)^{\frac{\gamma-1}{\gamma}} - 1 \right) \dot{m}_{\text{H}_2,\text{EL}}(t) & \forall t \\
P_{\text{CO}}(t) &\leq P_{\text{CO}}^{\max}(t) & \forall t
\end{aligned}$$

Hydrogen storage constraints

$$\begin{aligned}
m_{\text{H}_2,\text{sto}}(t) &= m_{\text{H}_2,\text{sto}}(t-1) + \eta_{\text{H}_2,\text{sto}}\Delta t (\dot{m}_{\text{H}_2,\text{hp}}(t) + \dot{m}_{\text{H}_2,\text{imp}}(t)) - \\
&\quad \frac{\Delta t}{\eta_{\text{H}_2,\text{sto}}} (\dot{m}_{\text{H}_2,\text{exp}}(t) + \dot{m}_{\text{H}_2,\text{FC}}(t)), \quad \forall t
\end{aligned}$$

$$\begin{aligned}
m_{\text{H}_2,\text{sto}}(t) &\leq m_{\text{H}_2,\text{sto}}^{\max}, & \forall t \\
m_{\text{H}_2,\text{sto}}(t_0) &= m_{\text{H}_2,\text{sto}}^{\max}/2 \\
m_{\text{H}_2,\text{sto}}(t_f) &= m_{\text{H}_2,\text{sto}}^{\max}/2
\end{aligned}$$

Heat pump constraints

$$\begin{aligned}
Q_{\text{HP}}(t) &= P_{\text{HP}}(t)\text{COP}, & \forall t \\
Q_{\text{HP}}(t) &\leq Q_{\text{HP}}^{\max}, & \forall t
\end{aligned}$$

Thermal energy storage constraints

$$\begin{aligned}
E_{\text{TES}}(t) &= E_{\text{TES}}(t-1) [1 - \epsilon_{\text{TES}}] + \eta_{\text{TES,in}} Q_{\text{TES,in}}(t) \Delta t - \frac{1}{\eta_{\text{TES,out}}} Q_{\text{TES,out}}(t) \Delta t, & \forall t \\
0 \leq Q_{\text{TES,in}}(t) &\leq r_{\text{TES,in}}^{\max} E_{\text{TES}}(t), & \forall t \\
0 \leq Q_{\text{TES,out}}(t) &\leq r_{\text{TES,out}}^{\max} E_{\text{TES}}(t), & \forall t \\
0 \leq E_{\text{TES}}(t) &\leq E_{\text{TES}}^{\max}, & \forall t \\
Q_{\text{TES,net}}(t) &= Q_{\text{TES,in}}(t) - Q_{\text{TES,out}}(t), & \forall t \\
E_{\text{TES}}(t_0) &= \frac{E_{\text{TES}}^{\max}}{2} \\
E_{\text{TES}}(t_f) &= \frac{E_{\text{TES}}^{\max}}{2}
\end{aligned}$$

Battery energy storage constraints

$$\begin{aligned}
E_{\text{BES}}(t) &= E_{\text{BES}}(t-1) [1 - \epsilon_{\text{BES}}] + \eta_{\text{BES,ch}} P_{\text{BES,ch}}(t) \Delta t - \frac{1}{\eta_{\text{BES,dis}}} P_{\text{BES,dis}}(t) \Delta t, & \forall t \\
0 \leq P_{\text{BES,ch}}(t) &\leq r_{\text{BES,ch}}^{\max} E_{\text{BES}}(t), & \forall t \\
0 \leq P_{\text{BES,dis}}(t) &\leq r_{\text{BES,dis}}^{\max} E_{\text{BES}}(t), & \forall t \\
E_{\text{BES}}^{\min} \leq E_{\text{BES}}(t) &\leq E_{\text{BES}}^{\max}, & \forall t \\
P_{\text{BES,net}}(t) &= P_{\text{BES,ch}}(t) - P_{\text{BES,dis}}(t), & \forall t \\
E_{\text{BES}}(t_0) &= \frac{E_{\text{BES}}^{\max}}{2} \\
E_{\text{BES}}(t_f) &= \frac{E_{\text{BES}}^{\max}}{2}
\end{aligned}$$

Photovoltaic system constraints

$$P_{\text{PV}}(t) = \phi_{\text{solar}}(t) A_{\text{PV}} \eta_{\text{PV}} \Delta t, \quad \forall t$$

Consumers constraints

$$\begin{aligned}
T_c(t) &= \zeta_c T_c(t-1) + [1 - \zeta_c] [T_{\text{amb}}(t-1) + R_c [Q_{\text{cons},c}(t-1) + Q_{\text{solar},c}(t-1)]] & \forall c, \forall t \\
\zeta_c &= e^{-\frac{\Delta t}{R_c C_c}} \\
T_c(t) &\leq T_c^{\max} + T_{\text{slack},c}(t) & \forall c, \forall t \\
T_c(t) &\geq T_c^{\min} & \forall c, \forall t \\
T_c(t_0) &= T_c^{\min} & \forall c \\
P_{\text{cons},c}(t) &= \frac{1}{\Delta t} (\beta_{\text{li}}(t) L_{\text{li},c} + \beta_{\text{ea}}(t) L_{\text{ea},c}) & \forall c, \forall t
\end{aligned}$$

A.2 Distributed optimisation

This section formulates the optimisation problems for each energy agent i that is used for the distributed coordination approach using the Exchange ADMM algorithm. To simplify the expressions, the augmented Lagrangians are formulated in vectorised form. Where \mathbf{x}_i^v represents the net output of the energy carrier v (heat or electricity) by the corresponding energy agent, $\bar{\mathbf{x}}^{v,k}$ represents the average total net output of all energy agents at iteration k , and N^v is the number of energy agents that participate in the *market* of that energy carrier.

$$\mathcal{L}_{\rho,i}^H = \frac{\rho^H}{2} \left\| N^H \bar{\mathbf{x}}^{H,k} - \mathbf{x}_i^{H,k} + \mathbf{x}_i^H \right\|_2^2 \quad (\text{A.2})$$

$$\mathcal{L}_{\rho,i}^E = \frac{\rho^E}{2} \left\| N^E \bar{\mathbf{x}}^{E,k} - \mathbf{x}_i^{E,k} + \mathbf{x}_i^E \right\|_2^2 \quad (\text{A.3})$$

(A.4)

Each of the following subsections presents the optimisation problem solved by each energy agent i for each iteration of the algorithm.

A.2.1 Hydrogen system agent

$$\begin{aligned} \underset{\dot{m}_{H_2,imp}, \dot{m}_{H_2,exp}, P_{H_2}, Q_{H_2}}{\text{minimize}} \quad & \sum_{t \in \mathcal{T}} (\dot{m}_{H_2,imp}(t)p^{H_2}(t) - \dot{m}_{H_2,exp}(t)p^{H_2}(t) \\ & - \lambda^E(t)P_{H_2}(t) + \lambda^H(t)Q_{H_2}(t))\Delta t + \mathcal{L}_{\rho,H_2}^H + \mathcal{L}_{\rho,H_2}^E \end{aligned}$$

subject to

$$\begin{aligned}
\dot{m}_{\text{H}_2,\text{imp}}(t) &\leq \dot{m}_{\text{H}_2,\text{imp}}^{\max}, & \forall t \\
\dot{m}_{\text{H}_2,\text{exp}}(t) &\leq \dot{m}_{\text{H}_2,\text{exp}}^{\max}, & \forall t \\
P_{\text{H}_2}(t) &= P_{\text{EL}}(t) + P_{\text{CO}}(t), & \forall t \\
Q_{\text{H}_2}(t) &= Q_{\text{EL,used}}(t) + Q_{\text{FC,used}}(t), & \forall t \\
P_{\text{EL}}(t) &\leq P_{\text{EL}}^{\max}, & \forall t \\
Q_{\text{EL,total}}(t) &= (P_{\text{EL}}(t) - \dot{m}_{\text{H}_2,\text{EK}}(t)\text{HHV}_{\text{H}_2})\eta_{\text{EL,th}}, & \forall t \\
Q_{\text{EL,total}}(t) &= Q_{\text{EL,used}}(t) + Q_{\text{EL,waste}}(t), & \forall t \\
\frac{\dot{m}_{\text{H}_2,\text{EL}}(t)\text{HHV}_{\text{H}_2}}{P_{\text{EL}}^{\max}} &\leq \alpha_{\text{EL},j} + \beta_{\text{EL},j}\frac{P_{\text{EL}}(t)}{P_{\text{EL}}^{\max}}, & \forall j \in [1, n+1], \forall t \\
P_{\text{FC}}(t) &\leq P_{\text{FC}}^{\max}, & \forall t \\
\dot{m}_{\text{H}_2,\text{FC}}(t) &\leq \dot{m}_{\text{H}_2,\text{FC}}^{\max}, & \forall t \\
Q_{\text{FC,total}}(t) &= (\dot{m}_{\text{H}_2,\text{FC}}(t)\text{HHV}_{\text{H}_2} - P_{\text{FC}}(t))\eta_{\text{FC,th}}, & \forall t \\
Q_{\text{FC,total}}(t) &= Q_{\text{FC,used}}(t) + Q_{\text{FC,waste}}(t), & \forall t \\
\frac{P_{\text{FC}}(t)}{\dot{m}_{\text{H}_2,\text{FC}}^{\max}\text{HHV}_{\text{H}_2}} &\leq \alpha_{\text{FC},j} + \beta_{\text{FC},j}\frac{\dot{m}_{\text{H}_2,\text{FC}}(t)}{\dot{m}_{\text{H}_2,\text{FC}}^{\max}}, & \forall j \in [1, n+1] \\
P_{\text{CO}}(t) &= \frac{RT_{\text{in}}\gamma}{M_{\text{H}_2}(\gamma-1)\eta_{\text{CO}}} \left(\left(\frac{P_{\text{out}}}{P_{\text{in}}} \right)^{\frac{\gamma-1}{\gamma}} - 1 \right) \dot{m}_{\text{H}_2,\text{EL}}(t) & \forall t \\
P_{\text{CO}}(t) &\leq P_{\text{CO}}^{\max}(t) & \forall t \\
m_{\text{H}_2,\text{sto}}(t) &= m_{\text{H}_2,\text{sto}}(t-1) + \eta_{\text{H}_2,\text{sto}}\Delta t (\dot{m}_{\text{H}_2,\text{hp}}(t) + \dot{m}_{\text{H}_2,\text{imp}}(t)) - \\
&\quad \frac{\Delta t}{\eta_{\text{H}_2,\text{sto}}} (\dot{m}_{\text{H}_2,\text{exp}}(t) + \dot{m}_{\text{H}_2,\text{FC}}(t)), & \forall t \\
m_{\text{H}_2,\text{sto}}(t) &\leq m_{\text{H}_2,\text{sto}}^{\max}, & \forall t \\
m_{\text{H}_2,\text{sto}}(t_0) &= m_{\text{H}_2,\text{sto}}^{\max}/2 \\
m_{\text{H}_2,\text{sto}}(t_f) &= m_{\text{H}_2,\text{sto}}^{\max}/2
\end{aligned}$$

A.2.2 Heat pump agent

$$\underset{P_{\text{HP}}, Q_{\text{HP}}}{\text{minimize}} \quad \sum_{t \in \mathcal{T}} (-\lambda^{\text{E}}(t)P_{\text{HP}}(t) + \lambda^{\text{H}}(t)Q_{\text{HP}}(t))\Delta t + \mathcal{L}_{\rho,\text{HP}}^{\text{H}} + \mathcal{L}_{\rho,\text{HP}}^{\text{E}}$$

subject to

$$\begin{aligned}
Q_{\text{HP}}(t) &= P_{\text{HP}}(t)\text{COP}, & \forall t \\
Q_{\text{HP}}(t) &\leq Q_{\text{HP}}^{\max}, & \forall t
\end{aligned}$$

A.2.3 TES agent

$$\begin{aligned}
& \underset{Q_{\text{TES},\text{net}}}{\text{minimize}} && \sum_{t \in \mathcal{T}} (\lambda^{\text{H}}(t) Q_{\text{TES},\text{net}}(t)) \Delta t + \mathcal{L}_{\rho,\text{TES}}^{\text{H}} \\
& \text{subject to} \\
E_{\text{TES}}(t) &= E_{\text{TES}}(t-1) [1 - \epsilon_{\text{TES}}] + \eta_{\text{TES,in}} Q_{\text{TES,in}}(t) \Delta t - \frac{1}{\eta_{\text{TES,out}}} Q_{\text{TES,out}}(t) \Delta t, & \forall t \\
0 \leq Q_{\text{TES,in}}(t) &\leq r_{\text{TES,in}}^{\max} E_{\text{TES}}(t), & \forall t \\
0 \leq Q_{\text{TES,out}}(t) &\leq r_{\text{TES,out}}^{\max} E_{\text{TES}}(t), & \forall t \\
0 \leq E_{\text{TES}}(t) &\leq E_{\text{TES}}^{\max}, & \forall t \\
Q_{\text{TES},\text{net}}(t) &= Q_{\text{TES,in}}(t) - Q_{\text{TES,out}}(t), & \forall t \\
E_{\text{TES}}(t_0) &= \frac{E_{\text{TES}}^{\max}}{2} \\
E_{\text{TES}}(t_f) &= \frac{E_{\text{TES}}^{\max}}{2}
\end{aligned}$$

A.2.4 BES agent

$$\begin{aligned}
& \underset{P_{\text{BES},\text{net}}}{\text{minimize}} && \sum_{t \in \mathcal{T}} (\lambda^{\text{E}}(t) P_{\text{BES},\text{net}}(t)) \Delta t + \mathcal{L}_{\rho,\text{BES}}^{\text{E}} \\
& \text{subject to} \\
E_{\text{BES}}(t) &= E_{\text{BES}}(t-1) [1 - \epsilon_{\text{BES}}] + \eta_{\text{BES,ch}} P_{\text{BES,ch}}(t) \Delta t - \frac{1}{\eta_{\text{BES,dis}}} P_{\text{BES,dis}}(t) \Delta t, & \forall t \\
0 \leq P_{\text{BES,ch}}(t) &\leq r_{\text{BES,ch}}^{\max} E_{\text{BES}}(t), & \forall t \\
0 \leq P_{\text{BES,dis}}(t) &\leq r_{\text{BES,dis}}^{\max} E_{\text{BES}}(t), & \forall t \\
E_{\text{BES}}^{\min} \leq E_{\text{BES}}(t) &\leq E_{\text{BES}}^{\max}, & \forall t \\
P_{\text{BES},\text{net}}(t) &= P_{\text{BES,ch}}(t) - P_{\text{BES,dis}}(t), & \forall t \\
E_{\text{BES}}(t_0) &= \frac{E_{\text{BES}}^{\max}}{2} \\
E_{\text{BES}}(t_f) &= \frac{E_{\text{BES}}^{\max}}{2}
\end{aligned}$$

A.2.5 Grid connection agent

$$\begin{aligned}
& \underset{P_{\text{imp}}, P_{\text{exp}}}{\text{minimize}} && \sum_{t \in \mathcal{T}} (P_{\text{imp}}(t) p_{\text{imp}}^{\text{E}}(t) - P_{\text{exp}}(t) p_{\text{exp}}^{\text{E}}(t) + \lambda^{\text{E}}(t) P_{\text{grid,net}}(t)) \Delta t + \mathcal{L}_{\rho,\text{grid}}^{\text{E}} \\
& \text{subject to}
\end{aligned}$$

$$\begin{aligned}
P_{\text{imp}}(t) &\leq P_{\text{imp}}^{\max}, & \forall t \\
P_{\text{exp}}(t) &\leq P_{\text{exp}}^{\max}, & \forall t \\
P_{\text{grid,net}}(t) &= P_{\text{imp}}(t) - P_{\text{exp}}(t), & \forall t
\end{aligned}$$

A.2.6 Consumer agent c

$$\begin{aligned}
\underset{P_{\text{cons},c}, Q_{\text{cons},c}}{\text{minimize}} \quad & \sum_{t \in \mathcal{T}} (\zeta_{\text{slack}} T_{\text{slack},c}(t) + \lambda^{\text{E}}(t) P_{\text{cons},c}(t) + \lambda^{\text{H}}(t) Q_{\text{cons},c}(t)) \Delta t \\
& + \mathcal{L}_{\rho, \text{cons},c}^{\text{H}} + \mathcal{L}_{\rho, \text{cons},c}^{\text{E}}
\end{aligned}$$

subject to

$$\begin{aligned}
T_c(t) &= \zeta_c T_c(t-1) + [1 - \zeta_c] [T_{\text{amb}}(t-1) + R_c [Q_{\text{cons},c}(t-1) + Q_{\text{solar},c}(t-1)]] \quad \forall t \\
\zeta_c &= e^{-\frac{\Delta t}{R_c C_c}} \\
T_c(t) &\leq T_c^{\max} + T_{\text{slack},c}(t) \quad \forall t \\
T_c(t) &\geq T_c^{\min} \quad \forall t \\
T_c(t_0) &= T_c^{\min} \\
P_{\text{cons},c}(t) &= \frac{1}{\Delta t} (\beta_{\text{li}}(t) L_{\text{li},c} + \beta_{\text{ea}}(t) L_{\text{ea},c}) \quad \forall t
\end{aligned}$$

Appendix B

Techno-economic parameters

This chapter contains the techno-economic parameters used to obtain the results from the case study presented in this report. Table B.2 presents all the technical parameters, Table B.1 presents the economic-related parameters for each technology.

Table B.1: *Economic-related parameters for the energy technologies modelled in the energy system.*

| Technology | Investment cost | O&M cost | Lifetime (y) | Source |
|------------------------|------------------------|--------------------------------|--------------|--------|
| PV system | 428 CHF/m ² | 2.6 CHF/(m ² ·year) | 25 | [41] |
| Battery energy storage | 285 CHF/kWh | 6.3 CHF/(kWh·year) | 12 | [42] |
| Thermal energy storage | 9 CHF/kWh | 0.14 CHF/(kWh·year) | 24 | [42] |
| PEM Electrolyser | 1'295 CHF/kW | 45.3 CHF/(kW·year) | 15 | [42] |
| PEM Fuel cell | 1'684 CHF/kW | 40 64.0 /(kW·year) | 14 | [42] |

Table B.2: Technical parameters for the energy technologies modelled in the energy system.

| Parameter | Value | Units | Source |
|---|---------|----------------|--------|
| <i>Heat pump</i> | | | |
| Maximum capacity (P_{HP}^{\max}) | 15 | kW | |
| Coefficient of performance (COP_{HP}) | 3.85 | - | [43] |
| <i>Electrolyser</i> | | | |
| Maximum capacity (P_{EL}^{\max}) | 10 | kW | |
| Nominal electrochemical efficiency (η_{EL}) | 0.5814 | - | [38] |
| Thermal efficiency ($\eta_{\text{EL,th}}$) | 0.95 | - | [16] |
| <i>Fuel cell</i> | | | |
| Maximum capacity (P_{FC}^{\max}) | 5 | kW | |
| Maximum mass flow ($\dot{m}_{\text{H}_2,\text{FC}}^{\max}$) | 0.29 | kg/h | |
| Nominal electrochemical efficiency (η_{FC}) | 0.4367 | - | [37] |
| Thermal efficiency ($\eta_{\text{FC,th}}$) | 0.95 | - | [16] |
| <i>Compressor</i> | | | |
| Maximum capacity (P_{CO}^{\max}) | 1 | kW | |
| Inlet pressure (P_{in}) | 30 | bar | |
| Outlet pressure (P_{out}) | 60 | bar | |
| Isentropic efficiency ($\eta_{\text{isentropic,CO}}$) | 0.80 | - | [22] |
| Mechanical efficiency ($\eta_{\text{mech,CO}}$) | 0.98 | - | [22] |
| Generator efficiency ($\eta_{\text{gen,CO}}$) | 0.96 | - | [22] |
| Total efficiency (η_{CO}) | 0.75 | - | [22] |
| <i>Hydrogen storage</i> | | | |
| Volume per tank ($V_{\text{H}_2,\text{sto}}$) | 0.85 | m ³ | |
| Pressure tank ($P_{\text{H}_2,\text{sto}}$) | 60 | bar | |
| Temperature tank ($T_{\text{H}_2,\text{sto}}$) | 60 | bar | |
| Number of tanks (n_{tanks}) | 4 | - | |
| Storage efficiency ($\eta_{\text{H}_2,\text{sto}}$) | 0.938 | - | [44] |
| <i>Battery energy storage</i> | | | |
| Maximum energy storage (E_{BES}^{\max}) | 30 | kWh | |
| Maximum charging rate ($r_{\text{BES,ch}}^{\max}$) | 0.25 | kW/kWh | [45] |
| Maximum discharging rate ($r_{\text{BES,dis}}^{\max}$) | 0.25 | kW/kWh | [45] |
| Charging efficiency ($\eta_{\text{BES,ch}}$) | 0.96 | - | [44] |
| Discharging efficiency ($\eta_{\text{BES,dis}}$) | 0.96 | - | [44] |
| Self-discharge rate (ϵ_{BES}) | 0.00054 | %/h | [44] |
| <i>Thermal energy storage</i> | | | |
| Maximum energy storage (E_{TES}^{\max}) | 17 | kWh | |
| Maximum input rate ($r_{\text{TES,in}}^{\max}$) | 0.25 | kW/kWh | [45] |
| Maximum output rate ($r_{\text{TES,out}}^{\max}$) | 0.25 | kW/kWh | [45] |
| Input efficiency ($\eta_{\text{TES,in}}$) | 0.91 | - | [44] |
| Output efficiency ($\eta_{\text{TES,out}}$) | 0.91 | - | [44] |
| Self-discharge rate (ϵ_{TES}) | 0.0097 | %/h | [44] |
| <i>PV</i> | | | |
| Panel area (A_{pv}) | 30 | m ² | |
| Efficiency (η_{pv}) | 0.17 | - | [44] |